REVIEW

Silicon Micro- and Nanofabrication for Medicine

Daniel Fine, Alessandro Grattoni, Randy Goodall, Shyam S. Bansal, Ciro Chiappini, Sharath Hosali, Anne L. van de Ven, Srimeenkashi Srinivasan, Xuewu Liu, Biana Godin, Louis Brousseau III, Iman K. Yazdi, Joseph Fernandez-Moure, Ennio Tasciotti, Hung-Jen Wu, Ye Hu, Steve Klemm, and Mauro Ferrari*

This manuscript constitutes a review of several innovative biomedical technologies fabricated using the precision and accuracy of silicon micro- and nanofabrication. The technologies to be reviewed are subcutaneous nanochannel drug delivery implants for the continuous tunable zero-order release of therapeutics, multi-stage logic embedded vectors for the targeted systemic distribution of both therapeutic and imaging contrast agents, silicon and porous silicon nanowires for investigating cellular interactions and processes as well as for molecular and drug delivery applications, porous silicon (pSi) as inclusions into biocomposites for tissue engineering, especially as it applies to bone repair and regrowth, and porous silica chips for proteomic profiling. In the case of the biocomposites, the specifically designed pSi inclusions not only add to the structural robustness, but can also promote tissue and bone regrowth, fight infection, and reduce pain by releasing stimulating factors and other therapeutic agents stored within their porous network. The common material thread throughout all of these constructs, silicon and its associated dielectrics (silicon dioxide, silicon nitride, etc.), can be precisely and accurately machined using the same scalable micro- and nanofabrication protocols that are ubiquitous within the semiconductor industry. These techniques lend themselves to the high throughput production of exquisitely defined and monodispersed nanoscale features that should eliminate architectural randomness as a source of experimental variation thereby potentially leading to more rapid clinical translation.

1. Introduction

From the invention of the first transistor in 1947[1] and the first integrated circuit (IC) in 1958,[2] the "top-down" techniques and processes used to achieve the highest possible density of active electronic components on a single semiconductor die have advanced at a dizzying pace (double the transistor and memory bit density every 18–24 months), while maintaining nearly constant areal manufacturing cost.[3] According to the *International Technology Road Map for Semiconductors*, a "fifteen year assessment of the semiconductor industry's future technology requirements", the current (2011) state-of-the-art for optical lithography is 24 nm (the physical gate length of a transistor) leading to an incredible 1.7 billion transistors per square centimeter.[4] Although the costs associated with the research, development, and implementation of the latest IC technology node can be significant, they are offset by continuously increasing demand for more advanced integrated circuit (IC) designs and architectures. This economic

Dr. D. Fine,[†] Dr. A. Grattoni,[†] Dr. S. S. Bansal, Dr. A. L. van de Ven, S. Srinivasan, Prof. X. Liu, Dr. B. Godin, Dr. L. Brousseau III, I. K. Yazdi, Dr. J. Fernandez-Moure, Dr. E. Tasciotti, Dr. H.-J. Wu, Prof. Y. Hu, Prof. M. Ferrari
Department of Nanomedicine
The Methodist Hospital Research Institute
Houston, TX, 77030, USA
E-mail: agrattoni@tmhs.org
Dr. R. Goodall, Dr. S. Hosali
NanoMedical Systems Inc., Austin, TX, 78741, USA
Dr. C. Chiappini
Department of Materials, Imperial College, London, SW7 2AZ, UK
Dr. S. Klemm
Leonardo Biosystems, Inc., Houston, TX, 77030, USA
I. K. Yazdi
Department of Biomedical Engineering
University of Houston
Houston, TX, 77204, USA
Prof. M. Ferrari
President, CEO,
and Ernest Cockrell Jr. Distinguished Endowed Chair,
The Methodist Hospital Research Institute
Houston, TX, 77030, USA
Prof. M. Ferrari
Department of Medicine
Weill Cornell Medical College
New York, NY, 10065, USA
Prof. M. Ferrari
Department of Bioengineering
Rice University
Houston, TX, 77005, USA
Prof. M. Ferrari
President, Alliance for NanoHealth, Houston, Texas 77030, USA
[†]These authors made equal contributions to this work

DOI: 10.1002/adhm.201200214

© 2013 WILEY-VCH Verlag GmbH & Co. KGaA, Weinheim

balance is usually reserved for the highest levels of computing power. Fortunately, many biomedical applications that use advanced silicon processing are well suited for non-leading edge *lithographic* technology generations (the multi-stage nanovectors described below are on the order of 600 nm or larger) meaning higher device yields and lower process cycle demand that lead to significantly reduced fabrication cost. **Figure 1** shows a visual representation of this dichotomy where biomedical devices and other "system-in-package" applications are fabricated with length scales that deviate from traditional trends in transistor scaling.[4] Many of these medical applications require and therefore substantially and increasingly benefit from the same continuously improving leading edge capabilities in other (non-lithographic) process areas that have been developed for advanced ICs, including nanoscale metallization and dielectric atomic layer deposition, chemical-mechanical polishing, precision multi-layer etches, and advanced metrology.

Thus with the same "top-down" fabrication processes developed over the last fifty years that produce high-performance microprocessors and memory chips, the engines of the Digital Age, nanoscale constructs for drug delivery, proteomic profiling, and bone repair have been manufactured with a high degree of both precision and accuracy. This is crucial for eliminating device variability as a source of experimental variation, for incorporating ever advancing capability at lower functional cost, for tuning nanoscale features for personalized medicine, and, ultimately, for gaining regulatory and clinical acceptance. As such, we present this overview of several of these innovative biomedical nanotechnologies for clinical applications.

This review is divided into 8 sections that include this introduction. Section 2 presents the biocompatibility and biodegrability, as well as the methods used to modify their surface properties, of silicon and its dielectrics. This section also covers the foreign body response of the in vivo environment to exogenously introduced entities. The beginning of Section 3 discusses implantable devices as they relate to dosing strategies and architectural designs and then hones in on the structural characteristics, history of development, and modeling of nanochannel membranes, including an elucidation of representative fabrication protocols used to manufacture them. This is followed by investigating electrokinetic transport as it relates to modulating drug delivery. Section 4 details porous silicon multistage nanovectors that are comprised of porous silicon particles whose shape, size, and surface properties have been rationally designed to maximize their loading capacity and accumulation in specific organs and tissues, especially tumors, after intravenous administration. In Section 5, the fabrication and biomedical applications of silicon and porous silicon nanoneedles and nanowires are investigated. Section 6 delves into the use of porous silicon inclusions in biocomposites for tissue engineering, and more specifically bone regeneration, in terms of its effects on the mechanical robustness of bone replacement scaffolds as well as the ability of these pSi particles to deliver important biomolecular cofactors and pharmaceuticals to promote collagen formation, mineralization, and chemotaxis. Proteomic profiling is covered in Section 7 as it relates to both biomarker discovery and tumor and metastasis staging. Finally, this review concludes in Section 8 with a recap of the important topics discussed in the previous sections as well as

Alessandro Grattoni is a Co-Chair and Assistant Member in the Department of Nanomedicine at The Methodist Hospital Research Institute. His research focuses on the development and clinical translation of implantable nanofluidic technologies for drug delivery, molecular sieving, and cell transplantation. Silicon-based nanochannel membranes are developed for the controlled delivery of therapeutics by exploiting nanoscale physics, achieving a constant or tunable sustained release of molecules for extended periods of time. His research projects have received the support of NASA and NanoMedical Systems, Inc., a company focused on the development and commercialization of the nanochannel Delivery System for clinical use.

Dr. Tasciotti is Co-Chair of the Department of Nanomedicine at the Methodist Hospital Research Institute and serves as the Director of the Regenerative Medicine Program and as Scientific Director of Surgical Advanced Technology Lab. He was the first to demonstrate the multistage delivery strategy for the loading and release of multiple nanoparticles from biodegradable first stage silica carriers, which was selected as cover story by Nature Nanotechnology and picked as one of the "5 big ideas in Nanomedicine" by Nature Medicine. He led the development of a fracture putty in a DARPA funded project entitled "BioNanoScaffolds for Post-Traumatic OsteoRegeneration"; a multidisciplinary study focused on the treatment of battlefield non-union long bone fractures.

Dr. Mauro Ferrari is President and CEO of The Methodist Hospital Research Institute, where he holds the Ernest Cockrell, Jr. Distinguished Endowed Chair, is the Director for the Institute for Academic Medicine as well as an Executive Vice President for The Methodist Hospital. Dr. Ferrari also is Senior Associate Dean and Professor of Medicine at Weill Cornell Medical College in New York, NY. Dr. Ferrari is president of the Alliance for NanoHealth in Houston, TX. Dr. Ferrari is one of the pioneers of biomedical nano/microtechnology research especially in their applications to drug delivery, cell transplantation, implantable bioreactors, and other innovative therapeutic modalities.

© 2013 WILEY-VCH Verlag GmbH & Co. KGaA, Weinheim

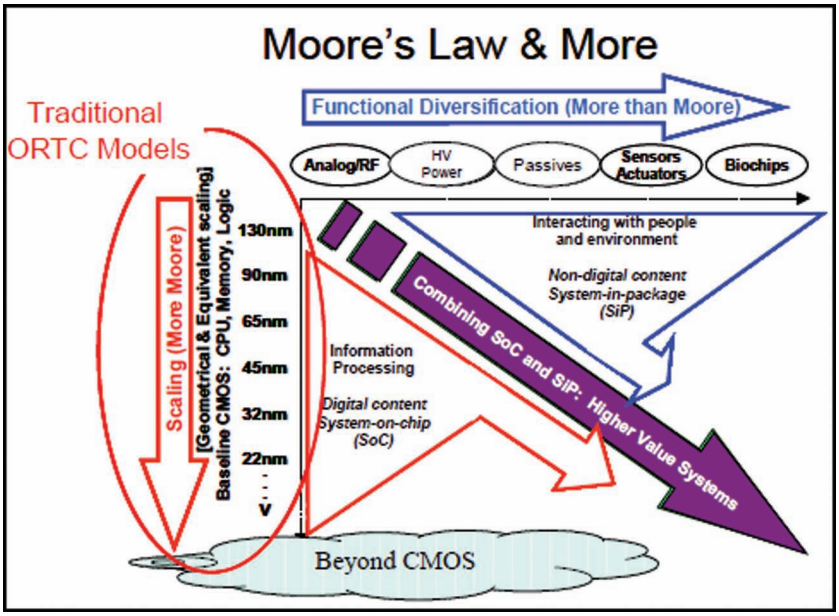

Figure 1. A representation of the divergence of device scaling between high performance computing and environmental and biological sensing application. Taken from "Semiconductor Industry Association. The International Technology Roadhmp for Semiconductors, 2009 Edition: Executive Summary, SEMATECH Austin, TX, 2009."

closing remarks on the economics of developing biomedical systems using silicon micro- and nanofabrication.

2. The Biocompatibility of Micro- and Nanofabrication Materials

2.1. Silicon and Its Dielectrics

In addition to exploiting their electrical properties to produce advanced ICs, highly refined silicon, the second most abundant element on the Earth's crust, and its dielectrics (SiO_2, Si_3N_4) have been used extensively for biomedical applications because of their previously demonstrated biocompatibility and mechanical stability, as well as the ease with which their surface properties and chemistry can be modified.[5] The silanol group can be easily activated at the surface of oxidized silicon to bind with organosilane molecules, which in turn are capable of providing diverse functional groups that can mediate a large array of specific bioconjugation strategies.[6] Silanes with amine, carboxyl, alkyl, epoxy, sulfhydryl, and aldehyde functional groups are commercially available, while optimized functionalization strategies in both the liquid and vapor phase have been widely developed and reported in both the scientific literature and for well-established commercial applications in very diverse fields. Once stable mono- or oligo-layers of silanes are formed on the silicon surface, then conventional bioconjugation strategies are employed to chemisorb or physisorb a wide array of bioactive molecules and nanoparticles on the silicon surface. As an example, Zhang et al.[5e] was able to achieve a 90% reduction in albumin adsorption for more than 4 hours on hydrophobic methylated surfaces modified with 0.05% Tween 20. Self-assembled polyethylene glycol (PEG) and monomethoxypoly(ethylene glycol) (MPEG) multilayers have also been functionalized on silicon surfaces and found to be capable of suppressing the adsorption of plasma proteins, platelets, fibroblasts, and HeLa cells.[5e]

While these silicon-based materials are generally harmless to the body and do not stimulate detrimental encapsulation, many are themselves directly degraded by the chemical/ionic environment in vivo. Implantable devices for long-term drug release with micro- and nanofabricated structures that experience continuous contact with body serum, both intravenously and subcutaneously, must therefore be fabricated with application-specific materials, coatings, and processes beyond those typically available in commercial MEMS fabrication facilities. These structural materials and nano-coatings, which include chemical vapor deposited silicon carbide and positive-to-negative stress-graded silicon nitride as well as atomic layer deposited oxides, along with their associated etch processes are frequently found only in advanced IC manufacturing facilities and have been anecdotally noted in biochip protection schemes by commercial developers of nanochannel devices.[7]

Porous silicon is not only biocompatible, but biodegradable as well. This is due to its high surface area that induces a rapid oxidation of Si in aqueous solution rendering it readily dissolvable.[8] The degradation product, orthosilicic acid, is a compound found naturally within the human body that has been shown to promote a number synergistic effects in relation to bone regeneration (discussed in Section 6.2). Particles fabricated out of porous silicon have been shown to be stable during storage, and then readily degradable in plasma, blood, and tissue.[9] A variety of cells, including endothelial cells and macrophages, also readily internalize porous silicon particles in vitro and in vivo with no adverse affects related to cell proliferation and particles partitioning to daughter cells during mitosis.[10] The release of cytokines from treated cells is similar to that of controls,[9a,10,11] suggesting that pSi particles are also non-immunogenic. No acute or chronic toxicity has been observed in healthy or tumor-bearing mice receiving multiple injections of these pSi particles.[12] Polymer coatings, including PEG and agarose, have been used to coat pSi particles to temporarily protect them from cellular degradation while the conjugation of antibodies or targeting moieties have facilitated the efficient delivery of payloads loaded in the pores to the right place at the right time in the right quantity.[6a,9a,13]

2.2. The Foreign Body Response

The biocompatibility of a foreign device is dictated by the type and extent of the cellular responses that it induces in the

© 2013 WILEY-VCH Verlag GmbH & Co. KGaA, Weinheim

surrounding tissue, a reaction typically referred to as the foreign body response (FBR). Implantation is an invasive procedure that causes localized tissue injury and initiates both acute and chronic inflammatory cascades that result in increased localized vascular permeability and the extravasation of a variety of proteins and immune cells, including albumin, complement factor 3, IgG, fibrinogen, fibronectin and vitronectin, intended to remove dead cellular debris.[14] These proteins adsorb to foreign bodies and act as identification tags for orchestrating the response of host cells, including inflammatory cells and fibroblasts. The rate and extent of protein adsorption on the surface of an implant is therefore one of the primary factors in determining its biocompatibility.[15] Studies have shown that specific adsorption of proteins like fibronectin and vitronectin on the surface of implants mediates cellular interactions, with surface topographies that are more receptive to these proteins also being more conducive to protein/cellular adhesion.[16] The types of protein molecules secreted at the implant surface also promote haptotaxis of polymorphonuclear cells (neutrophils and lymphocytes) towards the implant site and drive alterations in their morphology.[17] Various chemokinetic and chemotactic factors determine the rate and extent of this process, including various complement factors, bacterial fragments, leukotrienes, lymphokines, and fibronectin.[14] Once extravasated, neutrophils and lymphocytes start to accumulate at the tissue/implant interface and attract monocytes to the implant site.[18] These monocytes also respond to similar mediators as the polymorphonuclear cells, and, under their influence, mature into tissue macrophages that recognize the implant as a foreign body and try to engulf it.[14] Activation of macrophages further results in the release of various secretory products like superoxide anion, fibronectin, IL-1, extracellular matrix proteins, binding proteins, and coagulation factors that dictate subsequent cascade events.[19] These factors help in the remodeling of connective tissues and to regulate the extra-cellular environment.[20] The inability of macrophages to phagocytose the implants results in a frustrated state in which they fuse with each other to form giant cells resulting in granuloma formation and further promoting fibroblast migration. Proliferation and growth of fibroblasts further leads to the synthesis and deposition of collagen, a component of connective tissue and an important component in wound healing, and ultimately to fibrous encapsulation around the implant.[21]

Titanium and its alloys, a material base commonly used to fabricate drug delivery implants, have been demonstrated to have excellent biocompatibility, corrosion resistance, and mechanical strength. Studies performed with polymers coated with titanium derivatives (for easier preparation of thin sections[22]) in rats showed a fibrous encapsulation that was only 50–90 μm thick and decreased gradually with time.[21b] The connective tissue around the implants was found to consist primarily of collagen fibers forming concentric layers around the titanium implants with fibers oriented parallel to the implant surface.[21b] Furthermore, higher amounts of type-I collagen as compared to collagen III (an indicator of higher biocompatibility) was observed.[21b] The surrounding encapsulation was also found to be moderately infiltrated with inflammatory cells and fibroblasts.[23] A time dependent decrease in granulocytes and lymphocytes was observed at the site of implantation over a period of 4 weeks[23] with almost no detectable populations present after 4 weeks.[22] A similar trend was also reported with macrophages and giant cells.[22] As a result, titanium and its alloys have been extensively used for both dental and medical applications,[24] including for artificial hips, knees, bone plates, as screws for fracture fixation, pacemakers, dental prosthesis, overdentures, bridges, and crowns.[25] The excellent biocompatibility of commercially pure titanium originates from its tendency to react with oxygen and form an inert, stable, and thin layer of titanium dioxide at its surface. Furthermore, low electronic conductivity, high corrosion resistance, low ionization, an iso-electric point of around 5-6, and a dielectric constant comparable to water also makes it a biomaterial of choice for implants.[26]

The rate and extent of the inflammatory reaction depends not only on the composition and structure of a material but also on the implant's surface roughness, size, shape, and surface functionalization, which are usually determined by the manufacturing process and can be altered according to the intended biological function of the implants.[22] Various surface treatments, including sandblasting and acid etching (SLA),[27] plasma spray coating of hydroxyl apatite,[28] immobilization of extracellular matrix proteins,[29] layer by layer assembly of DNA by electrostatic self-assembly,[30] and electrospray deposition of enzymes like alkaline phosphatase,[31] can be used to further modulate the biocompatibility of implantable materials and bodies.

3. The nanochannel Delivery System (nDS)

From ion channels that control the diffusion of specific ions across the cell membrane[32] to chaetae rendered iridescent through a photonic crystal-like effect,[33] the natural world is replete with examples of organisms manipulating their physical environments using nanochannels. Nature uses a "bottom up" approach to manufacture these structures with an exquisite level of precision and accuracy derived from self-assembled protein building blocks that require constant maintenance to insure proper structure and function.[3] As of yet, however, no similar anthropogenic manufacturing process has succeeded in producing robust monodispersed nanochannels for long-term (greater than 6 months continuously) drug delivery using a similar bottom-up approach. Therefore, in this section we will limit our discussion to silicon-based nanofluidic membranes produced using the same top-down fabrication techniques and possessing the same biocompatible characteristics alluded to earlier. This discussion will also include a justification for continuous release and a glimpse into the possibilities for electrostatic and electrokinetic control (electroosmosis and/or electrophoresis) of analyte release, an important prerequisite for the realization of a self-regulating "NanoGland".

3.1. Modes of Drug Delivery

With most conventional routes of administration, including ingestion as well as subcutaneous, intramuscular, and intravenous injections, only a finite amount of drug can be delivered

© 2013 WILEY-VCH Verlag GmbH & Co. KGaA, Weinheim

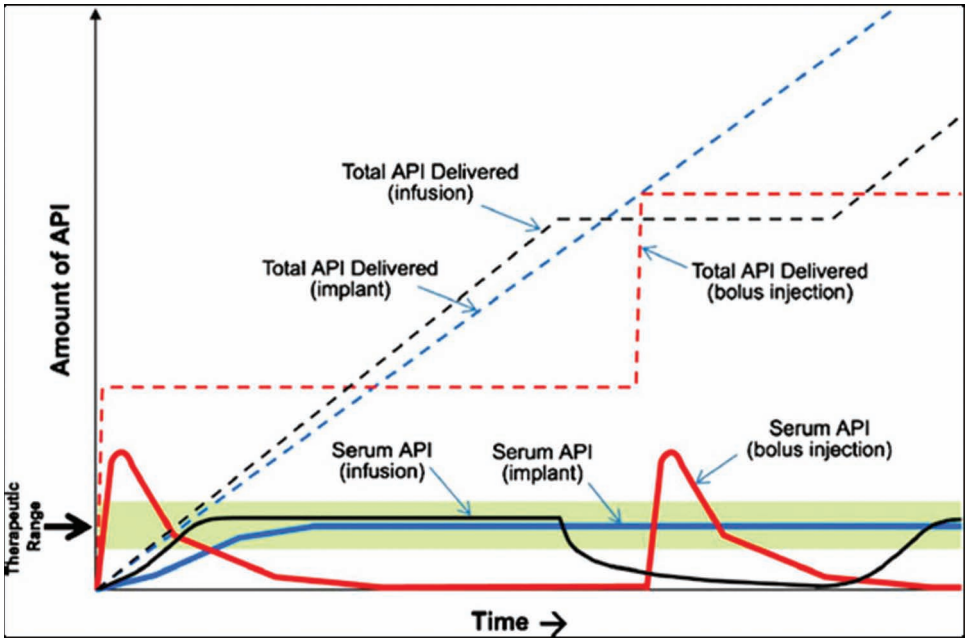

Figure 2. Profiles of drug delivered and drug concentration of an active pharmaceutical agent (API) in the plasma through bolus injection, infusion, or from zero-order release implant. Reproduced with permission.[41] Copyright 2011, Springer Science & Business Media.

at any given time. For pathologies requiring long-term intervention, this limitation necessitates a larger than optimal dose to maintain an average drug concentration within the therapeutic range. In the case of cytotoxic drugs, a category which includes most chemotherapeutics, the maximum tolerated dose (MDT) is delivered at intervals that allow for sufficient recovery from adverse side effects. New evidence suggests, however, that decreasing the amount and increasing the frequency of dosing can enhance the therapeutic index (the ratio of therapeutic to lethal dose) of many of these cytotoxic drugs while significantly reducing or eliminating systemic toxicity and thus leading to better overall clinical outcomes, a dosing regimen commonly referred to as metronomic delivery.[34] In addition, reducing the interval between doses may also help to prevent the acquisition of drug resistance by the pathologic target, an important concern for many chemotherapeutic regimens.[35]

The ultimate extension of metronomic delivery is continuous and constant drug release, also referred to as zero-order release. The zero-order release rate is carefully balanced with the in vivo drug elimination rate to achieve a therapeutic concentration while alleviating toxic accumulation.[35] Recent studies have verified the significant enhancements to therapeutic efficacy made possible by this drug delivery strategy.[36] The anti-angiogenic agents cyclophosphamide and methotrexate, drugs that many cancers have shown the propensity to become resistant to, have proven to be more effective inhibitors of tumor proliferation when constantly administered in this fashion.[37] The closest clinically available examples of continuous release are IV infusion and infusion pumps.[38] Unfortunately these methodologies require catheterization which could lead to infection, although experimental studies in which insulin pumps are fully implanted have been performed.[39] In addition, IV infusion has not proven to be tunable enough to prevent the eventual accumulation of toxic side effects and therefore also periodically requires lengthy recovery periods.[34c,40] **Figure 2** graphically compares and contrasts these different dosing regimens.[41]

3.2. Implantable Drug Delivery

Delivering drugs from implants offers the opportunity to precisely control the amount, release rate, and timing of pharmaceutical administration. Automatic and sustained delivery offers the added benefits of increasing patient compliance and improving quality of life.[42] Microchips possessing arrays of mini-reservoirs micromachined into a silicon substrate and capped with gold membranes that can be electrically ruptured are capable of the telemetrically controlled pulsatile release of a wide range of drug formulations[43] and have successfully been demonstrated in vivo in both a dog model for up to 6 months[44] and in humans for up to 20 days.[45] This very exciting architecture has one important limitation; it can only approximate zero-order release by increasing the pulse frequency. There are, however, several promising alternative implantable drug delivery architectures capable of achieving long-term zero-order delivery using a range of different actuation methods, both active and passive. Technologies that use active methods of delivery include implantable infusion pumps,[46] osmotic[47] and electroosmotic pumps,[48] and galvanic cells,[49] while passive delivery has been achieved largely through diffusive transport of analytes from biodegradable and nonbiodegradable polymers,[50] hydrogels,[51] porous inorganic materials, including TiO_2,[52] silica,[53] and alumina,[54] and nanoporous (block copolymer,[55] and ion milled[56]) and nanochanneled nanofluidic membranes.[57] Many of these alternative methods have also already been demonstrated in both animal models[55,58] and human preclinical trials,[45] while a few, including the Viadur™ implant based on the DUROS osmotic pump

© 2013 WILEY-VCH Verlag GmbH & Co. KGaA, Weinheim

(releases leuprolide acetate for up to one year),[47] as well as several versions of implantable polymers, including Implanon (birth control, sliastic tubing),[59] Sandostatin LAR (PLGA),[60] and Gliadel® (PCPP-SA)[61] to name a few, are already FDA approved and commercially available. For further reading, good reviews on many of these promising implantable drug release architectures can be found in these references,[62,63] and.[64]

3.3. The Development of Nanofluidic Membranes for Biomedical Applications

To date, nanofluidic membranes have been fabricated using a range of methods[65] from an array of materials, including silicon,[65a,66] silica,[65b] alumina,[67] silicon nitride,[57] carbon,[68] titanium dioxide,[69] polydimethylsiloxane,[70] SU-8,[71] and gold.[72] Silicon represents one of the more attractive material bases for manufacturing nanochannels because of the scalability, flexibility, precision, and accuracy of the processes and techniques used to machine it. By utilizing these silicon fabrication processes no structural feature of the nanochannels is left to chance or process randomness, while the nanochannel array's high degree of order helps to prevent undesirable protein absorption and mineralization that can be a problem for membranes with more chaotic nanostructure.[73] At least one study demonstrated stable in vivo release rates from silicon nanofluidic membranes for up to 6 months with little to no effect from fibrotic encapsulation for the molecules tested.[58] Silicon nanochannels with depths as small as 2 nm have been fabricated using anodically bonded Pyrex to cap 2 nm deep nanotrenches[74] (see **Figure 3**), while a sacrificial metal embedded in silicon nitride has been used to fabricate massively parallel nanochannels of less than 3 nm in depth.[75]

The first examples of nanofludic membranes produced using silicon micro- and nanofabrication techniques were reported by Kittilsland et al. in 1990[76] followed by Chu et al. in 1995.[65a] The 1990 report showed the filtration of particles as small as 50 nm while the 1995 work further reduced the threshold, demonstrating nanofilters possessing monodispersed nanochannels with critical dimensions as small as 20 nm.[65a] These nanofilters consisted of a 9 µm thick polysilicon layer supported by a silicon substrate with nanochannels that were generated by etching a thin sacrificial SiO_2 layer embedded within the membrane structure. The effective nanochannel size was therefore controlled by tuning the thickness of the oxide layer. Despite their thin structure these membranes were shown to be capable of withstanding differential pressures of approximately 1.4 atm.

3.3.1. Immunoisolating Biocapsules

For several decades, cell transplantation has been investigated and used in the clinic for the treatment of a number of pathologies. For Type 1 diabetes, pancreatic islets, microstructures in the pancreas that contain the body's insulin secreting cells, have been transplanted into diabetic patients in order to restore the mechanisms that maintain normoglycemia. Frequently these transplanted cells are intravenously infused and directly exposed to the bloodstream, but can often trigger an innate immune response within the host, including complements[77]

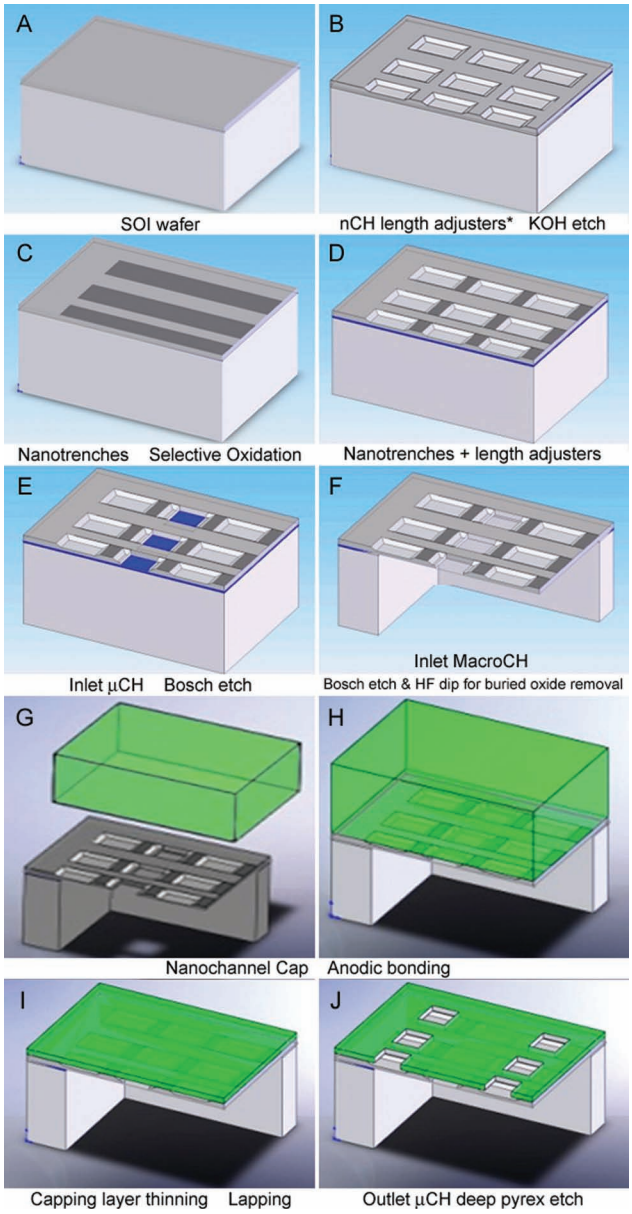

Figure 3. An example of a sequence of process steps for fabricating a nanofluidic membrane. A) The process begins by using a piranha cleaning solution of H_2O_2 and H_2SO_4 (ratio of 1 to 2) to clean a silicon-on-insulator substrate (SOI, 30 micron top silicon device layer, 400 nm buried oxide layer, 500 µm bottom silicon handle wafer). B) Mixports are then etched into the device layer with a solution of KOH to adjust the final length of the nanochannels. C) or D) Trenches with the desired nanometer depth are then machined into the device layer using selective oxidation of the surface through a silicon nitride oxidation mask. E) Microchannels through the device layer are then etched down to the buried oxide using a Bosch reactive ion etching process (deep silicon etch). F) Macrochannels are then etched through the handle wafer from the other side of the SOI substrate also with a deep silicon etch followed by removal of the buried oxide between the macro- and microchannels using HF. G) and H) A Pyrex glass wafer is then anodically bonded to the device layer of the SOI substrate to cap the nanotrenches. I) This is followed by a lapping procedure to thin the Pyrex wafer to 20 µm or less. J) Finally, outlet micrchannels are then etched through the Pyrex also using a reactive ion etch. Reproduced with permission.[75] Copyright 2010, The Royal Society of Chemistry (RSC).

© 2013 WILEY-VCH Verlag GmbH & Co. KGaA, Weinheim

and coagulation, due to their non-hematological and allogeneic origin. This immune response serves as the first-line of defense against foreign objects, eliciting a thrombotic and/or inflammatory reaction, referred to as the instant blood-mediated inflammatory reaction (IBMIR), which destroys the foreign cells immediately after their implantation.[78] Thus, the success of transplantation depends on protecting the implanted cells from immunorejection and maintaining their viability and functionality through neovascularization at the site of implantation, biological stimulation of the cells, and maintenance of an appropriate implant morphology.[79] In the case of pancreatic islets, patients are treated with systemic immunosuppressive therapy to inhibit immuno- and clotting reactions following transplantation. For this purpose, and despite their limited efficacy, drugs such as heparin,[80] thrombin[81] or protein tissue factor inhibitors[82] are administered at regular intervals for extended durations. These treatments are commonly associated with significant side effects, including internal bleeding and infections. Other methods have therefore also been developed to protect the cells within the host body to circumvent the deleterious side effects of these immunosuppressive regimens. Prior to transplantation, cells have been pretreated through PEGylation of their surface to avoid direct contact with blood components. This process increases the cell viability and biological activity by preventing the adsorption of proteins and the activation of the immunoresponse cascade[83] through an increase of the cellular surface hydrophilicity.

Immunoisolation represents a fascinating alternative to the aforementioned transplantation methods. In this technique, the transplanted cells are provided with a physical barrier capable of protecting them from the host immune system. This approach involves shielding cells using a semi-permeable membrane that allows for the diffusion of small molecules, such as oxygen, nutrients and hormones, while impeding the permeation of large molecules, such as antibodies or inflammatory cells.[84] The encapsulation provides the additional advantage of confining the transplanted cells into a finite three-dimensional space that more closely mimics their natural environment. Various materials have been investigated for the fabrication of suitable platforms for immunoisolating encapsulation. Most of the previously developed strategies have been based on polymeric materials. Microcapsules for intravascular implantation[85] have been directly injected into blood vessels to promote a fast insulin-secretion response and a rapid adjustment to blood-glucose levels and are generally made of hollow polymeric fibers (e.g,. of polyacrilonitrile and polyvinylchloride[86]). Despite the biocompatibility of the materials, such capsules can potentially lead to thrombosis and therefore require administration of anticoagulants.[85,87] Other polymers and hydrogels, including alginate, nitrocellulose acetate, Poly(L-lysine)/PEG copolymers,[88] agarose[89] and chitosan,[90] have also been used for extravascular macro- and microcapsules. Implanted subcutaneously or intraperitoneally, these macro- and microcapsules are less likely to represent significant risks to patients. Despite the enormous research efforts focused on these polymeric and hydrogel-based biocapsules, however, such materials present limitations, including broad pore-size distributions, chemical instability and degradation, and limited mechanical strength, all factors that may ultimately impede their clinical application.[91]

Biocompatible ceramic and ceramic/metal composites offer valuable alternatives to the polymeric approach. A large number of ceramic/metal composites are already currently in use in the clinic in a range of applications from orthopedics to cardiovascular devices. These materials have also shown great potential for cell transplantation because of their increased biocompatibility, inertness to biological molecules, and significant mechanical robustness. Among these ceramics, silicon offers a well defined and highly reproducible structure, based on the top-down methods of fabrication previously discussed, ideal for the development of biohybrid capsules. Previously, Desai et al.[92,93] achieved biocompatible encapsulation of pancreatic islets by manufacturing immunoisolating capsules using a pair of the aforementioned nanofilters reported by Chu et al. (1995). These nanofilters, possessing 78 nm nanochannels, were bonded back to back using bonding materials that were analyzed and optimized by Hansford et al. The bonding materials investigated included 2 types of silicones and three different methacrylates.[94] Of these, the low T_g methacrylates proved to be the most suitable candidates for biohybrid devices, presenting with adequate mechanical adhesion strength and maintaining complete inertness with respect to the growth of HeLa cells. Once loaded in the nanofilters and incubated in cell culture plates, the encapsulated islets were able to respond to glucose stimuli for over 4 weeks while maintaining superior functionality with respect to unencapsulated islets. It was hypothesized that this enhanced functionality and viability was the result of the three-dimensional matrix environment provided by encapsulation, in contrast to the significant dissociation experienced by the free islets. In following experiments[95] with similar capsules presenting 18, 66, and 78 nm nanochannels, Desai et al. also examined the in vivo biocompatibility of the immunoisolating capsules loaded with primary islet cells and insulinoma cell lines in mice and rat models. After intraperitoneal implantation the biocapsules were found free from significant fibrotic encapsulation-based channel blockage and degradation. Furthermore, the encapsulated cells remained viable and maintained glucose- stimulated insulin secretion. Later, Smith et al.[96] confirmed the results obtained by Desai et al., using the same nanofilters developed by Chu et al. In this study, nanofluidic membranes with 7–50 nm nanochannels were employed to perform dynamic perfusion measurements and showed superior glucose and insulin diffusion through the membrane compared to commercially available immunoisolating membranes. These results were attributed to the physical characteristics of the nanofluidic membranes, including the elevated channel distribution density and minimal membrane thickness (5 μm). Recently, novel micro-nanochanneled silicon devices have been developed through an academic/industrial collaboration (Fine, Grattoni et al. and NanoMedical Systems, Inc., Austin, TX) with robust mechanical properties and highly selective semi-permeability to be suitable for auto- and allotransplantation of pancreatic islets (see **Figure 4**).

Besides silicon, other approaches have been developed based on aluminum oxide (alumina). La Flamme et al.[5c] assessed the biocompatibility of PEGylated nanoporous alumina membranes with host tissues. The implantation of such biocapsules in the intraperitoneal cavity of rats induced only a transient inflammatory response. These devices also showed the ability

© 2013 WILEY-VCH Verlag GmbH & Co. KGaA, Weinheim

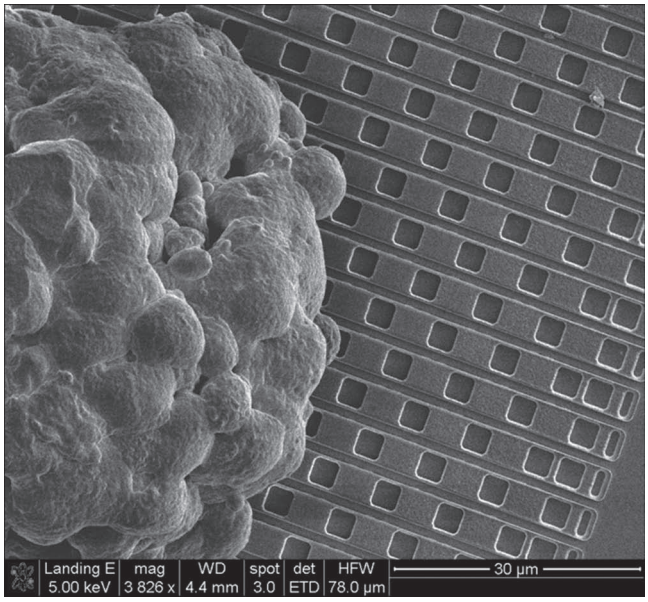

Figure 4. A scanning electron micrograph image of a human pancreatic islet on the surface of a silicon nanofluidic membrane developed by Fine, Grattoni et al. and NanoMedical Systems, Inc. (Austin, TX).

to support the viability of islets during in vitro experiments.[97] Separately, Lee et al.[98] developed a self-assembled porous alumina array for immunoisolation devices with a final pore size of 14.6 nm and coated with polyethylene oxide (PEO) in order to reduce surface protein absorption and prevent the elicitation of an immune reaction. The filter presented high permeability to nutrients, excellent mechanical stability, and the possibility for tuning geometrical parameters such as porosity, disk size, and thickness.

Other attempts were made with titanium/titanium oxide composites. TiO_2 nanotubular structures fabricated by an anodization process have been developed as controlled drug eluting coatings[24] for cardiovascular stents and implantable medical devices. Minjing et al.[99] developed a Ti supported TiO_2 membrane (600 µm thick) using a sol gel technique with tetrabutyl titanate. The membranes were characterized by quantifying the retention rate of IgG, bovine serum albumin, ovalbumin, trypsin, and glucose. The retention characteristics showed a significant dependence on the membrane sintering temperature. When sintered at 600 °C, the membranes could fully retain proteins presenting a molecular weight larger than 156 kDa, while allowing for the permeation of smaller molecules. As such, this study represents an interesting attempt that requires further developments to be applicable to islet immunoisolation.

Despite several decades of laboratory work, large human trials, and the enormous effort spent on the technological advancement of pancreatic islet immunoisolation, no immunoisolation approach has been successfully translated to the clinic. The 5 year success rate of islet transplantation is under 20% and the viability of transplanted islets still requires pharmacology-based immunosuppression. New strategies are needed to dramatically increase the viability and efficiency of the encapsulated islets. Recent studies have shown that the bone hormone osteocalcin can drive islet growth and insulin production.[100] In addition, new targets for cell transplantation have emerged with the pluripotent possibilities offered by bone marrow (mesenchymal) stem cells (MSC) that have been shown to differentiate into a variety of tissues, including cells that produce insulin.[101] A promising approach could therefore consist of encapsulating devices that could effectively house the islets or insulin-producing MSCs to shield them from the body's natural protective defenses while delivering molecules such as osteocalcin and VEGF to promote long term cellular viability and neovascularization.

3.3.2. Nanofluidic Membranes for Drug Delivery

The potential of nanofluidic membrane devices for drug delivery was demonstrated in 2004 with a different nanofluidic architecture than was reported by Chu et al. that was used to release glucose and then later interferon alpha. These devices had nanochannels that were fabricated with horizontal nanotrenches capped with anodically bonded Pyrex in a similar fashion to the previously mention 2 nm nanochannels (the 2 nm membranes were produced several years after these prototypes).[102] Despite the impressive transmembrane pressures these 1 mm thick devices could sustain (500 µm silicon substrate bonded to a 500 µm Pyrex substrate), these membranes required horizontal microchannels to interface the nanochannels to the inlet and outlet ports resulting in a low nanochannel density and thus extremely low release rates. A year later a third micromachined nanofluidic membrane prototype for drug delivery was reported that resembled more closely the original 1995 nanofilter design.[57] This prototype had sufficiently high release rates from its vertically integrated nanochannels but was mechanically weak. This weakness resulted from both process specific aspect ratio limitations of the nanochannels as well as the fundamental relationship between nanochannel length and membrane thickness. As the diffusion time through the nanochannels is the rate limiting step, the membrane needed to be thin to achieve a high rate of drug release. This inherent lack of mechanical stability necessitated a fourth design that combined short horizontally machined nanochannels with vertically integrated micro- and macrochannels.[75] These devices coupled rapid clinically relevant release rates, ~30 µg/day for interferon α-2b[41] similar to the aforementioned vertical nanochannel membranes,[57] with high mechanical robustness, as demonstrated by applied transmembrane pressures that could exceed 400 psi for the initial prototype and 600 psi for the commercial product without rupturing the membrane. High mechanical robustness is an important feature given the high osmotic pressures the membrane may be subjected to.[103] **Figure 5** shows a schematic representation and SEM micrograph of this newest membrane architecture (the process flow can be found in reference[75]). **Figure 6** demonstrates the linear release of several analytes in vitro.[75] Animal experiments to assess the in vivo long-term operation of these new nanofluidic membrane prototypes are ongoing.

3.3.3. Nanoconfinement

Classical diffusion along a concentration gradient can be analytically described by Fick's first law:

© 2013 WILEY-VCH Verlag GmbH & Co. KGaA, Weinheim

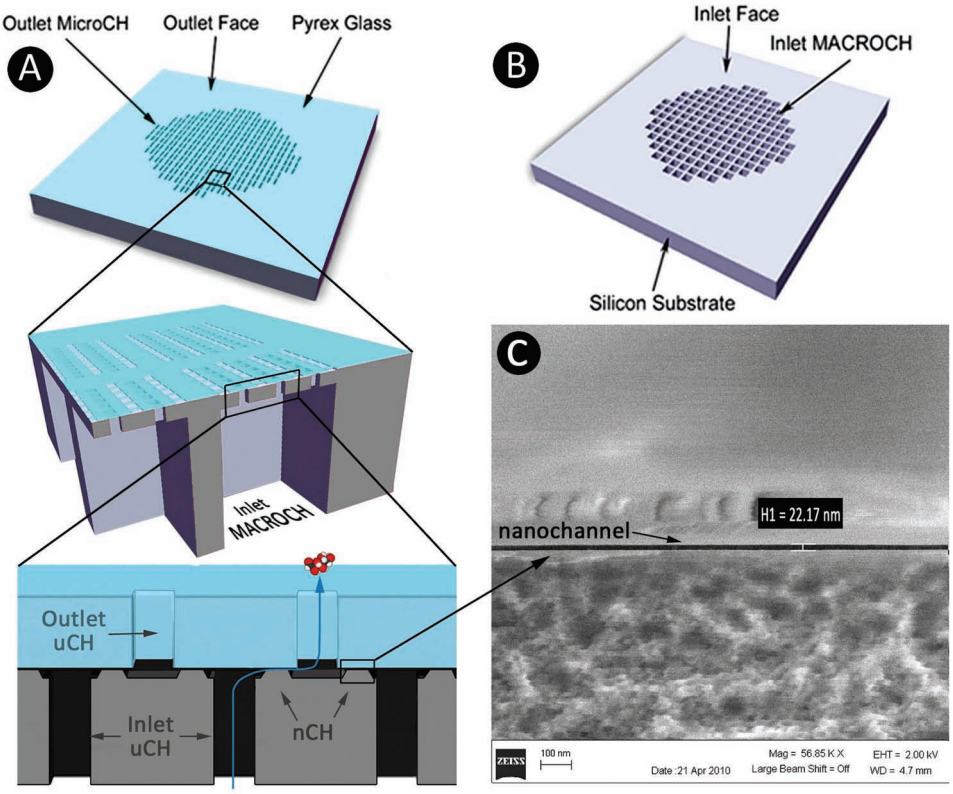

Figure 5. A,B) present schematic representations of a nanoscale delivery system (nDS) membrane. C) is a scanning electron micrograph of the nanochannel outlet of the nDS. The nanochannel was imaged by fracturing an nDS membrane using a mechanical clamp. Reproduced with permission.[75] Copyright 2010, The Royal Society of Chemistry (RSC).

$$J_A = -D_{AB}\nabla c_A \tag{3.1}$$

where J_A is the flux of solute A, D_{AB} is the diffusion coefficient of solute A in solvent B, c_A is the concentration of solute A, and the negative sign denotes flow down the gradient. From Fick's first law, a relation can be derived that describes the quantity of mass transferred across a semipermeable membrane between two closed fluid filled compartments as a function of time:

$$Q_A(t) = \left(c^0_{A1} - c^0_{A2}\right)\frac{V_1V_2}{V_1+V_2}\left(1-e^{-\lambda_A t}\right) \tag{3.2}$$

with

$$\lambda_A = \left(\frac{D_{AB}\,S}{V_1\,L}\right)\left[1+\frac{V_1}{V_2}\right]$$

where $Q_A(t)$ is the mass of drug, with diffusion coefficient D_{AB}, released from the source compartment, with starting concentration c^0_{A1} and volume V_1, to the sink compartment, with starting concentration c^0_{A2} and volume V_2, through a membrane of thickness L with a total fluidic channel cross section of S.[104]

When solutions are confined in nanoscale fluidic channels (nanochannels) with at least one size dimension on the order of the size of the diffusing analyte, however, these relations no longer hold. Due to the constriction of the available volume for diffusion from three dimensions to one or two dimensions, as well as significantly increased analyte-to-channel wall interactions, mass transport across nanochannels changes from the classical Fickian exponential decay to a saturated concentration independent zero-order behavior.[55,75,105] Membranes that incorporate nanochannels can therefore generate a constant drug release from a passive device that requires no moving or electronic components and can be incorporated into implants with a wide range of source reservoir volumes and geometries. Early efforts to describe nanoconfined diffusive transport revolved around the idea of hindered transport in which nanoconfinement resulted in an adjustment to the diffusion coefficient.[38] More recently, these models involved the hierarchical application of multiple analytical and computational methods over several length scales, including Finite Element Analysis (FEA) and Molecular Dynamics Simulations (MDS), as a result of the complexity of the molecular interactions and forces that dominate in nanochannels.[106]

3.3.4. Application Focus: Chemoprevention

Carcinogenesis, the process or processes that cause normal cells to mutate into cancer cells, requires the cellular acquisition of several important "capabilities", including evasion of apoptosis, self-sufficiency in growth signals, insensitivity to anti-growth signals, sustained angiogenesis, limitless replicative potential, and tissue invasion and metastasis (from Hanahan D, Weinberg RA. "The Hallmarks of Cancer").[107] The carcinogenic cascades that lead to these "capabilities" involve a combination of factors, including diet, environmental

© 2013 WILEY-VCH Verlag GmbH & Co. KGaA, Weinheim

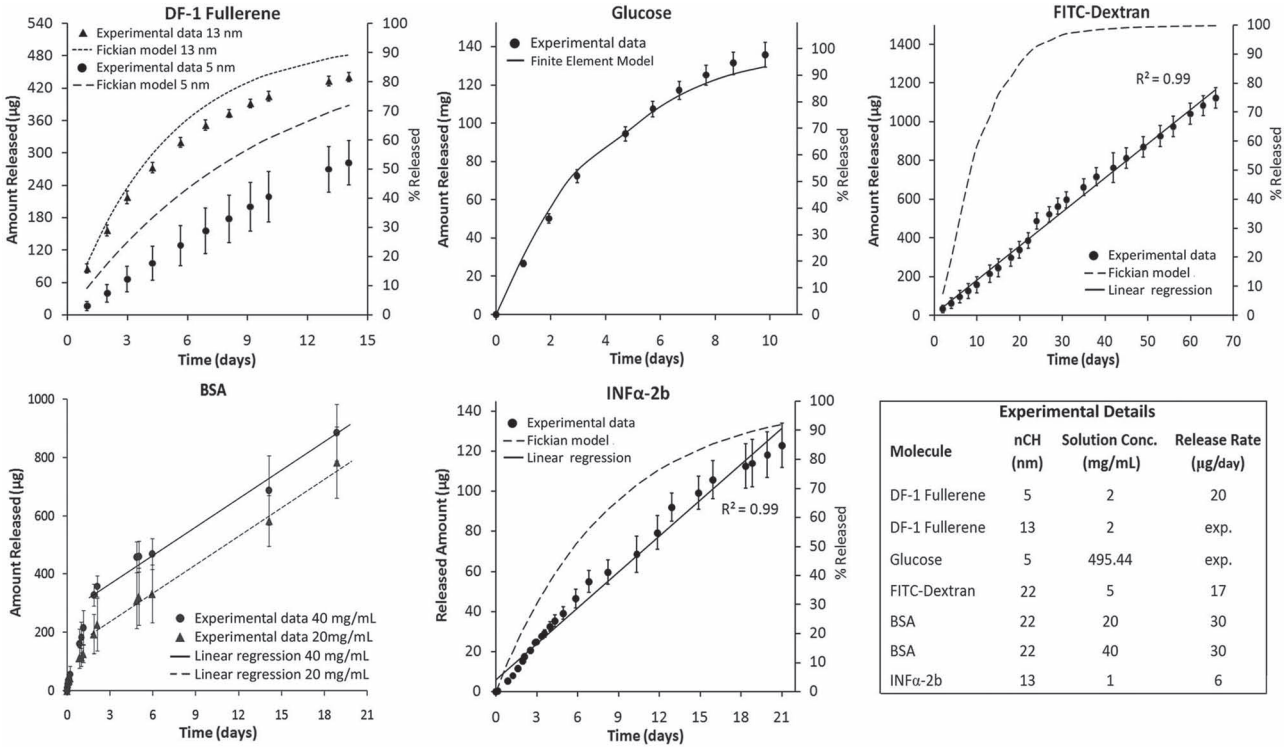

Experimental Details

Molecule	nCH (nm)	Solution Conc. (mg/mL)	Release Rate (μg/day)
DF-1 Fullerene	5	2	20
DF-1 Fullerene	13	2	exp.
Glucose	5	495.44	exp.
FITC-Dextran	22	5	17
BSA	22	20	30
BSA	22	40	30
INFα-2b	13	1	6

Figure 6. The theoretical and experimental release profiles of the 5 molecules tested using custom designed diffusion chambers. The analytical calculation for dendritic fullerene 1, fluorescein isothiocyanate conjugated dextran, and interferon a-2b are based on Fickian diffusion (see Table 2 for diffusion constants). For glucose, a numerical calculation based on three dimensional finite element analysis is presented. For bovine serum albumin (BSA), two starting source concentrations of 20 and 40 mg/mL were used which released 26.11 and 14.76%, respectively, with identical release rates (after a stabilization period). By using both starting concentrations, linear release could be demonstrated for up to 63.05% of the total amount of loaded BSA from the 40 mg/mL solution with an experimental duration of only 21 days (once the release rates were verified to be equivalent) as opposed to the 126 days that would be required given the approximate release rate of 30 mg/day. Reproduced with permission.[75] Copyright 2010, The Royal Society of Chemistry (RSC)

and occupational conditions, and genetic and epigenetic traits, that operate in conjunction and may be characterized by long symptom-free latent periods ranging from months to years.[108] Chemoprevention, a term coined by Michael Sporn over 30 years ago, refers to the inhibition, blunting, or reversal of these carcinogenic cascades by using natural or synthetic agents.[109] To be effective, these chemopreventive agents must therefore be administered slowly and continuously for extended duration or as long as the cascade initiator or propagator is present.[108] Epidemiological studies have clearly shown that long-term (years) continuous consumption of chemopreventives like turmeric (a source of curcumin) in southeast Asia, especially in India, has lead to a decreased incidence of a variety of cancers, including colon cancer.[110] However, most of these chemopreventives (curcumin, ellagic acid, quercetin) are often water insoluble and undergo rapid hepatic metabolism in the body resulting in poor bio-availability when administered orally and thus require higher doses.[108] In a series of papers, Bansal et al., showed that the continuous low-dose administration of chemopreventives like curcumin by polymeric implants not only safely provided controlled continuous release into the systemic circulation,[111] but also achieved significantly higher plasma concentrations as compared to oral doses that were 20–30 fold higher.[112] Furthermore, this method of administration proved to be more effective at altering hepatic cytochromes as compared to dietary curcumin over a 3 month period.[112] Nanochannel delivery systems (nDSs) in a chemoprevention setting can not only enable continuous administration of such agents, but can also avoid first pass hepatic metabolism by direct administration into the systemic circulation. Furthermore, due to the monodispersity and size of the nanochannels, the drug release is devoid of any burst release phenomenon and does not continuously decrease in a fashion similar to polymeric implants. nDS implants should therefore enhance bioavailability leading to drastically reduced effective doses while improving patient compliance for treatments requiring months to years of drug administration.

3.4. Electrokinetic Control of Analytes from Silicon Nanofluidic Membranes

Although one of the primary advantages of passive release nanofluidic membranes is the lack of moving and electrical components, to realize the temporal synchronization that is an important aspect of chronotherapy[113] or the self-regulation based on biofeedback vital to eventually achieving an artificial gland requires active control.[114] In the case of nanofluidic membranes, one of the more effective methods for implementing active

 © 2013 WILEY-VCH Verlag GmbH & Co. KGaA, Weinheim

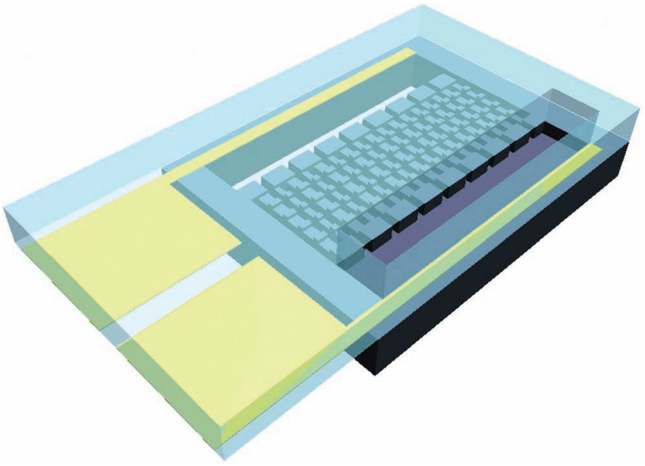

Figure 7. A schematic representation of a low-voltage electrokinetic device for drug delivery. Reproduced with permission.[117] Copyright 2011, The Royal Society of Chemistry (RSC)

control is by integrating electrodes directly on the membrane to exploit electrokinetic transport phenomena with the application of longitudinal and/or transverse electric fields.[68,74,115] Electrophoresis, the migration of charged particles under an externally applied electric field, is attractive as it does not require net fluid flow whereas electroosmosis, the net flow of the bulk fluid induced by viscous coupling to the ions migrating in the Debye layer at the fluid/nanochannel wall interface, can be used to deliver uncharged analytes.[116] Direct electrokinetic actuation of the analyte containing fluid in the nanochannels also eliminates the necessity of having a separate electroosmotic pumping chamber, but with the added restriction that solution formulations cannot be optimized for inducing efficient electroosmotic flows and the potential for biofouling is increased leading to an inability to maintain a continuous and consistent sheet of charge in the Debye layer.[48,49] Recently, Fine, Grattoni, et al. reported a low-voltage electrokinetic nanochannel membrane based on the thick anodically bonded horizontal nanochannel design described earlier.[117] This device was capable of both amplification and flow reversal of analyte delivery while consuming only 104 μWatts under an applied bias of 2 VDC. **Figure 7** shows a schematic of the device, while **Figures 8** and **9** show the amplification and flow reversal of analyte release for fluorescein isothiocyanate conjugated bovine serum albumin and lysozyme.[117]

3.4.1. Application Focus: Chronotherapy

Chronotherapy is the science of administering therapeutics in accordance with circadian variations in the human body.[118] Circadian patterns are regulated by the suprachiasmatic nuclei (SCN) within the hypothalamus[119] that maintains homeostasis by regulating the release of a range of hormones from endocrine glands in a synchronized rhythmic pattern in response to various social and environmental signals, such as ambient lighting conditions.[119] As an example: thyroid stimulating hormone (TSH), the growth hormone (GH) prolactin, melatonin, and atrial natriuretic peptide are mostly active at midnight; adreno-cortico-trophic hormone (ACTH), follicle stimulating hormone (FSH), luteinizing hormone (LH), testosterone, and cortisol are predominantly active early in the morning; and serum total proteins and triglycerides are usually synthesized around noon.[118] Recent studies have suggested a similar rhythmic trend in the precipitation of various diseases: rheumatoid arthritis,[120] stroke,[121] and pulmonary embolism[122] more often occur during the early hours of the morning; while peptic ulcers and gout are prevalent at night.[123] Therefore, drug delivery systems, including the telemetrically controlled pulsatile microchips or electrokinetically controlled nanofluidic membranes described earlier, that can be designed to release a drug at the most suitable time of the day to mimic normal physiological function, especially in hormone deficient patients, or when pathological conditions are most prevalent, allowing for maximal efficacy with minimal doses, would be highly desirable for chronotherapeutic applications.

4. Porous Silicon MultiStage Nanovectors

4.1. Nanovectors as "Magic Bullets"

In the early 1900s, Paul Ehrlich, a recipient of the Nobel Prize in Medicine, suggested an avant-garde concept: A "magic bullet" in which toxins are co-delivered with targeted agents to selectively kill disease-causing cells.[124] Since that time, advances in the understanding of various pathophysiological mechanisms have facilitated the identification of specific molecular signatures and transport differentials that can be leveraged to treat disease. From a biological perspective, the "magic bullet" was first realized with the discovery of molecularly-targeted therapeutics, including monoclonal antibodies, small interfering RNAs (siRNAs), and other disease-specific agents.

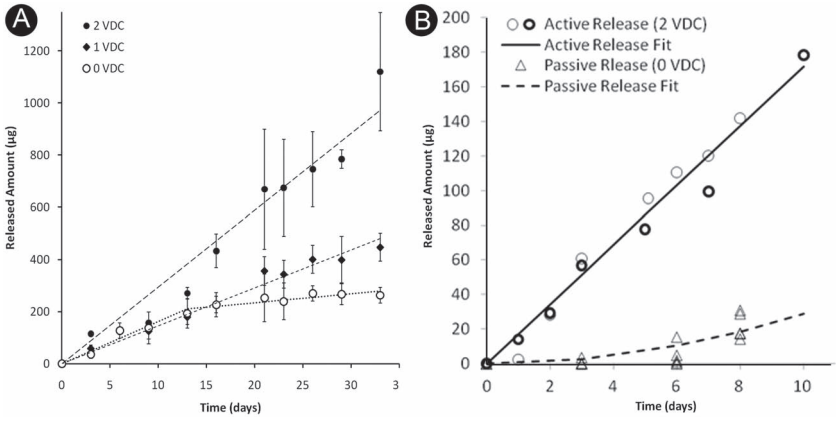

Figure 8. A) Cumulative release data of FITC–BSA. The error bars are calculated from the standard deviation of three replicates for each bias condition. B) Cumulative release data for lysozyme. Data points from two replicates are included for the active release whereas 5 replicates are included for the passive release. Reproduced with permission.[117] Copyright 2011, The Royal Society of Chemistry (RSC)

© 2013 WILEY-VCH Verlag GmbH & Co. KGaA, Weinheim

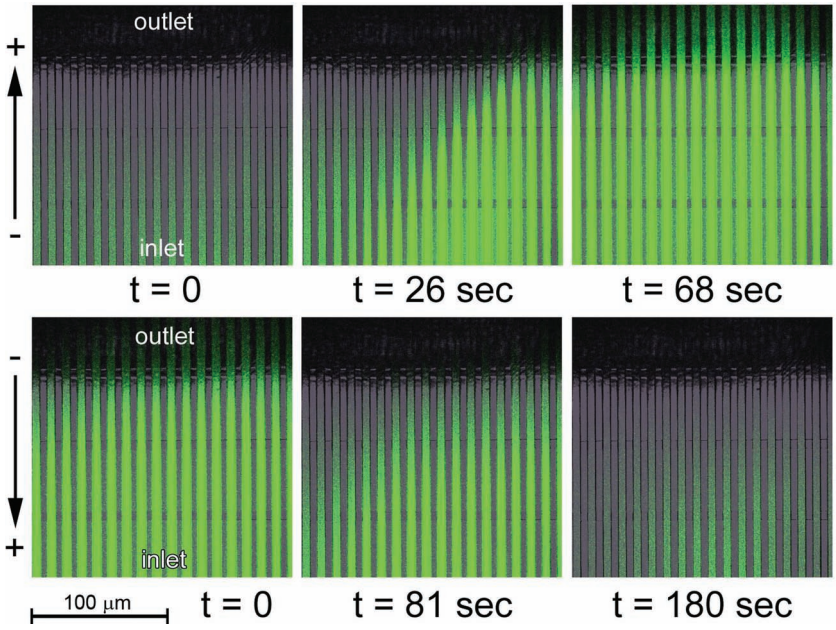

Figure 9. Fluorescent microscope images depicting FITC–BSA under both forward and reverse bias (3 VDC for both), demonstrating reversibility of the molecular transport. Reproduced with permission.[117] Copyright 2011, The Royal Society of Chemistry (RSC)

Remarkable progress has been made in finding new and efficient therapies against a variety of diseases. Dozens of molecularly targeted therapeutics have been approved by the FDA for cancer alone.[125] Many other molecules have exhibited potent therapeutic effects at the cellular and molecular level, but their clinical translation has proven challenging. This is primarily attributed to: 1) unfavorable physicochemical drug properties (e.g. the insolubility of drugs such as paclitaxel in aqueous solutions[126]), 2) instability/degradation within the blood (e.g. rapid degradation of siRNA[127]), and 3) biophysical transport barriers en route to the target tissue.[128] While the first two obstacles make certain drugs generally unacceptable for intravenous administration in "naked" form, the third obstacle, the presence of sequential biophysical barriers, prevents otherwise acceptable molecules from reaching their targets. As a result, the accumulation of therapeutic agents in disease loci is poor, with only 0.01–0.001% of administered molecules reaching their target tissue.[128b,c]

In cancer, for example, biophysical barriers to intravenous drug delivery include capture by the reticulo-endothelial system, pathological disruptions to blood flow, enzymatic degradation, endothelial impermeability, positive intratumoral pressure, cellular and subcellular membrane impermeability, and cellular efflux by molecular pumps.[128a,129] Each of these barriers needs to be overcome to enable optimal therapeutic efficacy. A logical solution is to decouple drug transport and drug activity. This idea is the driving force behind therapeutic nanovectors, which are comprised of two or more components that function synergistically to deliver cytotoxic drugs in a targeted manner.

Therapeutic nanovectors were first introduced to the field of medicine in the mid-1990s, and continue to be used primarily in oncology. Beginning with FDA approval of liposomal doxorubicin against Kaposi's sarcoma,[130] a range of nanocarrier-based drug delivery systems have reached clinical and pre-clinical stages of development. These nanovectors feature a variety of chemical compositions, physical features, and surface functionalities for fulfilling specific tasks within the body.[131] The library of particles generated to date is very large, coupled with an increasing awareness that several design considerations are critical for clinical success.

Nanovectors can be divided into three general sub-classes or generations (see **Figure 10**).[130a,c,131b,132] In this taxonomy, first-generation nanovectors act as a simple drug encapsulation mechanism. Encapsulation serves to increase drug solubility or stability within the blood, and allows drugs to accumulate within tumors through a passive mechanism called Enhanced Permeation and Retention (EPR).[133] Liposomes are the main representatives of this generation.[134] Other nanovectors in this category include polymeric particles,[135] polymer-drug conjugates,[136] polymer micelles,[137] and dendrimers.[138] Common surface modifications for 1st generation nanovectors include PEGylation[134a,139] and altering the zeta potential of the vector through chemical modification.

Second-generation nanovectors have specific modifications to the nanoparticle surface or the nanoparticle body to provide functions beyond passive drug delivery. Such nanovectors possess the ability to target their therapeutic action through molecule-specific recognition, remote activation, or responsiveness to the environment. These second-generation nanovectors have evolved through progressive enhancements of first-generation particles.[13,131c,134a,140] Common enhancements include the

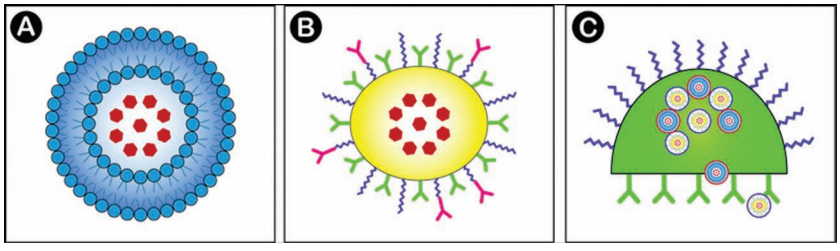

Figure 10. A) First-generation nanovectors (e.g., liposomes) comprised of a container and an active principle. They localize in the tumor by the mechanism of enhanced permeation and retention (EPR) that involves enhanced permeability of the tumor neovasculature. B) Second-generation nanovectors possess the ability to target their therapeutic action through molecule-specific recognition, remote activation, or responsiveness to the environment. C) Third-generation nanovectors (e.g. multi-stage vehicles) are capable of more complex functions, such as time-dependent deployment of multiple waves of active nanoparticles across different biological barriers and different subcellular targets. Reproduced with permission.[130]

© 2013 WILEY-VCH Verlag GmbH & Co. KGaA, Weinheim

addition of antibodies, receptor ligands, aptamers, small peptides, and phage-display peptides for molecule-specific targeting.[9a,141] It is important to note that there are currently no such nanovectors approved for clinical use.

It is unlikely that a single material or particle will be able to overcome all of the biophysical barriers mentioned above. For this reason, third-generation nanovectors have been proposed (see Figure 10C). These multi-compartmental constructs are comprised of multiple nanovectors, each of which plays a discrete task when injected into the body. Ferrari et al. provided the first successful demonstration of Multi-Stage Vectors (MSVs),[142] a construct that provides one of the predominant emblematic representations of this category. These vectors are comprised of porous silicon particles (1st stage) that are loaded with therapeutic or diagnostic nanoparticles (2nd stage). Their rational design, fabrication, biocompatibility, and application are discussed in further detail below.

4.2. Rationally Designed MSVs

MSVs are engineered to have multiple, discrete components that act in a synergistic and time-sensitive manner.[142,143] Each component (or stage) has a specific sequential function in vivo. A major strength of the MSV approach is that the size, shape, and surface properties of the 1st stage carrier vectors may be modulated independently of their therapeutic cargo in order to improve their ability to reach the disease site and locally deliver drugs. With simple changes to their physicochemical and biophysical properties, the 1st stage vector may be programmed to have specific functions, such as a long circulation time,[9b] tailored intravascular margination behavior,[144] and controlled loading of cargo, including nanoparticles, bioactive molecules, imaging agents, and combinations thereof.[142] By appropriately functionalizing the vector surface, particles can be programmed for cell uptake[10,11,145] and intracellular drug release.[12] Such first-stage vectors are rationally designed through the use of mathematical models that are calibrated and validated using quantitative in vitro and in vivo experiments.

The majority of the published work on nanovectors focuses on spherical particles, which are the most common product of thermodynamically-driven biomaterial self-assembly. Examples include liposomes, polymeric micelles, polymeric nanoparticles, and metallic nanoparticles. Recent evidence has shown, however, that nanovector geometry is an important design consideration that impacts vector behavior at the scale of cells, tissues, and organs. Nanovector geometry has been predicted to affect vector transport, cell-particle interactions, endocytosis and phagocytosis, and vesiculation.[131b,146] These findings have been reported for a variety of nanovector materials, including polymeric particles,[147] carbon and metal-based particles,[148] and silicon particles.[10,11,145,149]

4.2.1. Intracellular Uptake of MSVs

Several mathematical models and design maps were proposed to explain the effect of nanovector geometry on intracellular uptake. The rate of intracellular uptake can be described through a first-order kinetic law where the intracellular concentration, $C_i(t)$, increases with time according to the following relationship:

$$\frac{d\tilde{C}_i(t)}{dt} = k_{int}\left[\chi - \tilde{C}_i(t)\right] \quad (4.1)$$

where τ_w is the wrapping time of the nanovector by the cell membrane and is related to the nanovector geometry (size, shape) and surface chemistry (zeta potential, specific ligands). Modeling of receptor-mediated internalization based on energetics has shown that there is a minimal threshold for the particle radius to enable intracellular uptake. Below this threshold, intracellular uptake becomes energetically unfavorable. Similarly, if the particle radius is too large, the particle is only partially wrapped and fails to internalize.[146b,146e] This phenomenon favors the uptake of non-spherical particles comprised of a long and short axis. The overall rate of internalization is dependent on the particle volume and aspect ratio.[146d,146e]

4.2.2. Biodistribution of MSVs

Modulating physical MSV properties to increase or decrease cellular uptake also impacts their overall biodistribution following injection. Particles of different shapes and sizes preferentially accumulate in specific organs.[150] This behavior is likely due, at least in part, to the ability of non-spherical particles to marginate under laminar flow conditions. This lateral drift serves to increase the probability of particles contacting the vascular walls, which in turn increases their probability of adhesion.[144] For the case of *plateloid* vectors, both in vitro and in vivo experiments support a role for local blood flow conditions in determining what sizes of particle will best adhere to the endothelium.[150b]

Intravital microscopy studies have revealed that MSV geometry plays a fundamental role in the ability of particles to reach and accumulate within tumors. Tumor-bearing mice injected with rationally designed particles show a preferential accumulation of plateloid-shaped particles.[150b] Interestingly, 1000 × 400 nm plateloid particles are favored over larger and smaller plateloid particles of similar aspect ratio (see **Figure 11**). The ability of these particles to accumulate in tumors increases when molecular-specific targeting moieties are added to the particle surface, with the smallest particles showing the greatest increase. These MSVs appear to primarily line the walls of the tumor vasculature, rather than extravasating into the tumor interstitium. Mathematical modeling of these behaviors suggests that blood shear rates determine the preferential particle diameter, while cell-particle interactions (influenced by number and affinity of receptors on the endothelial surface) determine the number of particles that adhere.[150b]

Taken together, these studies suggest that MSV geometry must be considered at multiple biological scales. The development of powerful new tools including intravital microscopy can allow us to track individual particles as they undergo a variety of dynamic events.[150b] Such quantitative data may be used to calibrate and validate mathematical models.[151] Future advances in comprehensive multi-scale design maps, which consider MSV transport, cell-specific recognition, adhesion, and uptake under a variety of physiological/biophysical conditions, will allow us to better identify the key design parameters for specific applications.

© 2013 WILEY-VCH Verlag GmbH & Co. KGaA, Weinheim

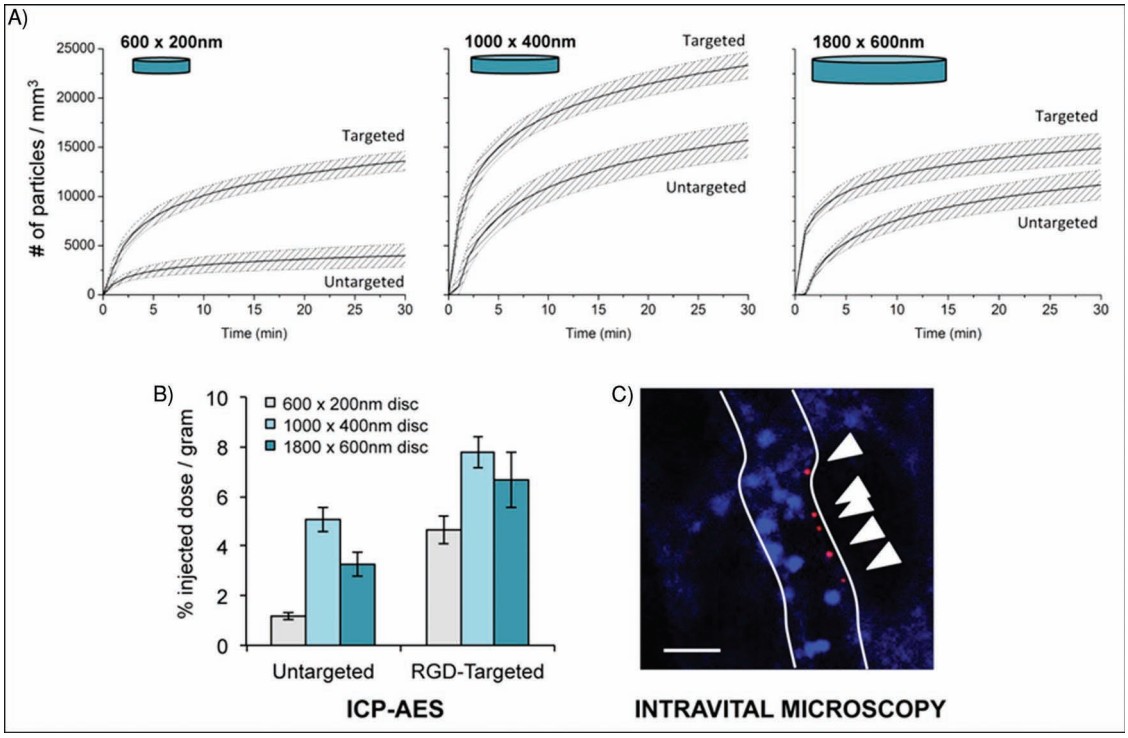

Figure 11. Preferential accumulation of plateloid MSVs in melanoma tumors. A) Time-dependent accumulation of 600 × 200 nm, 1000 × 400 nm, and 1800 × 600 nm plateloid particles targeted with and without an RGD-4C peptide, as measured using intravital microscopy. B) Independent validation of particle accumulation trends using inductively coupled plasma–atomic emission spectroscopy (ICP-AES). Cumulative particle uptake is expressed as the percentage of the injected dose normalized by the mass. C) Stills extracted from the intravital microscopy videos reveal that micron-size MSVs, such as the 1000 × 400 nm particles shown here, predominantly accumulate within the tumor vasculature. (scale bar, 25 µm). Adapted with permission.[150] Copyright 2010, Elsevier.

4.3. Porous Silicon as a Material for MSV Fabrication

The MSV concept requires that 1st stage particles provide an extensive surface area for nesting 2nd stage nanometer-sized particles such as liposomes, micelles, carbon nanotubes, and other organic or inorganic nanoparticles.[142] Porous silicon was selected for the fabrication of 1st stage carrier particles due to the features summarized in **Figure 12**. This material has been explored for numerous biomedical applications based on its readily modifiable physicochemical and biophysical properties.[8c,152] Its biodegradable nature, coupled with the availability of sophisticated tools and processes available from the silicon semiconductor industry, makes porous silicon an ideal material for synthesizing injectable MSVs.

Precise control over 1st stage particle size, shape, surface, loading, and release properties, enabled by top-down fabrication approaches and electrochemical etching, is required for clinical translation.[153] In general, the fabrication protocols consist of two steps: formation of a nanoporous silicon film followed by photolithographic patterning of the particles within the film. By altering the order of this process flow, both hemispherical and discoidal porous silicon particles can be fabricated. The geometry of the porous silicon particles is precisely defined by changing the photolithographic mask while the porosity, pore size, and pore morphology are controlled by parameters including silicon doping, electric current, and concentration of hydrofluoric acid

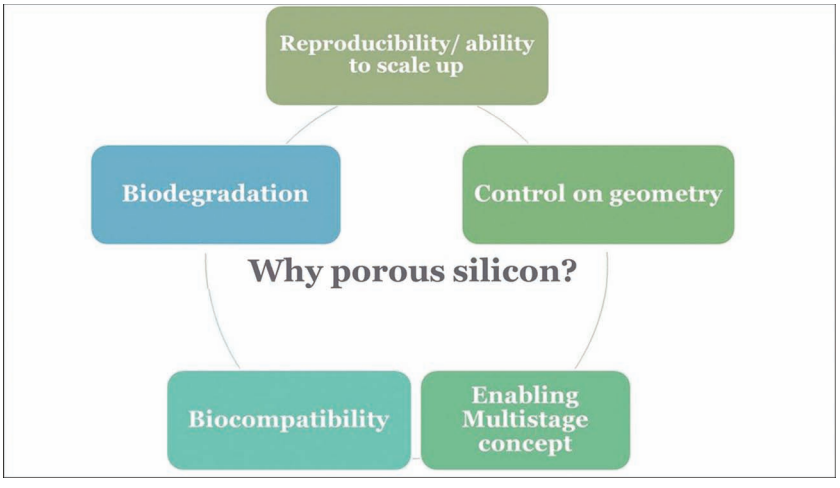

Figure 12. The reasons behind the choice of porous silicon for MSV fabrication.

© 2013 WILEY-VCH Verlag GmbH & Co. KGaA, Weinheim

(HF) solutions. Multiple protocols were developed by Liu and colleagues, allowing the fabrication of particles in a variety of shapes and sizes, with external dimensions ranging from 100 nm to hundreds of microns, and pore diameters in the range of 5–150 nm. **Figure 13** highlights some examples.

The fabrication protocol for the hemispherical particles was detailed by Chiappini et al.[153b] A silicon wafer is coated with a dielectric film (silicon nitride) followed by photolithographic patterning of an array of circles with an appropriate diameter and pitch. The circle pattern is then transferred into the dielectric layer using a Reactive Ion Etch (RIE). A second RIE into the silicon defines the trenches that nucleate the particles with different topological profiles. Subsequently, a 2-step electrochemical etch process forms the particles with desired porosity, pore size, and thickness. The contour of the lateral electrochemical etch undercut is determined by the current distribution and follows the profile of the pre-etched trench. The depth of the trenches determines the hemispherical particle aspect ratio. A highly porous release layer is then formed that is strong enough to retain the particles on the substrate, allowing for extensive washing to eliminate residues from processing solutions such as HF, but fragile enough to be broken by sonication to release intact particles into isopropyl alcohol.

The protocol for the fabrication of the discoidal particles involves first preparing a porous silicon film and then photolithographically patterning it.[154] Full wafer porosification eliminates potentially distorting effects introduced by non-uniform current distribution during the electrochemical etch while still allowing for independent control over the porous structure (porosity and pore size). A major technical hurdle had to be overcome, however, in order to perform direct patterning of pSi: photoresist adsorbed within the pores creates non-uniformities in the photolithographic micropatterns that disrupt the subsequent RIE. A novel sealing strategy was adapted using Low Pressure Chemical Vapor Deposition (LPCVD) of Low Temperature Oxide (LTO). After the electrochemical etch of the double layered porous silicon films (particle and release layers), the porous films are sealed by LTO, and an array of circles is patterned on top of the LTO film. A CF_4 RIE is then performed to etch through both the LTO and the two porous silicon layers. The particles are then washed and released in a similar fashion using sonication.

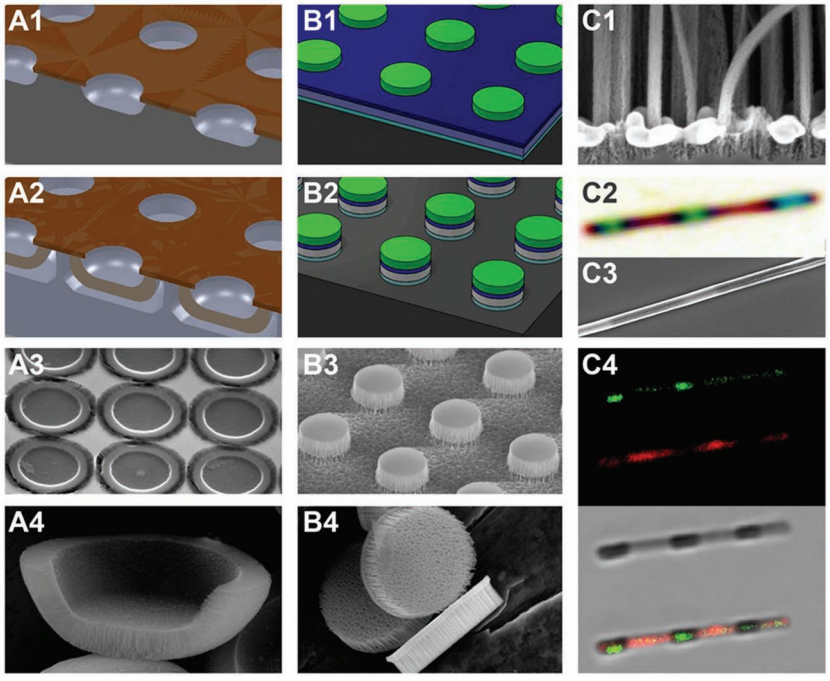

Figure 13. Fabrication of 1st stage particles: A1: Patterned silicon nitride (SiN) layer and trenches etched into silicon. A2: Electrochemically etched particles with release layer. A3: A scanning electron micrograph of an example hemispherical particle array on a wafer after removal of SiN. A4: A scanning electron micrograph of a cross-section of a hemispherical 1st stage vector (ranging from 900 to 3200 nm in diameter). B1: Photoresist pattern on LTO capped porous silicon film with release layer. B2: Particle array on wafer after RIE. B3: A scanning electron micrograph of an example plateloid S1MP array on a wafer after Low Temperature Oxide (LTO) removal. B4: A scanning electron micrograph of a released plateloid S1MPs (ranging from 400 to 1000 nm in diameter). C1: A scanning electron micrograph of a silver nanopattern etched into silicon forming porous silicon nanowires. C2: Nanowire barcode under white light. C3: A scanning electron micrograph of a nanowire barcode. C4: 3-channel confocal micrographs of a nanowire barcode with green Q-dots loaded in the small pore segment and red Q-dots in the larger pore segment. Adapted with permission.[143] Copyright 2011, The American Chemical Society.

4.4. In vitro and in vivo Experiments with MSVs

MSVs are being developed for a variety of applications, including therapeutic, diagnostic, and pre-clinical imaging applications. As part of the optimization process, studies have looked at cell-particle interactions, drug loading and therapeutic efficacy, MSV targeting through both passive and active means, and the diagnostic characteristics of porous silicon particle 1st stage carriers. Highlights of these studies are described in further detail below.

In vitro studies were performed to understand the mode of silicon particle interaction with macrophages and endothelial cells. Particle internalization involves actin-dependent mechanisms, including phagocytosis (engulfment of particles with pseudopodia-like extensions) and macropinocytosis (membrane ruffle formation). The kinetics of internalization are dependent on cell type. The $t_{1/2}$ of internalization was calculated to be around 16 min for endothelial cells.[149] Macrophages engulf particles even more rapidly,[155] with $t_{1/2}$ decreasing as particle size is decreased.[156] Surface modification of the particles results in differential uptake by the cells. Silicon particles with negative and positive surface charge are internalized by both macrophages and endothelial cells; however, positive particles are preferred by endothelial cells.[10] PEGylation of the particles greatly inhibits the internalization process (see **Figure 14**).[145a]

© 2013 WILEY-VCH Verlag GmbH & Co. KGaA, Weinheim

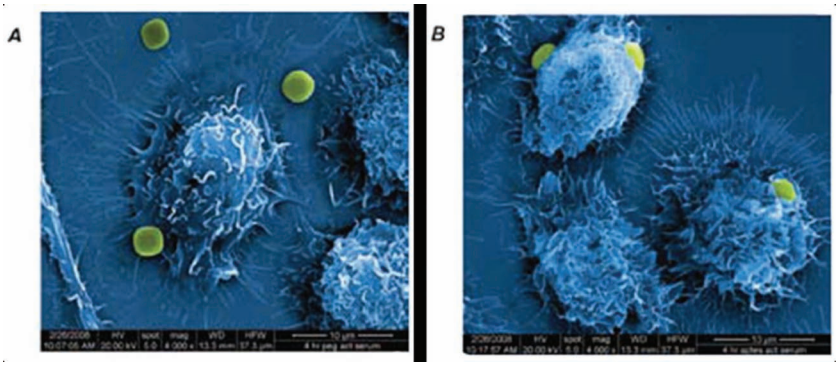

Figure 14. Scanning Electron Micrographs of J744 mouse macrophages incubated with (A) PEGylated (5000MW PEG) and (B) positively charged porous silicon particles. Reproduced with permission.[ab] Copyright 2008, The Controlled Release Society.

Internalized porous silicon particles are trapped within endosomes; however, their cargo may be programmed to perform specific tasks within or between cells. For example, amine-modified Super Paramagnetic Iron Oxide Nanoparticles (SPIONs) released from internalized 1st stage carriers undergo endosomal sorting into multivesicular bodies (MVBs) and are secreted from the cell.[11,157] There is great interest in using such MVBs as a means for cell-to-cell communication. Conversely, chitosan-coated SPIONs released from internalized carriers are capable of escaping the endosomes.[11,158] Interestingly, this phenomenon is not observed for freely internalized chitosan-coated particles, suggesting that the 1st stage nanovector can provide a "protective" effect for maintaining the bioactivity of the 2nd stage nanovectors. The intracellular partitioning of such 2nd stage nanovectors may be leveraged to selectively deliver agents to specific cellular organelles or to participate in the cross-talk between cells and the microenvironment.

The protective effect of the MSV strategy is best appreciated in vivo, where a single i.v. administration of siRNA-loaded liposomes encapsulated in 1st stage carriers showed sustained silencing of the EphA2 gene for up to 3 weeks in orthotopic ovarian cancer models.[12] This treatment also decreased tumor burden, angiogenesis, and cell proliferation when compared to non-coding control and naked siRNA-loaded liposomes (both of which are administered twice a week with an overall 2-times higher dose) (see **Figure 15**). One of the main hurdles in siRNA therapy to date is the inability to deliver siRNA to specific cells of interest while maintaining its bioactivity.[127]

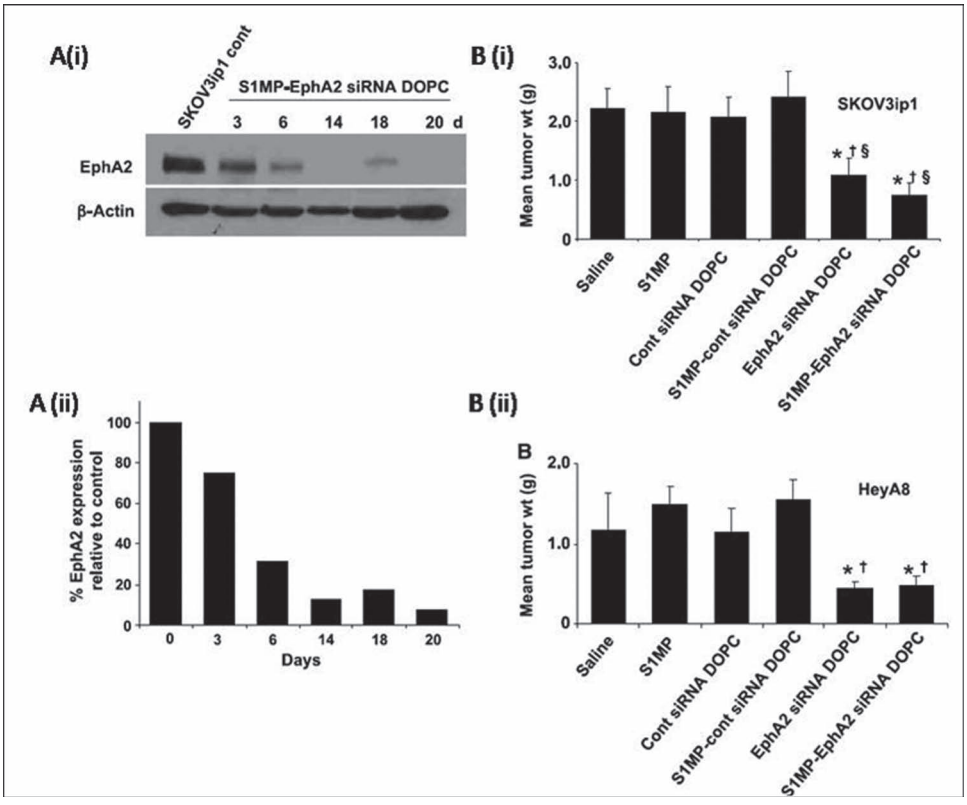

Figure 15. Nude mice bearing SKOV3ip1 ovarian tumors were randomly allocated to one of six treatment groups: saline, 1st stage silicon particles (S1MP), nonsilencing control containing siRNA loaded in DOPC liposomes (cont-siRNA-DOPC), S1MP-nonsilencing control-siRNA-DOPC, EphA2-siRNA-DOPC, or S1MP-EphA2-siRNA-DOPC. A) Evidence of in vivo gene silencing as measured by western blot (i) and desimetric analysis (ii). B) Therapeutic efficacy of sustained EphA2-siRNA-DOPC delivery by S1MP shown as reduction of SKOV3ip1 (i) and HeyA8 (ii) tumor burden. Adapted with permission.[12] Copyright 2010, The American Association of Cancer Research.

© 2013 WILEY-VCH Verlag GmbH & Co. KGaA, Weinheim

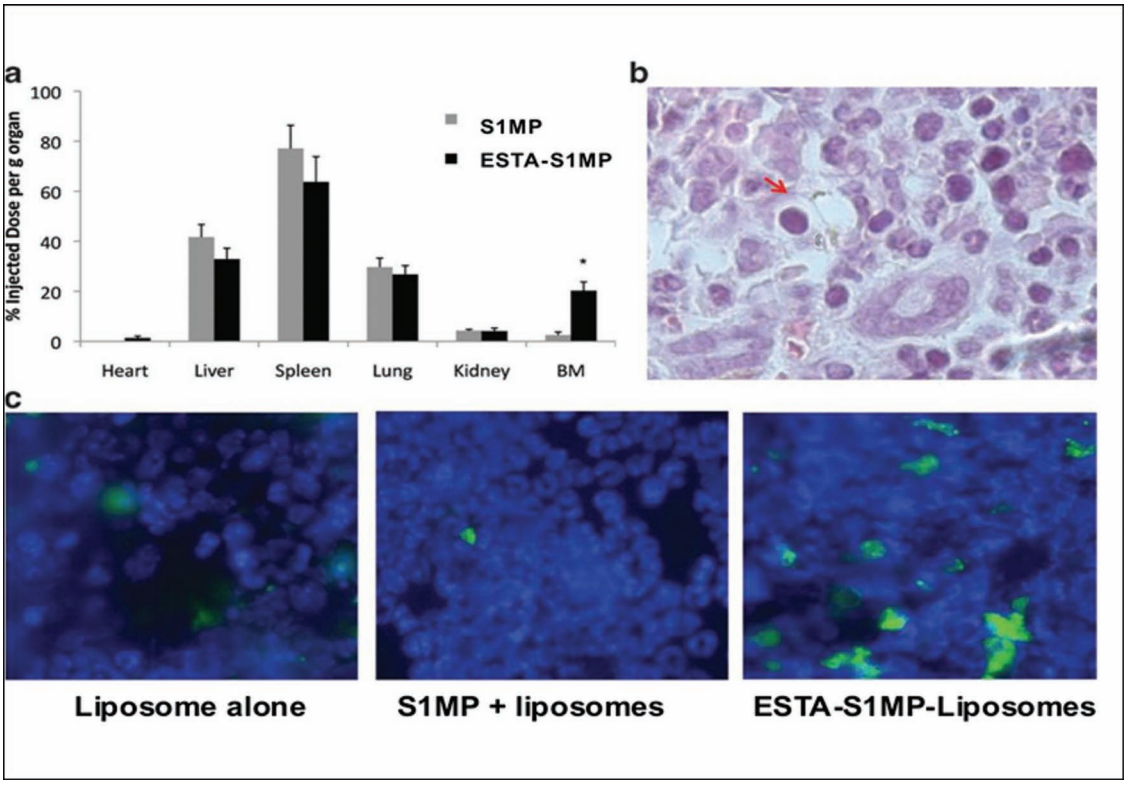

Figure 16. a) Silicon content analysis by ICP-AES for the evaluation of the biodistribution of E-selectin-thioaptamer 1st stage particles (ESTA-S1MP)* $P < 0.05$. b) ESTA–S1MP localization in the bone marrow visualized in a decalcified, paraffi n-embedded section. c) Fluorescence microscopy images to analyze accumulation of Paclitaxel-loaded liposomes in bone marrow tissue after i.v. administration in ESTA-S1MP. Green: Oregon green encapsulated liposomes; blue: Hoechst 33342. Adapted with permission.[160]

Systemically administered MSVs may be a promising solution, since they appear to preserve siRNA bioactivity from enzymatic degradation for a prolonged period of time.

MSVs have also successfully been demonstrated for in vivo applications requiring molecular-specific targeting. E-selectin, also referred to as a "vascular" selectin, is an inducible molecule expressed on activated endothelium, as well as constitutively expressed on bone marrow and dermal microvasculature.[159] To evaluate the possibility of targeting the bone marrow, thioaptamers targeting E-selectin (ESTA) were conjugated onto first-stage carriers and tested in vivo. Accumulation of up to 20% of injected MSVs per gram bone marrow was observed. When liposomes containing paclitaxel were loaded inside E-selectin targeted MSVs (see **Figure 16**), a 200 fold higher concentration of targeted liposomes was delivered to the bone marrow as compared to untargeted liposomes.[160] This work opens up the possibility of delivering chemotherapeutics to the bone marrow, a common niche for metastases of multiple cancer types.

In parallel with these therapeutic applications, MSVs are being developed as imaging contrast agents for diagnostic applications. 1st stage porous silicon particles are readily loaded with a variety of SPION formulations[158] and are being investigated as potential MRI contrast agents. The packaging of gadolium-based contrast agents into porous silicon particles also offers superior MRI images.[161] Particles loaded with gadonanotubes, for example, exhibit 50 times larger relaxivity values as compared to clinically available gadolinium-based contrast agents. This phenomenon is thought to be attributed to the geometrical confinement of the gadonanotubes and their organization within the pores. Similarly, silicon particles loaded with gold nanoshells show enhanced heating over free nanoshells when irradiated with a near infrared (NIR) laser, likely due to surface polaron interactions between the tightly packed nanoshells.[162]

Fluorescent tagging of the 1st stage particles with NIR dyes enables monitoring of MSV biodistribution in vivo using optical imaging[9c] (see **Figure 17**). Higher resolution techniques, such as quantitative real-time intravital microscopy, allow individual particle dynamics to be tracked as they flow through the vasculature, associate with cells, and accumulate in different organs (see **Figure 18**).[151,156] Using this approach, the effect of modulating particle size and shape on the number as well as the rate at which particles accumulate in different organs has been demonstrated. What is particularly exciting about intravital microscopy is that the role of each MSV component can be studied sequentially with sub-cellular resolution. This has the potential to provide fundamental insights into mechanisms that regulate nanotherapeutic delivery, uptake, and treatment response.

Taken together, these studies indicate that the MSV concept is truly starting to be realized. A flexible biocompatible material now exists that can be synthesized with a variety of physical

© 2013 WILEY-VCH Verlag GmbH & Co. KGaA, Weinheim

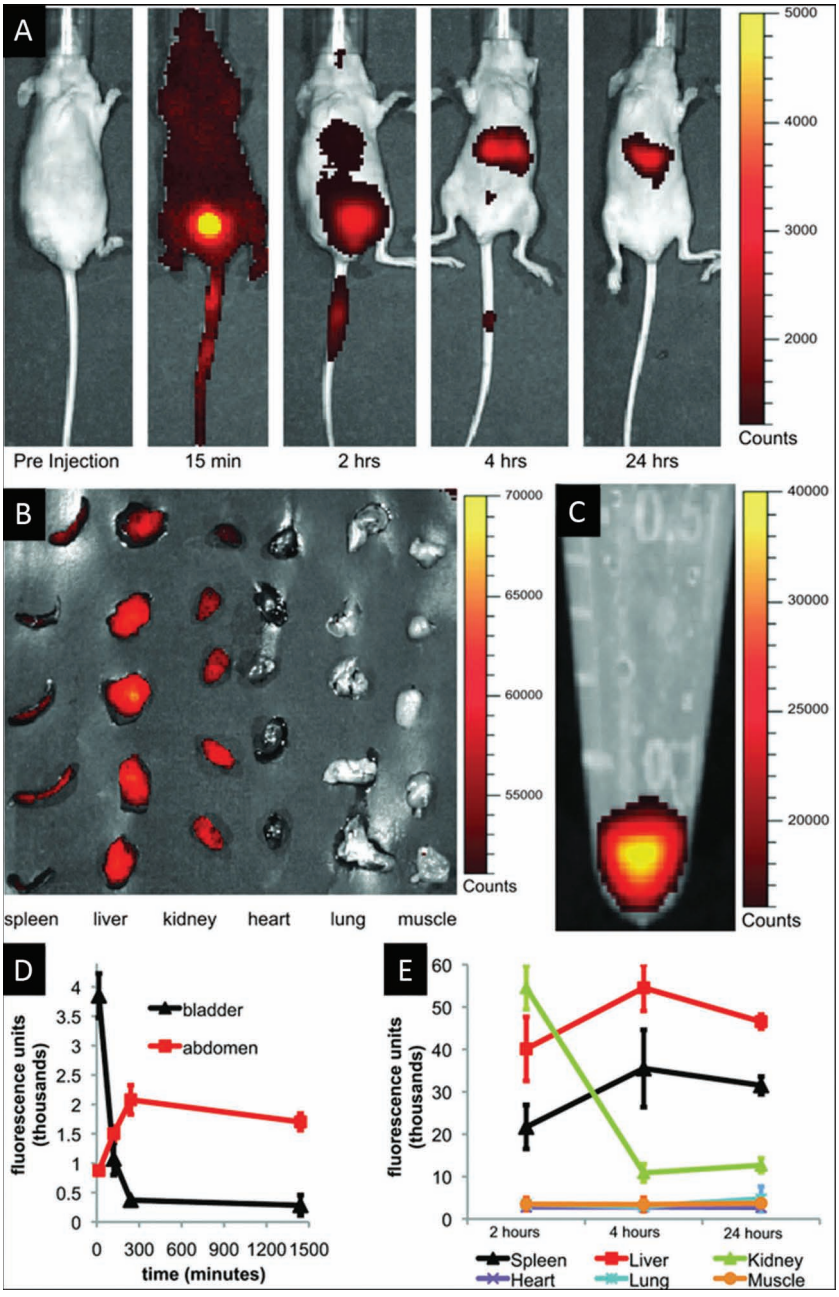

Figure 17. In vivo NIR imaging following intravenous administration of S1MPs tagged with Dylight 750. A) Representative pictures of mice injected with S1MPs and followed for 24 hours in a whole-animal imaging study (n = 5). B) Organs collected after sacrificing the animal for ICP-AES analysis (time point 2 hours). C) A NIR image of the vial containing the suspension of particles injected in each animal. D) Quantification of the fluorescence in the abdomen (spleen, liver, and kidneys) and in the bladder. E) Postmortem evaluation of the accumulation of the fluorescence signal in the different organs and tissues. Adapted with permission[9c] Copyright 2011, Decker Publishing, Inc.

features, loaded with therapeutic or diagnostic cargos, and functionalized to have specific targeting and release kinetics. The multi-component nature of the MSVs provides unique functionalities such as the protection of sensitive cargos and the ability to target specific cells. In the future, it is likely that these MSVs will find use as both clinical agents and pre-clinical tools for the study of diseases requiring innovative solutions for biobarrier avoidance.

5. Silicon and Porous Silicon Nanowires

5.1. Silicon Nanowires (SiNWs): Investigating Fundamental Intracellular and Intercellular Properties and Interactions

Nanowires have previously been demonstrated to aid in the investigation of biological interactions when employed as a controlled system for mimicking the structural and functional properties of biological filamentous nanostructures. Silicon nanowires (SiNWs) in particular have been employed as a f-actin mimics to study the behavior of the myosin motor protein, showing that in one-dimensional confinement myosin possess a ballistic motion behavior not seen with two-dimesional confinement.[163] When structured to replicate the arrangement of the extracellular matrix, SiNWs can provide insightful information on the optimal architecture to guide cell proliferation, morphology and localization.[164] The one-dimensional nature of nanowires also allow for interfacing them with cells, gaining access to the intracellular compartment with minimal disruption to cellular processes thus providing significant advantages for the development of nanodelivery systems and diagnostic nanoprobes.[165] The high aspect ratio of nanowires and nanotubes mimic that of naturally occurring filamentous phages and act as Trojan horses to induce cellular uptake, even for an overall size much larger than that allowed for spherical objects.[166] In the so-called spearing strategy, colloidal suspensions of nanowires and nanotubes can be introduced within cells bypassing the endolysosomal system to deliver biolabile molecules directly to the site of action, enhancing both bioavailability and bioactivity.[167]

AFM manipulated SiNW can deliver nucleic acids within a large variety of cells, with lower cytotoxicity and higher efficiency than conventional physical access approaches such as electroporation and patch clamping.[168] As a further, higher throughput step, cells can be grown over arrays of vertically aligned nanowires, which can deliver a large variety of bioactive molecules without disrupting their proliferation.[165a] Interfacing nanowire electrodes within the cytosol of excitable cells is a minimally invasive tool to study triggering and

© 2013 WILEY-VCH Verlag GmbH & Co. KGaA, Weinheim

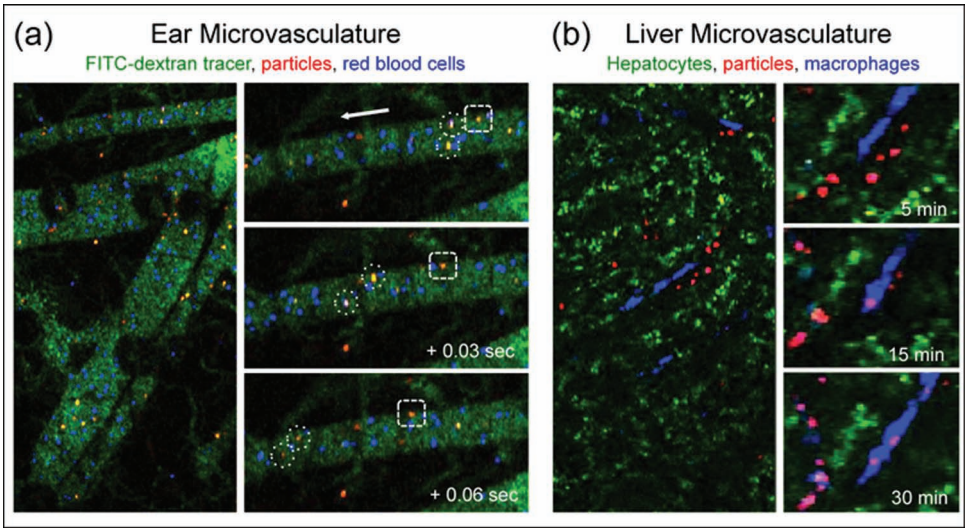

Figure 18. a) Dynamics of individual 1000 × 400 nm plateloid silicon particles (shown in red) imaged noninvasively in the microvasculature of the mouse ear. The circles and boxes distinguish particles flowing at different rates. b) Time-dependent uptake of porous silicon particles by macrophages residing in the liver of a wild-type mouse, as measured from the time of injection. Adapted with permission.[151] Copyright 2012, the American Institute of Physics.

propagation of action potentials in multiple cells simultaneously, providing a viable strategy for neuronal network mapping and sustained monitoring of the activity of multiple cardiomyocytes.[169]

The cytocompatibility and the versatility of SiNW, due to their ease and variety of synthetic methods, large availability, high reproducibility, facile bioconjugation, direct electronics integration, and advanced micro- and nanofabrication toolset, has made SiNW the nanowire of choice for most of these fundamental and applied investigations. As silicon nanowire-based biomaterial technologies gain further traction and more momentum builds towards developing new strategies that optimize their biological interactions, the performance of SiNWs is set to improve as well as cement and expand their current relevance in the biomedical field.

5.2. Synthesis of SiNWs

Most traditional top-down approaches result in the formation of either nanowires or nanopillars (depending on orientation) and usually involve lithographic patterning of the desired structures, followed by a series of etching procedures. Top-down approaches grant fine control over the geometry, density and arrangement of nanowires. These approaches allow for facile synthesis of nanowires with specified length and controlled geometry that can be varied along their axes, but are challenged when forming large arrays of nanopillars with constant diameter.[170] Among bottom-up strategies, vapor-liquid-solid (VLS) interface synthesis is by far the most common. In this approach a vapor phase silicon precursor is absorbed into and supersaturates a nanoparticle catalyst deposited on a surface, inducing crystal growth at the nanoparticle-surface interface.[171] The size of the nanoparticle determines the diameter of the nanowire, with the possibility of controling its electronic properties by introducing silicon dopants in the gas phase.[172] Several variants of this synthetic technique exist, exploiting laser ablation,[173] plasma ions,[174] and liquid phase[175] and molecular beam epitaxy[176] to enhance the specificity and quality of the produced nanowires. This approach grants limited control over the direction of the nanowire growth and their axial geometry, along with an inability to determine their arrangement or density unless assisted by an independent top-down or bottom-up patterning technique.[177] As such, a combination of top-down and bottom-up fabrication methods are typically used to great effect.

5.3. Porous Silicon Nanowires (pNWs): Possibilities for Extending Nanowire Applicability to Diagnosis and Drug Delivery

Porous silicon nanowires (pNWs) are poised to combine the biomedical relevance of silicon nanowires with that derived from porous silicon to develop emergent properties unique to these one-dimensional high surface area photonic nanocrystals. pNWs delivered or interfaced to cells or introduced in biological media can controllably biodegrade into harmless orthosilicic acid, differently from their solid nanowire counterparts.[153a] As such, pNWs are advantageous for a wide range of applications where disposing or removing the nanowires once they have exhausted their function is impractical. Furthermore, pNWs inherit the photonic properties of porous silicon, showing a porosity dependent reflectance and photoemission spectrum that can be synergistically leveraged alongside the pNW's biodegradability to develop intracellular barcode nanowire reporters (see **Figure 19**). The photonic crystal structure of pNWs, analogously to what is routinely done with porous silicon layers, can be integrated into biosensing applications that employ a change in optical thickness observed upon a

© 2013 WILEY-VCH Verlag GmbH & Co. KGaA, Weinheim

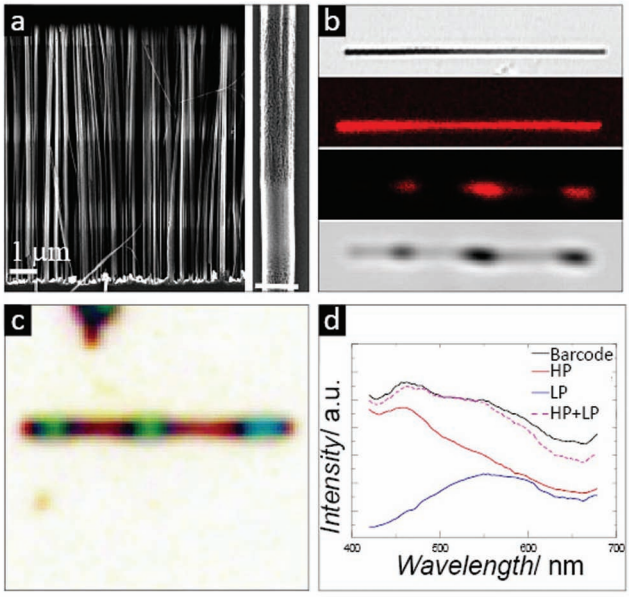

Figure 19. Porous silicon nanobarcodes. By controlling the porosity along the nanowire axis, segments with different photonic properties are generated, which can be detected by reflection, transmission and fluorescence microscopy. (a) SEM micrograph of porous silicon nanobarcodes showing multiple segments with different porosity. (b) Fluorescence, at 500 nm (red), and bright field (greyscale) confocal microscopy images of a single segment nanobarcode (top) and a six segment, dual color nanobarcode (bottom). (c) Reflectance microscopy image of the same two-color six segment nanobarcode. (d) Comparison of the fluorescence emission spectrum of high porosity nanowires (HP), low porosity nanowires (LP), and nanobarcodes composed of high-porosity and low-porosity segments. The spectrum associated with the nanobarcodes matches well with the superposition of the HP and LP spectra. Adapted with permission.[153a]

biorecognition event as a reporter.[178] By forming pNWs with variable porosity along their axis, it is possible to encode a unique tag within the wire that can be recognized at a later stage during biological interactions.

The porous matrix of pNWs allows for efficient loading and sustained release of different classes of biomolecules and nanoparticles,[142,145b,152d] as well as pH operated nanovalves that can cap the pore openings and trigger environmentally responsive release.[179] Control over the porosity of the nanowires determines their mechanical properties and can be optimized for interfacing in cell culture.[180] pNWs can also be structured into large vertical arrays similarly to SiNWs.[181] As pNWs possess superior drug delivery versatility and are biodegradable, they could provide a better platform for localized intracellular delivery of bioactive agents intracellularly, and perhaps ultimately, intravitally.

5.4. Synthesis of pNWs

Metal assisted chemical etch (MACE) is a recently developed hybrid approach which allows the formation of vertical sidewalls to generate nanowires with aspect ratios in excess of 1000.[153a,181,182] In MACE, anisotropic etching of Si in the <100> direction is mediated by noble metal layers deposited on the silicon surface.[183] As the Si is etched directly underneath the metal nanoparticles in an oxidizing solution of hydrofluoric acid, the deposition pattern can be controlled to form vertically aligned nanowires and nanopillars with desired cross sections and arrangements. Alternatively noble metal nanoparticles can be deposited on the surface by electroless deposition resulting in a dense forest of randomly arranged, randomly shaped silicon nanowires and nanoribbons. The crystallinity of the substrate is preserved in the resulting nanowires alongside its electronic characteristics. By controlling the nature of the noble metal employed and the composition of the etchant solution, it is possible to determine the sidewall geometry and roughness, the etch rate, and the maximum aspect ratio achievable.

MACE is the simplest strategy for direct synthesis of porous nanowires.[153a] By controlling the resistivity of the substrate and etching conditions, MACE can synthesize solid nanowires (sNWs), porous nanowires (pNWs), porous nanowires over porous silicon layers (pNWs+PS), or porous silicon layers (PS). A smooth and regular transition from sNWs towards pNWs and pNWs+PS results from increasing the concentration of H_2O_2 in an aqueous solution of HF. A similar behavior presents when the resistivity of the substrate is lowered given the same etching conditions (see **Figure 20**). This regular and smooth transition allows for controlling the porosity of the pNWs by tuning either the H_2O_2 concentration or substrate resistivity. By controlling the concentration of H_2O_2 in the solution over time, it is possible to synthesize porous silicon nanobarcodes. Porosification occurs almost exclusively at the etching front, thus porosity can be controlled along the nanowire axis simply by changing the etch conditions as the etch front progresses (see Figure 20a).[153]

The mechanism of action of MACE is still widely debated, but a consensus is forming on the basics of the etching reaction.[183] In the consensus view, the noble metal catalyzes the oxidation of silicon underneath to silicon oxide at the expense of the oxidizing agent in solution that is reduced at the metal interface. Once the silicon oxide is formed it is attacked by the hydrofluoric acid in solution. While the redox reaction can occur even in the absence of the metal, its presence facilitates charge transfer between the semiconductor and the solution, inducing preferential etch at its interface. The mechanism by which porosification occurs alongside the etch is even more debated. Initially, models were proposed whereby the primary deposited metal (in nanoparticle or layer form) was responsible for the bulk etch and secondary particles nucleating at defect sites by re-deposition of ions shed by the primary particles were responsible for the porosification.[182] These initial models are now surpassed by the accumulation of conflicting experimental evidence: (i) no metal nanoparticles (or metal elemental signatures) are observed within the pores throughout the nanowires, while some particles are observed at the base of nanowires with a size that is not consistent with the pores and a location suggesting that they are primarily deposited particles; (ii) when pNWs+PS are formed, no metal nanoparticles are observed within the PS layer and all the visible particles are localized at the pNW/PS interface. Thus the formation of the PS layer cannot be attributed to nanoparticles, (iii) when pNWs+PS layers are formed, straight pores, orthogonal to the

© 2013 WILEY-VCH Verlag GmbH & Co. KGaA, Weinheim

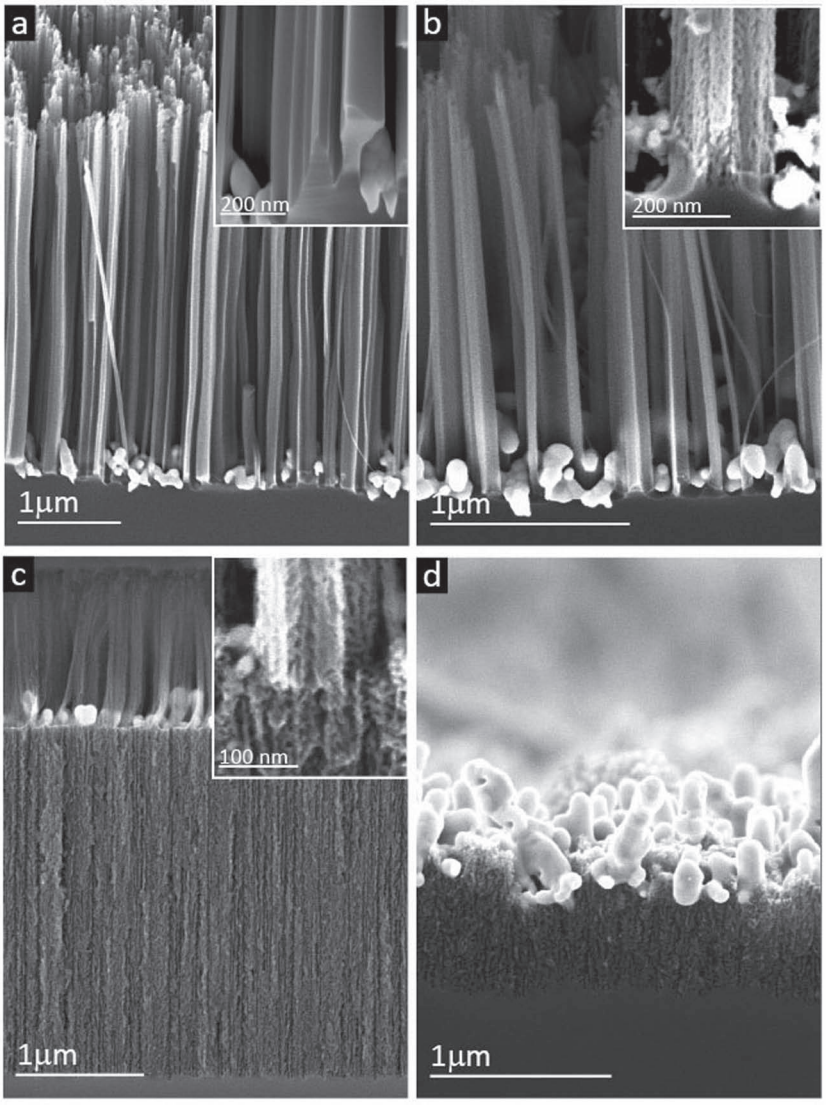

Figure 20. Cross-sectional scanning electron micrographs of the different silicon morphologies of silicon nanowires obtained by metal-assisted etch. The inset is a magnification of the sample shown in the cross section focusing on the structure of a single nanowire. a) Solid silicon nanowires (sNWs). b) Porous silicon nanowires (pNWs). c) Thick porous silicon nanowires on top of a porous silicon layer (pNWs+PS). d) A porous silicon layer (PS). Adapted with permission.[153a]

original Si surface are present that run continuously from within the tip of the pNWs to the bottom of the PS interface, indicating that the porous layer was formed first and then part of it was etched into nanowires, suggesting that the two processes occur alongside but are independent in nature; (iv) To further support the independent nature of the two processes, when pNWs or partially porosified nanowires are formed, the pores originate from the sidewalls and grow towards the core of the wire, indicating that the etch occurs first, and porosification afterwards; (v) The addition of ethanol to the etch solution slows the rate of etch of the nanowires but does not slow significantly the porosification process inducing the formation of PS or pNWs+PS instead of pNWs, and further supporting the independent nature of the two processes. An alternative model proposes that positive charges (holes) injected locally at the metal/semiconductor interface, provided they are in excess of what is necessary to mediate localized oxidation, can migrate within the semiconductor and induce preferential oxidation at defect sites, thus mediating porosification.[182] While this model provides a more suitable explanation of the preferential porosification at the etch front which is observed in the formation of porous nanobarcodes, it is unable to explain the rapid porosification of substrates without any metal deposited (i.e. wherein no catalytic charge transfer occurs) when placed in a solution where metal ions are present due to the simultaneous or preceding MACE etch of another substrate.

We recently proposed an alternative model based on our experimental findings and the independent observation that porosification, in the absence of nanowire formation or any form of etch, can be induced and controlled in many HF/oxidant metal salt solutions.[184] In our model porosification and etch are two independent processes occurring alongside each other. Etch is catalyzed by the metal layer deposited on the surface, while porosification is catalyzed by metal ions in solution. Assuming a comparable catalytic activity per unit mass for the ions in solution and metal nanoparticles, the prevalence of etch or porosification is determined by the relative abundance of ions in solution with respect to deposited metal. As ions are constantly formed by oxidation of the metal and get reduced by interaction with the semiconductor, it can be assumed that the steady-state concentration of ions in solution is determined by the concentration of oxidant present, as the available local semiconductor surface for interaction can be considered constant. In fact with increasing concentration of H_2O_2, a shift towards a higher porosification rate occurs, as determined by the progressive formation of sNWs, pNWs, and pNWs+PS, as well as an associated increase in pore size and porosity. Solid wires are formed at low ion concentration as most of the ions that become solvated interact with the semiconductor in the vicinity of the original metal particles and are quickly neutralized and locally recondensed into metal particles. As the concentration of H_2O_2 increases the ions can diffuse further away from their site of origin before being neutralized, and can be more readily re-ionized to catalyze multiple sequential reactions. This is reflected by the migration towards pNWs as H_2O_2 concentration increases and even further by the formation of a porous layer up to several microns away from the localization sites of the metal particles at very high H_2O_2 concentrations. In principle this model is analogous to the one

© 2013 WILEY-VCH Verlag GmbH & Co. KGaA, Weinheim

previously proposed whereby the diffusion of excess local charges in the semiconductor mediates porosification. In this model though it is the diffusion of excess local charge carried by the ions in solution that mediates porosification, allowing for an extension of the description of the experimental findings from the case when solid metal is present at the semiconductor interface to that when solid metal is absent.

Alternatively to MACE, solid nanowires can be formed by more traditional top-down or bottom-up approaches, and subsequently porosified by either electrochemical or stain etch. While this approach may provide more control on the formation of solid wires as the more traditional strategies are better estabilished than MACE, the porosification step is undermined by erosion of the wire leading to poor uniformity, breakages, and low reproducibility.

6. Porous Silicon for Tissue Engineering Applications

Tissue engineering has become a growing multidisciplinary field that utilizes cells, biomaterials, and drug delivery systems for the development of tissue constructs to augment, repair or replace injured tissues.[185] There are three main challenges that must be overcome to engineer functional three-dimensional tissues: the development of biomimetic materials, the achievement of locally efficacious levels of bioactive molecules, and the induction of cellular metabolism towards an appropriate phenotype for tissue growth.[186] Research on nano-biomaterials has introduced a new generation of substrates that can promote tissue healing through controllable physical and chemical properties.[185b,187] A tissue engineering scaffold should meet four major criteria: high porosity while retaining its three-dimensional structure, biocompatibility and bioresorbability with a tunable rate to match tissue growth, appropriate surface chemistries for cellular growth, and mechanical properties that are matched to the surrounding tissue. The engineering of a three-dimensional construct starts with the choice of a nano-biomaterial that closely simulates the properties of the tissue to be repaired. The ideal scaffold should mimic the composition of the extracellular matrix, promote cell viability and enhance cell proliferation, retain controllable degradation rates, and have a high degree of immune tolerance.[188]

6.1. Possibilities for Biomimetic Materials: Polymers, Hydrogels, and Bioactive Glasses

Three broad categories of nano-biomaterials extensively explored for tissue engineering applications are based on polymers, hydrogels, and inorganic ceramics.[187,189] Polymer scaffolds have the advantages of highly tunable chemical and physical properties and great fabrication flexibility, while hydrogel compositions more closely match that of the extracellular matrix.[189a,190] Bioactive glasses have been extensively investigated and reported on in the literature because of their demonstrated potential to regenerate hard and soft tissue and to release ionic biological stimuli that promote cell proliferation by gene activation.[189c,191] They have also been shown to induce specific biological activity both in vitro[192] and in vivo based on specific surface reactions that lead to the formation of hydroxycarbonate apatite (HCA). This HCA layer helps to form firm bonds with both soft and hard tissue,[193] as well as promote osteointegration as a result of their high degree of similarity to the HCA layer in the mineral phase of bone.[194] Furthermore, their degradation byproducts positively affect gene expression and osteogenesis.[195] As a result, bioactive glasses have been predominantly used in bone formation and regeneration applications in vivo,[196] where these bioactive glasses have been found to accelerate new bone regeneration, especially as compared to synthetic hydroxyapatite (HA).[197] Additionally, recent reports have also demonstrated the usefulness of bioactive glasses for soft tissue engineering because of their angiogenic potential. Overall, bioactive glass has a unique set of features, including controllable degradation rate, the production of an HCA-like layer for firm bonding to hard and soft tissues, and the release of ions during their degradation, which benefits osteogenesis and angiogenesis. In all cases, however, scaffold degradation needs to temporally coincide with host-generated tissue formation.

Unfortunately, many of these nano-biomaterials still lack sufficient mechanical strength to be used in muscolo-skeletal tissue engineering.[198] Recently, Tasciotti, Decuzzi, Ferrari, et al. has introduced a novel blend of composite nano-biomaterials (biocomposite scaffolds) containing pSi as both a bioactive and structural component[199] able to address both the biological and micromechanical needs of bone tissue engineering.

6.2. Porosous Silicon as a Functional Component for Bone Repair

Porous silicon (pSi) is of particular interest among biomaterials since its mechanical properties and elastic modulus can be tuned as a function of its porosity.[8c] pSi Micro- and nanoparticles, with different sizes, shapes, porosities, aspect ratios and surface properties,[9a,13,142,153b,190] have been incorporated into a polymeric scaffold to enhance its micromechanical stability for use in bone repair. To identify the optimal geometries and material properties of the reinforcing pSi particles, mathematical models have been developed to predict the impact of variations in the Young's and shear moduli of the composite material.[200] The equivalent poly-inclusion approach (within the effective medium theory) was employed to predict the elastic properties of a composite with inclusions of different shapes, sizes, material properties, and volume concentrations. **Figure 21** shows a schematic representation of the composite, made up of a polymer matrix with pores and reinforcing pSi particles. The model suggested that the best strategy to optimize the elastic properties of a bone repairing material was to generate spherical pores within the polymer matrix and to disperse highly anisotropic and stiff pSi nanoparticles throughout the composite.

In **Figure 22**B, the elastic modulus E of a biocomposite scaffold, Poly(propylene fumarate)-pSi (PPFpSi), is plotted against the pSi volume concentration (α_s). The original PPF had an elastic modulus of 2 GPa, whereas for $\alpha_s = 1$ the elastic modulus of pSi was obtained. The overall elastic modulus (E) was

 © 2013 WILEY-VCH Verlag GmbH & Co. KGaA, Weinheim

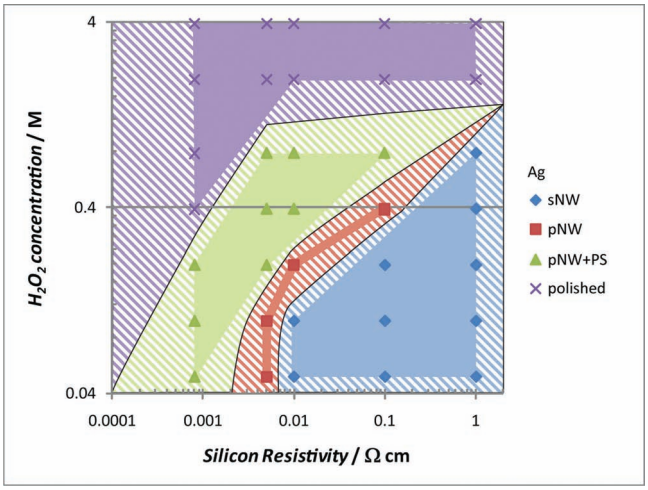

Figure 21. Phase diagram showing the different nanowire morphologies obtained as a function of H_2O_2 concentration and Si substrate resistivity during Ag mediated etch. Increasing the concentration of H_2O_2 and increasing the Si conductivity are associated with a smooth transition from sNWs to pNWs to pNWs+PS to polished surfaces. Adapted with permission.[153a]

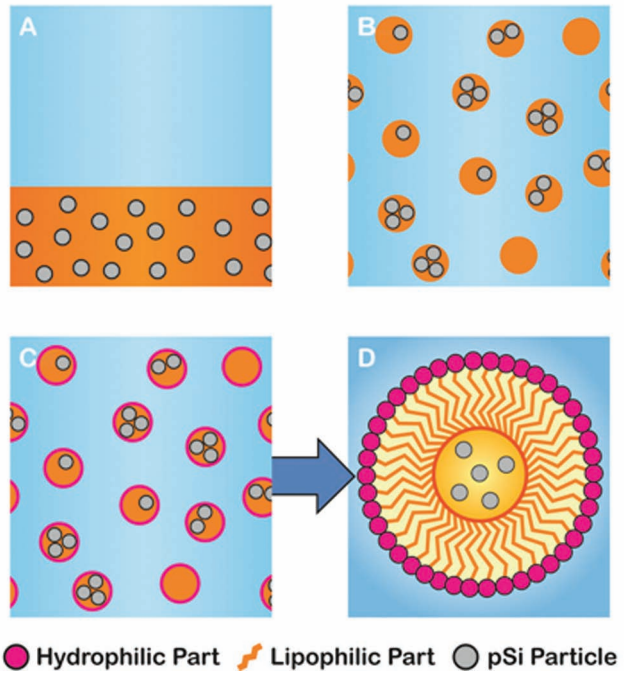

Figure 23. A schematic diagram of PLGA/pSi microsphere fabrication by means of the S/O/W emulsion method. A) A PLGA/pSi suspension is poured into the water phase. B) The suspension is then emulsified in the water phase. C) Surfactants are added to stabilize the structures. D) A cartoon depicting the final composition of the PLGA/pSi microsphere (components not to scale). Reproduced with permission.[190]

calculated using this approximate relationship of porosity (α_p) and pSi reinforcement:

$$E \approx 3.23\alpha_s - -2.98\alpha_p + 2[\text{GPa}] \quad (6.1)$$

Notably, the elastic properties of the biocomposite improved with increasing pSi content (α_s) and decreasing overall porosity (α_p). For a porous polymeric scaffold reinforced with 10% weight per volume pSi, it was mathematically shown and experimentally validated that the optimal mechanical properties could be achieved by dispersing pSi nanoparticles with specific aspect ratios and shapes into the scaffold complex. In particular, discoidal or platelet-like pSi particles showed better enhancement than rod shaped or fibril-like particles. The biochemical properties of these pSi inclusions were further tuned, using the fabrication techniques previously described, to obtain uniform micro- and nanocarriers with specifically designed pore size, high surface area, highly interconnected porosity, and functionalized surfaces capable of accommo-dating various types of payloads within the biocomposite and protecting them from degradation.[73b,201] Additionally, pSi possesses intrinsic bioactivity in simulated body fluid, with the pSi degradation byproduct, orthosilicic acid, able to promote collagen formation and facilitate the deposition of calcium and mineralization, thus stimulating bone regeneration.[190,201a,b]

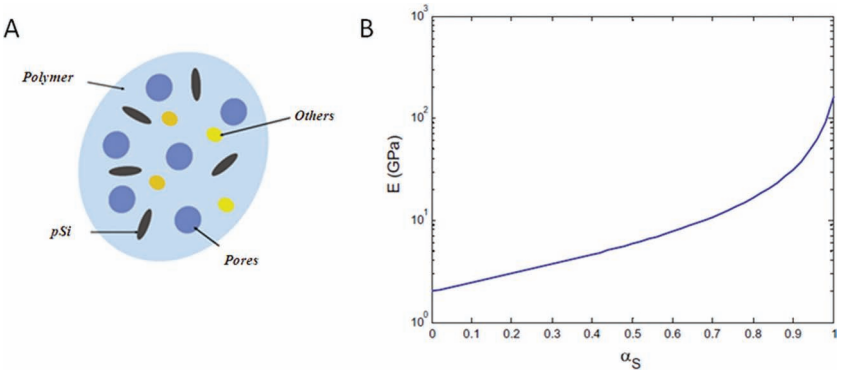

Figure 22. A) A schematic presenting porous silicon (pSi) particles and pores embedded in a polymeric matrix. (The pores and pSi particles have arbitrary shapes and are randomly oriented. They are not to scale.) B) The Young's modulus *E* as a function of pSi volume concentration within the matrix. Reproduced with permission.[200] Copyright 2010, Elsevier.

6.3. pSi/PLGA Composites

To further extend the storage time, stabilization, and release of growth and differentiating factors, Fan, et al. adapted the solid/oil/water emulsion method to encapsulate pSi particles with Poly(DL-Lactide-Co-Glycolide) (PLGA) (see **Figure 23**). PLGA is an FDA approved biodegradable polymer widely used in drug delivery applications.[201c,202] Its degradation rate and material properties can be tuned by changing its constituent monomer ratios and/or polymer molecular weight to obtain the controlled delivery of pharmaceutical agents.[203] In the experiments detailed here, PLGA was formulated to obtain

© 2013 WILEY-VCH Verlag GmbH & Co. KGaA, Weinheim

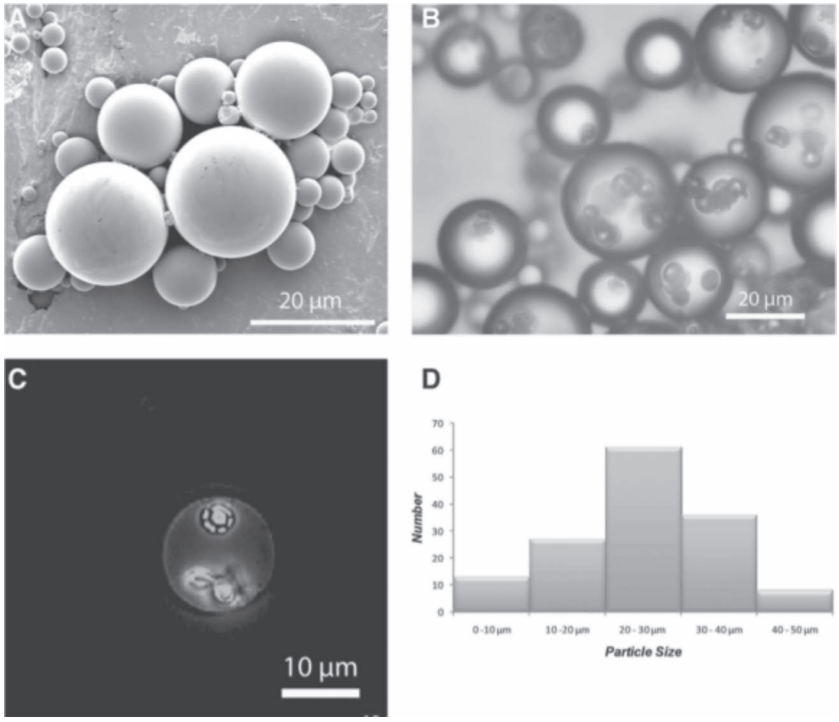

Figure 24. Physical characterization and size distribution of PLGA/pSi microspheres. A) SEM image of presorted microspheres. B) An optical microscopy image showing the presence of pSi particles enclosed in the larger PLGA spheres. C) Fluorescence microscope image and (D) size distribution of PLGA/pSi microspheres displaying a uniform product centered around 25 µm. Reproduced with permission.[190]

multilayer coatings with tunable properties. The polymeric shell was able to seal the pSi pores, thus preventing early payload release, as well as control the degradation of the carrier and extend the release of the biomolecules in time (see **Figure 24**). Compared with pSi, a larger quantity of biomolecules could be loaded and stored into the pSi/PLGA composite microspheres. To enhance the biostability of drug molecules during the formation of the PLGA shell, the pSi particles were lyophilized prior to encapsulation. pSi surface chemical properties were also optimized to improve loading and stabilization of the payload. Depending on the isoelectric properties of the loaded molecules, the surface of the pSi was chemically modified in order to obtain more stable electrostatic interactions.[152c,201d] The loading of biomolecules into the pSi pores prior to PLGA encapsulation minimized their hydrolytic degrada-tion in the solutions used during PLGA fabrication.

Subsequent studies demonstrated that the PLGA coating played a significant role in managing molecular release kinetics. A higher concentration of PLGA resulted in thicker coating layers with higher density and, consequently, slower release rates. **Figure 25** shows the release of FITC-BSA from pSi particles, PLGA microspheres, and PLGA/pSi composite microspheres. In the case of pSi or PLGA microparticles, BSA was released with a massive initial burst and then reached the plateau within three days. In contrast, PLGA/pSi composite microspheres released their payload at a continuous rate for over four weeks. Two release phases were observed: a minor fraction was released during the early phase due to the diffusion of the payload from the outer PLGA layers, followed by a subsequent long time frame phase when the payload was released from the embedded pSi particles. The acidic degradation byproducts of PLGA particles are known to lower the pH of the surroundings and have been known to cause unexpected inflammatory responses.[203c] The degradation of PLGA/pSi composite microparticles was therefore investigated to determine the net result of orthosilicic acid and PLGA metabolism. It was found that the pH values of the composite degradation remained within physiological limits for four weeks and cre-ated a more biologically favorable microenvironment for any cellular response.[204] It was concluded that the silicic acid neutralizes the acidic products of the PLGA degradation. pSi particles also have the ability to increase mineralization by stabilizing both calcium phosphate nucleation and the osteoac tive mineral phase.[73b] To investigate the enhancement of mineral deposition from pSi in PLGA/pSi composites, PLGA/pSi and PLGA microspheres were incubated in osteogenic media for 21 days and confirmed the uniform deposition of minerals only on the surface of the PLGA/pSi microspheres. This study suggested that the pSi contained within the PLGA composite microspheres could stimulate intensive production of a mineralized layer on the surface of microspheres. This phenomenon was validated in an in vivo model of bone regeneration (manuscript in preparation) and concluded that pSi can be used to further enhance the osteoconductive

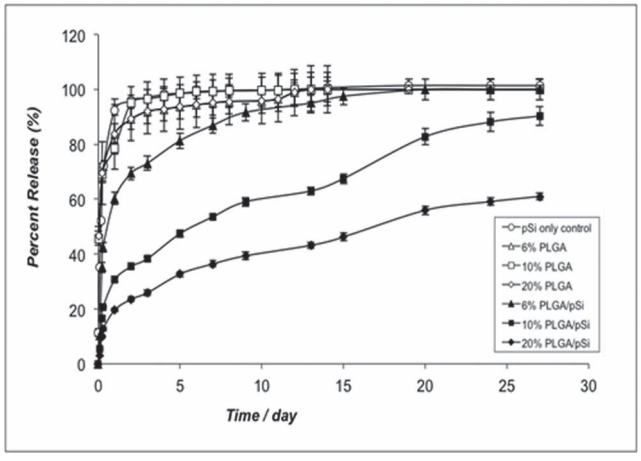

Figure 25. The release profiles of FITC-BSA from different formulations of PLGA and PLGA/pSi microspheres over a four week period. pSi particles and PLGA microspheres (6%, 10%, and 20%) showed a massive initial burst release of protein within 3 days. However, the addition of pSi to the PLGA microparticles (6%, 10%, and 20%) significantly reduced the initial burst leading to a more sustained release rate. Reproduced with permission.[190]

© 2013 WILEY-VCH Verlag GmbH & Co. KGaA, Weinheim

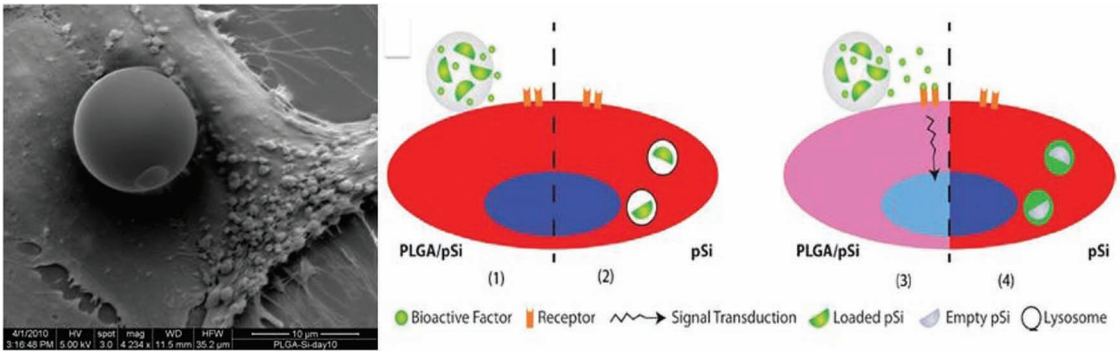

Figure 26. Scanning electron microscopy image (left panel) of an uninternalized PLGA/pSi particle. A schematic diagram of the mechanism of action of PLGA/pSi microspheres as compared to pSi (right two panels). Following internalization, pSi is entrapped within lysosomes (#2 and #4) while the PLGA/pSi microparticles are not endocytosed and release their payloads outside the cells for maximal bioactivity (B3 and B4). Reproduced with permission.[190]

potential of a scaffold, while simultaneously allowing the release of bioactive molecules, thus serving a dual role in bone tissue engineering.[205] Most growth factors and differentiating biomolecules function by binding to receptors on the cell surface to start active transmembrane signal transduction. When bioactive stimuli are trans-ported by nanoscale carriers, they often get internalized either by their primary targets or by macrophages and other cells of the immune or reticulo-endothelial system, thus minimizing their therapeutic efficacy.[14,206] The size of the PLGA-pSi composite microspheres prevented internalization and provided a hydrophobic barrier to lytic enzymes released by the cells. The ability to escape internalization provides the advantages of releasing the growth factor closer to the external cellular membrane where they are naturally active and pre-venting exposure of the payload to the lysosomal environment (see **Figure 26**).[190,201a,b]

6.4. pSi as Molecular Reservoirs for Releasing Stimulating Factors in Biocomposite Scaffolds

By using a combination of synthetic and natural biomaterials able to enrich the microstructural environment (optimizing fiber diameter, orientation and porosity) it is possible to enhance the recruitment of stem cells from the surrounding tissues.[8b,152c] Achieving successful cellular colonization within the scaffold and maintaining differentiated cell phenotypes through interactions with the scaffold are crucial requirements for a successful implant.[8c,190,199] Early cellularization and scaffold infiltration promote functional integration at the cell-material interface and support three dimensional tissue formation.[73b] Mechanical, chemical, or electrical signals are crucial to induce the phenotypic maturation of the cells and to maintain the development of functional tissue. The optimization of scaffolds has laid a foundation for the growth and integration of mature cells in tissue constructs. The success of tissue-engineered constructs rely both mechanically and biologically on proper cell localization, phenotypic maturation, and integration. pSi has been used as a vehicle for the delivery of differentiating signals that play specific roles in osteogenic maturation.[190,207] As a carrier system, pSi has been shown to provide sustained release of stimulating factors for osteogenic and neurogenic differentiation.[190,208] pSi was used to deliver Bone Morphogenic Protein-2 (BMP-2) to induce the differentiation and proliferation of osteogenic progenitors in conjunction with amphiphilic peptides in a collagen sponge. The use of pSi not only allowed for efficient release of functional BMP-2 but also enhanced mineral deposition in the extracellular matrix.[190] Through the control of payload release in a time and spatially dependent fashion, not only is differentiation influenced, but cellular recruitment as well.[209] The delivery of osteogenic factors for mesenchymal stem cell (MSC) induction has also been shown to function in chemotaxis of stem cells to the site of injury to aid in repair. Through the localized delivery of these factors, the potential for wound healing can be enhanced by attracting a greater number of cells with reparative potential to the site of an injury. It has been extensively reported that the factors released during this process are often multifunctional with the ability to induce maturation, proliferation, and chemotaxis.[210] By providing a local biochemical gradient through the controlled release of loaded chemical factors from pSi, MSC chemotaxis is enhanced.[211] With increased numbers of MSC at the site of repair a greater number of naïve cells can be stimulated leading to enhanced ECM deposition for construct integration. A final benefit of the ue of pSi in the manipulation of cell fate is the potential for increased cell survival through the delivery of proper inductive factors.[190,212] **Figure 27** confirms the uniform distribution of cells and pSi throughout the pore network of a collagen scaffold.

7. Nanoporous Silica Chips for Exploring Novel Biomarkers from Human Blood

The complexity of the circulating proteome within the human body presents one of the greatest challenges to protein biomarker discovery. Many techniques are currently available for the detection and identification of proteins of interest in blood, including western blot analysis,[213] immunohistochemical analysis, enzyme-linked immunosorbent assays (ELISA),

© 2013 WILEY-VCH Verlag GmbH & Co. KGaA, Weinheim

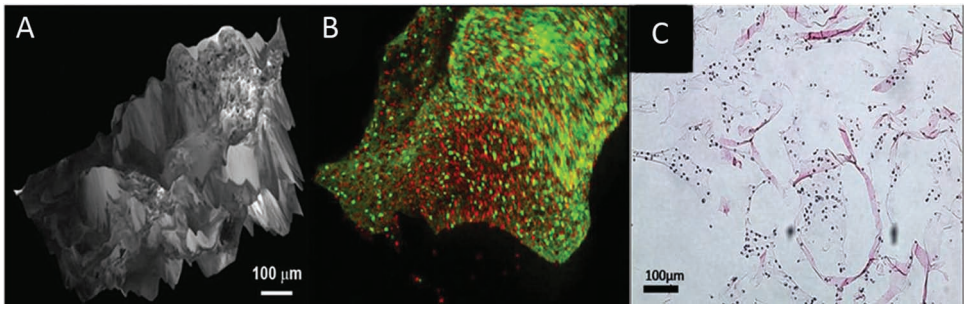

Figure 27. Confocal microscopy images of a collagen bioactive sponge (A) loaded with MSC (green) and pSi microparticles (red) (B). An even distribution of cells and pSi microparticles was observed throughout the scaffold. After overnight culture, histologically stained sections of the scaffolds showed cells attached to and proliferating throughout the scaffold (C). Taken from "Multi-Composite Bioactive Osteogenic Sponges Featuring Mesenchymal Stem Cells, Platelet-Rich Plasma, Nanoporous Silicon Enclosures, and Peptide Amphiphiles for Rapid Bone Regeneration" Matthew B. Murphy, Daniel Blashki, Rachel M. Buchanan, Dongmei Fan, Enrica De Rosa, Ramille N. Shah, et al. (Figure 5) J. Funct. Biomater. 2011, 2(2), 39-66; doi:10.3390/jfb2020039. Reproduced by permission of MDPI.

nuclear magnetic resonance techniques, x-ray diffraction, and mass spectrometry (MS). Because of its relative easy-of-use, non-invasiveness, and rapidity, matrix assisted laser desorption ionization time-of-flight mass spectroscopy (MALDI TOF MS) has become the method of choice for the analysis and discovery of proteomic patterns from complex biological samples. The large number of proteins and peptides that must be screened, however, combined with their wide range of size dispersity and relative abundance can make processing a major obstacle to identifying new biomarkers.

To address this problem, advanced separation techniques have been introduced to reduce the complexity of the samples. Accordingly, protein-based nanotechnology methods, such as nanoporous silica chips, have become an essential technique for enabling the detection of proteins on the order of zeptograms. Highly abundant proteins in plasma or serum samples mask the presence of low abundant species and hinder their identification in MS spectra. Approaches such as two-dimensional polyacrylamide gel-electrophoresis (2D-PAGE) and shotgun proteomics methods are labor-intensive low throughput procedures, offering limited suitability for enriching low molecular weight (LMW) protein signatures.[214] Size selection of proteins in pore gradients within silicon and silicon dioxide offers tunability over several key factors, including pore size, shape, and chemical functionalization, but has yet to be transformed into a reliable method.[215]

7.1. Tailoring Nanoporous Silica Chips for Fractionating and Enriching Low Molecular Weight Proteins and Peptides

Nanoporous silica chips (NSC) containing nanoscale pores were developed to achieve sample fractionation for the enrichment of LMW proteins, peptides, and their associated fragments resulting from enzymatic degradation. The nanoscale pores discriminate LMW proteins from complex biological samples via size-exclusion-based depletion. A combination of a bottom-up sol gel approach with industrially developed top-down silicon deposition techniques (spin coating, vapor phase deposition, etc.) provide a strategy to precisely engineer and control pore size, shape, and morphology to improve the fractionation of the smaller proteins and peptides. Additionally, the selectivity of specific species (for example phosphorylated proteins) can be further improved via the modification of the surface chemistry of the nanoporous silica thin films, for instance to preferentially enrich LMW phosphoproteins.[216] A general strategy for performing fractionation is depicted in **Figure 28**. The sample fractionation process starts with incubating a complex biological sample on the NSCs, followed by

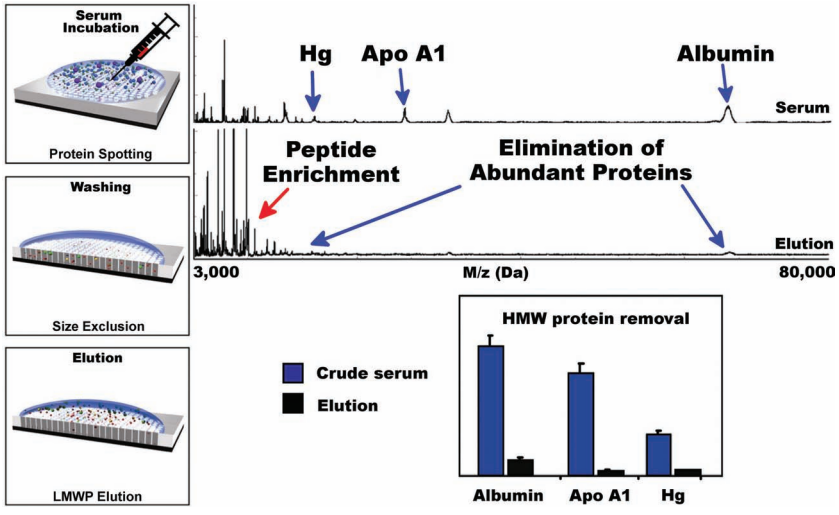

Figure 28. Left panels: the process of on-chip fractionation. After sample spotting on the surface, low molecular weight (LMW) proteins and peptides are trapped in the pores while the larger species remain outside the pores and are removed during the subsequent washing steps. The enriched fractions are then eluted and analyzed by MALDI-TOF. Top and bottom panel: MS spectra and a histogram plot showing the efficacy of on-chip fractionation for the enrichment of LMW proteins and the removal of large proteins.

© 2013 WILEY-VCH Verlag GmbH & Co. KGaA, Weinheim

a buffer wash to remove the excluded HMW proteome. LMW proteins and peptides captured by the nanopores are then eluted with an organic solvent rinse to transfer the sample to a MALDI target plate. Potential protein and peptide biomarkers are identified from the mass spectrum acquired by MALDI TOF MS. The protein profiles can be further refined using different MS modalities, such as liquid chromatography-mass spectrometry (LC-MS), on the LMW enriched samples.

The nanotexture of mesoporous silica films, along with their functionalized derivatives, can be tailored to selectively harvest a range of low molecular weight proteins.[217] The transmission electron micrographs (TEM) in **Figure 29** illustrate the pore size and geometry of different types of fabricated NSCs. The NSCs, with pore sizes ranging from 2.0 to 9.0 nm and possessing an array of different 3-dimensional internal structures, have been successfully fabricated to allow for recovered fractions with different molecular weight cut-offs and molecular characteristics, as shown in Figure 29 (top-right panel). An NSC presenting with a hexagonal pore structure significantly enriches ACTH and insulin peptides, while the recovery rate for substance P and a-Endorphin peptides is higher with NSCs presenting with a cubic structure (see Figure 29, bottom panel). The association of the LMW proteins and peptides is further mediated either by electrostatic interactions directly with the charged silica surface of by ionic or molecular intermediaries, such as metal ions (Zr^{4+} and Ti^{4+}). Thus, differentially configured NSCs can be used either alone or in combination to enrich the interesting LMW species to improve the resolution of detection.

7.2. The Staging of Metastatic Breast Cancer after Invasion of the Lungs Using NSCs

According to the American Cancer Society, cancer mortality rates have been steadily declining due in large part to improvements in early detection and treatment, as well as efforts to promote prevention. These developments have in large part been derived from significant investment towards uncovering the molecular-level alterations of metabolism and cell

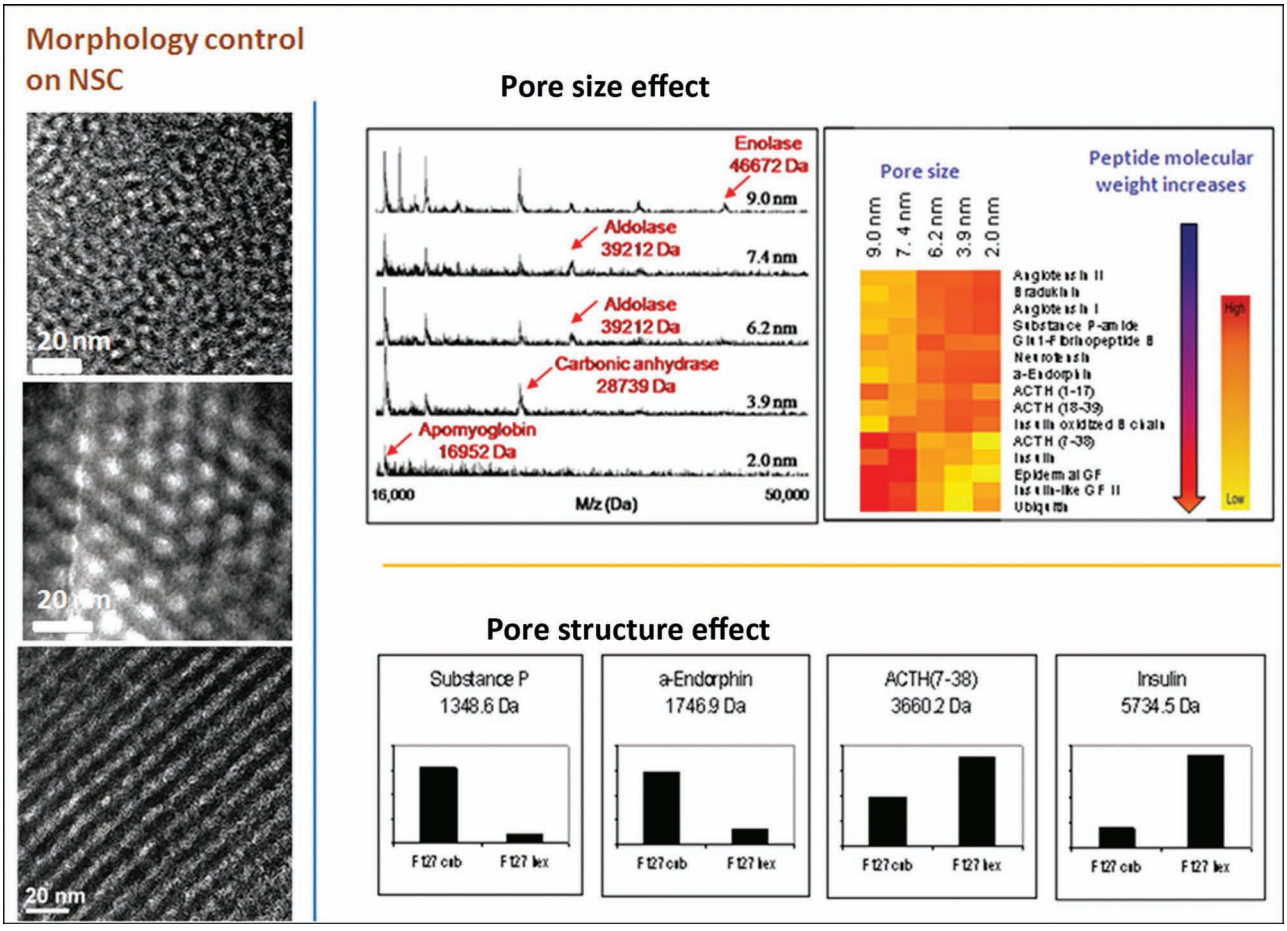

Figure 29. The effect of pore size and structure on the selective enrichment of LMW peptides from a complex biological sample. A MALDI spectra (top right panel) demonstrates the correlation between pore size and molecular weight cut-off for NSCs of varying pore size. A bar graph of the intensity of detection (bottom right panel) illustrates selectivity of the 3-D cubic or hexagonal NSCs for specific peptide recovery. Left panel: A transmission electron micrograph of the pore size and structure of different NSC configurations. Reproduced with permission.[217a] Copyright 2010, The American Chemical Society.

© 2013 WILEY-VCH Verlag GmbH & Co. KGaA, Weinheim

signaling pathways that are associated with different types and stages of cancer. As tumor cells evolve into larger structures, specific sets of proteins involved in angiogenesis, extracellular matrix formation, apoptosis, cell growth and invasion are shed into the circulatory system, providing opportunities for disease surveillance that leads to early therapeutic intervention.[218] Of particular interest are the low molecular weight proteins and peptides that are often obfuscated by larger and more abundant species such as immunoglobulin and albumin that account for more than 90% of the blood proteome.[219] The key challenge has been of a dual nature: highly sensitive detection of these low abundance targets with high specificity, and their efficient separation from complex clinical samples (such as blood). pSi can potentially address both challenges at once, benefiting both new biomarker discovery as well as new diagnostic applications.

The lung is one of the most frequent sites of breast cancer metastasis, accounting for approximately 60% of all patients. In 21% of these cases, the lung is the only metastatic organ. Its aggressive nature, high rate of recurrence, and resistance to common targeted therapies is attributed to the lack of estrogen receptors (ER), progesterone receptors (PR), and HER2 receptors (HER2). Patients in this subgroup must revert to conventional cytotoxic chemotherapy, including anthracycline and taxane, while enduring the substantial burden of adverse side-effects. While these conventional chemotherapies coupled with radiation therapy are initially effective in controlling this lung metastasized breast cancer growth, patients will frequently relapse over time.

With the on-chip fractionation technique, unique expression signatures have successfully been identified that correlate with different stages of metastatic breast cancer.[220] Fan et al. analyzed serum samples from nude mice with lung metastasized MDA-MB-231 human breast cancer, a triple negative cell line lacking expression of ER, PR, and HER2. The serum samples were collected from nude mice without tumor cell injection, at breast cancer lung metastasis early stage (BCLM-ES), and at late stage (BCLM-LS) of disease progression and processed on NSCs for LMW protein fractionation. The isolated samples were analyzed by MALDI-TOF MS with the generated spectra further analyzed by principle component analysis (PCA). As shown in **Figure 30**C, the vertical scatter plots for the eight specific biomarkers exhibited expression level variability from specific LMW proteins or peptides that distinctly correlate to the three different stages of lung metastasized breast cancer. Further characterization of the variations of these possible biomarkers will be required to determine

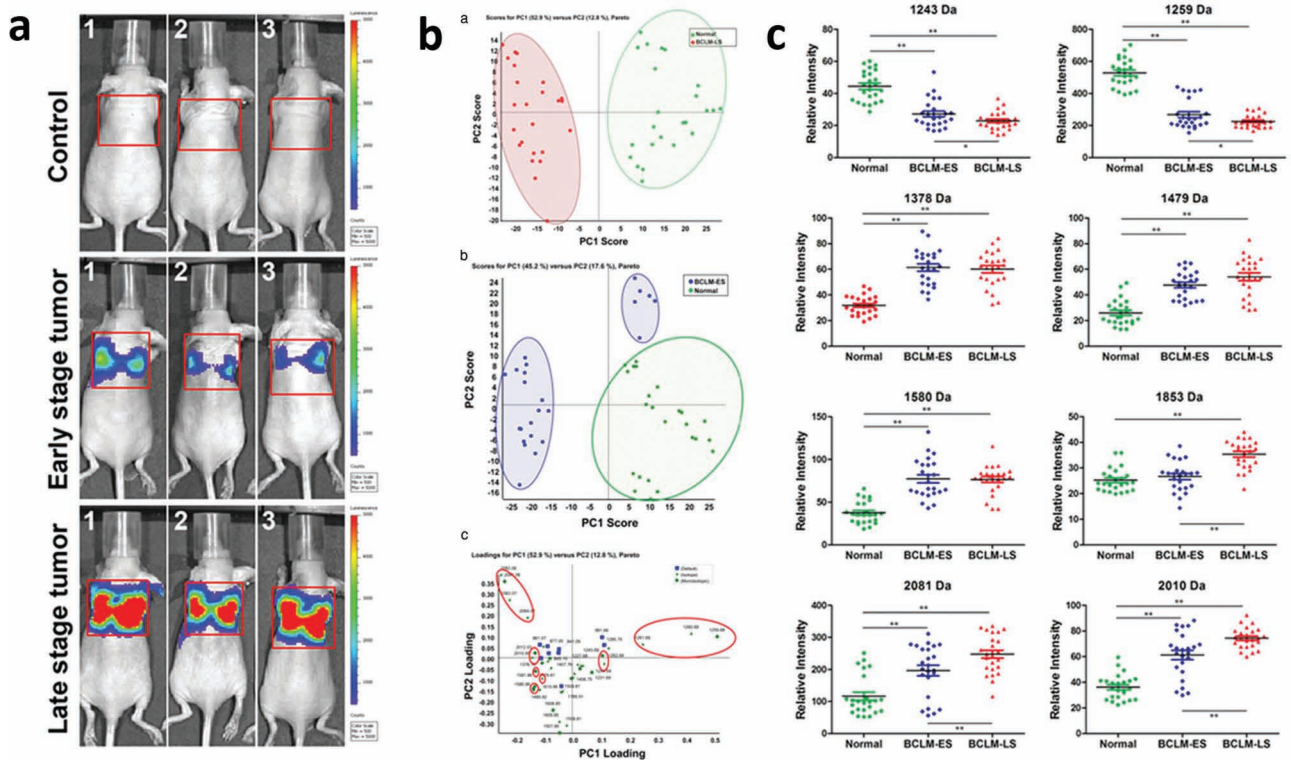

Figure 30. Staging of Metastatic Breast Cancer on NSCs. a) The MDA-MB-231 human breast cancer cells were engineered with a luciferase gene. Tumor growth was monitored with bioluminescence using a Xenogen IVIS 200 imaging system. b) Principle component analysis (PCA) of control, BCLM-ES, and BCLM-LS groups. PC1 and PC2 scores obtained after PCA analysis of the replicated MALDI-TOF MS data sets in three groups. Top: The scores plot of PC1/PC2 between the BCLM-LS and control groups; Mid: The scores plot of PC1/PC2 between the BCLM-ES and control groups; Bottom: The loading plots specific for PC1/PC2 between BCLM-LS and control groups. Highlighted ions clusters represent specific peptides for classification into these two groups. c) Different expressed biomarker candidates between control and breast cancer-based lung metastase in mouse serum. Eight biomarker candidates were detected. **represents p-value lower than 0.01, * represents p-value lower than 0.05. Reproduced by permission.[220] Copyright 2012, The Royal Society.

© 2013 WILEY-VCH Verlag GmbH & Co. KGaA, Weinheim

whether these proteins and peptides are truly indicative of cancer progression.

7.3. Challenges and Perspectives

Cancer represents a class of pathologies containing more than 100 subtypes whose primary distinguishing characteristics are their tissue of origin and the type and nature of the specific molecular and metabolic pathway alterations that lead to their initiation. Their diagnostic and prognostic classification is still quite limited and does not reflect inter-patient and intra-tumoral heterogeneity. These limitations impede precise histological diagnosis requiring new molecular markers to improve diagnosis, prognosis, and predictions of therapeutic response. Increasing knowledge of the molecular alterations driving disease progression can provide researchers, pharmacists, and clinicians with possible molecular targets that can be used to generate new diagnostic strategies.

There is no doubt, however, that completely defining the human proteome is going to involve a much different set of challenges than sequencing the human genome. Due to the lack of a coherent pipeline connecting biomarker discovery and well-developed validation methods, the contribution of MS-based proteomics methods to clinical applications has been disappointing. The need for developing novel pathways forward for protein biomarker discovery and integrating the advantages from multiple techniques can be a driving force for providing the critical bridge between discovery and validation while limiting development resources to those biomarker candidates with the highest likelihood of success. There is reason to remain optimistic that widespread use of evolving technologies, including microarrays, microfluidics, and nanopore-based assays similar to the platform described herein, could facilitate the development of better methods to detect disease at earlier and more treatable stages and to evaluate the effects of new therapeutic strategies in a timely manner.

8. Conclusions

This manuscript has detailed several exciting technologies that have been developed using the same highly precise and accurate silicon micro- and nanofabrication techniques invented and deployed in the semiconductor industry to produce high performance ICs. The myriad process technology refinements that have been developed to maintain the rate of transistor and memory cell scaling per unit area dictated by Moore's Law has yielded significant benefits that can be leveraged for the precise and accurate manufacture of silicon-based drug delivery, diagnostic, and treatment systems possessing advantageous nanoscale features. These refinements not only include lithography (although 200–500 nm structures with 50-nm overlay accuracy are sufficient for the near future), but metal and dielectric deposition (including atomic layer deposition), etching (including complex multi-stack and deep silicon plasma etching), cleaning, and nanoscale metrology (including angstrom resolution ellipsometry, SEM, TEM, and microscale compositional analytical methods) as well.

Drug delivery through nanochannel membranes allows for the long-term zero-order passive release of analytes from an implant with no moving or electrical components. These membranes have been used to deliver therapeutic doses of a variety of clinically important molecules in vitro and in vivo, including but not limited to interferon α-2b, Avastin (not shown), and leuprolide (not shown). Electrokinetically controlled nanochannels for use in applications that necessitate temporal modulation have also been demonstrated. Industrially scalable prototype manufacturing has been established, including bio-protection layers compatible with high-volume semiconductor manufacturing. Finally, predictive models of these nanofluidic architectures have shown great potential for detailing the behavior of molecules in nanoconfinement.

The nanochannel membranes produced by NanoMedical Systems leverage advanced semiconductor manufacturing by targeting 200 mm and larger silicon wafers and utilizing only advanced materials and processes that are both silicon and biology compatible. This requirement excludes materials that constitute electronic contaminates, such as gold and mobile ion-bearing glasses like Pyrex, which are often used in bio-MEMS designs. The number of masks (a key cost driver) is also minimized. During volume production, hundreds of drug release chips, each with millions of nanochannels identically sized down to 3 nm, can be manufactured on 200 mm wafers at a production cost of a few hundred dollars. This enables the packaging of these chips into injection molded drug delivery implants for long-term constant release of high-potency, and often high-cost, therapeutics for a net addition of only a few dollars per day.[7]

The concept of multistage nanovectors is a new frontier in cancer therapeutics. Nanovectors act and respond sequentially to circumvent the many biobarriers that exist between the delivery point (i.e. injection site) and the therapeutic target (e.g., a tumor site). Through the development of a set of mathematical tools to guide their rational design, non-spherical biocompatible multistage silicon vectors, both hemispherical and discoidal, can be fabricated with high precision using top-down processing techniques, including photolithography. These nanovectors have unique and favorable margination properties in blood vessels to overcome unfavorable hemodynamic forces. They can also carry an array of different payloads simultaneously which facilitates their use in both diagnostics as well as therapy.

The combination of established lithographic patterning and plasma etching with emerging electrochemical anodization techniques (described in Section 4.3) has also provided a "sweet spot" of increased yield and reduced costs in the case of the porous silicon MultiStage Nanovectors. Advancements in processing and manufacturing technology have introduced 200 mm and 300 mm diameter wafers with 450 mm wafers now in development so that increased particle density with decreasing areal cost have already dramatically dropped the cost per dosage unit over that achieved in 4 inch academic research clean room laboratories.[4] Additional economy of scale improvements will further reduce costs once continuous semi-automated production has been established. Compared to some current "advanced" delivery systems that are selling at extreme premiums over the basic drugs,[221] it is apparent that the MSV

© 2013 WILEY-VCH Verlag GmbH & Co. KGaA, Weinheim

platform not only has clinical advantages of reduced toxicity and improved performance, but also has the potential to provide financial benefits as well.[222]

Silicon and porous silicon nanowires have the potential to manipulate cells at the molecular level. These high aspect ratio probes can be used to fundamentally investigate intracellular and intercellular interactions as well as deliver molecules into the cytoplasm with minimal disruption to normal cellular homeostasis. Porous silicon nanowires are also biodegradable, a property that may enable their eventual application towards drug delivery and diagnostic imaging applications.

Porous silicon (pSi) particles of differing size, shape, orientation, concentration, and physico-chemical properties have been incorporated into multi-phase non-homogeneous composite biomaterials that consist of an enveloping polymeric matrix containing several second phase reinforcements in addition to the pSi particles. These variously shaped pSi inclusions not only serve to reinforce the matrix, but can also release biologically active molecules to initiate important recruitment and differentiation cascades. With standard industrial silicon micro- and nanofabrication technologies, it is anticipated that potential scale-up and manufacture will not pose insurmountable problems. pSi is increasingly seen as a structural alternative to hydroxyapatite for bone replacement with many possible uses in orthopedic medical implants as bone graft substitutes, scaffolds for bone repair and regeneration, pastes for spinal fusion, and substrates for controlled drug delivery.

Finally, the accurate quantification of low abundance and low molecular weight proteins given the high dynamic range of both protein quantities and sizes in vivo is one of the greatest challenges to the study of the human proteome. With the assistance of MS-based technologies and biostatistical methods, we have developed nanoporous silica chips (NSC) for the capture and identification of peptides and low molecular weight proteins in complex biological samples, including human serum and plasma. NSC-based fractionation facilitates depletion of the abundant high molecular weight (HMW) proteins and promotes enrichment of the LMW protein and peptide species. By finely tuning the pore size and the physicochemical properties inside the pores, we have demonstrated substantial control over the molecular weight cut-off.

The technologies noted in this review will undergird new classes of products that represent the vanguard of a new era in patient care. As medical researchers and engineers gain access to ever more leading edge R&D semiconductor facilities established to maintain Moore's Law, healthcare will join with the semiconductor industry in directing and investing in the broad advancement of nanofabrication that is already and will continue to transform society well into the 21st century.

9. Conflict of Interest

Mauro Ferrari is the founding scientist and a member of the Board of Directors of Leonardo Biosystems, and NanoMedical Systems, Inc., and a member of the Board of Directors of Arrowhead Research Corporation, and hereby discloses potential financial interests in those companies. In addition, Ennio Tasciotti and Xuewu Liu also declare a financial interest in Leonardo Biosystems, while Daniel Fine, Alessandro Grattoni, and Xuewu Liu declare a financial interest in NanoMedical Systems, Inc.

The other authors disclosed no potential conflicts of interest.

Acknowledgements

The Authors would like to thank the Microelectronics Research Center at the University of Texas at Austin, Austin, TX for use of their facilities. The Authors would also like to acknowledge financial support from the following sources: NASA (NNJ06HE06A and NNX08AW91G), the Department of Defense (DODW81XWH-09-1-0212, DODW81XWH-11-02-0168), the National Institutes of Health (NIHU54CA143837 (CTO, PS-OC), NIH1U54CA151668-01 (TCCN, CCN), NIHU54CA143837 (NCI), R01CA128797 (NCI), R33CA122864 (NCI)), the Ernest Cockrell Jr. Distinguished Endowed Chair, the Alliance for NanoHealth (ANH) (Seed Grant and graduate student fellowship), the State of Texas Emerging Technology Fund (ETF) and NanoMedical Systems (NMS).

Specific Author Contributions: D.F. and R.G. (Sections 1,2,3, and 8), S.S.B. and A.G. (Sections 1–3), C.C. (Sections 2 and 5), Sharath Hosali (Section 3), A. L.v.d.V., S. S., X.L., B.G. (Section 4), L.B. III (Section 6 and 7), I.K.Y. and J. F.-M. (Section 6), E.T. (Sections 2,3 and 6), H.-J.W. and Y.H. (Section 7), S.K. (Section 8), and M.F. contributed to all sections.

Received: June 22, 2012
Revised: August 31, 2012
Published online: April 15, 2013

[1] W. F. Brinkman, D. E. Haggan, W. W. Troutman, *IEEE J. Solid-St Circ.* **1997**, *32*, 1858.
[2] J. S. Kilby, *IEEE Trans. Electron. Dev.* **1976**, *23*, 648.
[3] B. K. Teo, X. H. Sun, *J. Clust. Sci.* **2006**, *17*, 529.
[4] SEMATECH **2009**.
[5] a) G. Voskerician, M. S. Shive, R. S. Shawgo, H. Von Recum, J. M. Anderson, M. J. Cima, R. Langer, *Biomaterials* **2003**, *24*, 1959; b) Y. C. Wang, M. Ferrari, *J. Mater. Sci.* **2000**, *35*, 4923; c) K. E. La Flamme, K. C. Popat, L. Leoni, E. Markiewicz, T. J. La Tempa, B. B. Roman, C. A. Grimes, T. A. Desai, *Biomaterials* **2007**, *28*, 2638; d) M. Q. Zhang, T. Desai, M. Ferrari, *Biomaterials* **1998**, *19*, 953; e) M. Q. Zhang, M. Ferrari, *Biotechnol. Bioeng.* **1997**, *56*, 618.
[6] a) D. Rother, T. Sen, D. East, I. J. Bruce, *Nanomedicine-Uk* **2011**, *6*, 281; b) G. Hermanson, *Bioconjugate Techniques, 2nd Edition*, Academic Press, **2008**.
[7] Commercial Perspective Provided by NanoMedical Systems, Inc.
[8] a) L. T. Canham, *Adv. Mater.* **1995**, *7*, 1033; b) S. H. C. Anderson, H. Elliott, D. J. Wallis, L. T. Canham, J. J. Powell, *Phys. Status Solidi A* **2003**, *197*, 331; c) E. J. Anglin, L. Cheng, W. R. Freeman, M. J. Sailor, *Adv. Drug Delivery Rev.* **2008**, *60*, 1266.
[9] a) B. Godin, J. Gu, R. E. Serda, R. Bhavane, E. Tasciotti, C. Chiappini, X. Liu, T. Tanaka, P. Decuzzi, M. Ferrari, *J. Biomed. Mater. Res. A* **2010**, *94*, 1236; b) B. Godin, J. Gu, R. E. Serda, S. Ferrati, X. Liu, C. Chiappini, T. Tanaka, P. Decuzzi, M. Ferrari, *Controlled Release Newsl* **2008**, *25*, 9; c) E. Tasciotti, B. Godin, J. O. Martinez, C. Chiappini, R. Bhavane, X. Liu, M. Ferrari, *Mol. Imaging* **2011**, *10*, 56; d) T. Tanaka, B. Godin, R. Bhavane, R. Nieves-Alicea, J. Gu, X. Liu, C. Chiappini, J. R. Fakhoury, S. Amra, A. Ewing, Q. Li, I. J. Fidler, M. Ferrari, *Int. J. Pharm.* **2010**, *402*, 190.
[10] R. E. Serda, S. Ferrati, B. Godin, E. Tasciotti, X. Liu, M. Ferrari, *Nanoscale* **2009**, *1*, 250.

 © 2013 WILEY-VCH Verlag GmbH & Co. KGaA, Weinheim

[11] R. E. Serda, A. Mack, A. L. van de Ven, S. Ferrati, K. Dunner Jr., B. Godin, C. Chiappini, M. Landry, L. Brousseau, X. Liu, A. J. Bean, M. Ferrari, *Small* **2010**, *6*, 2691.
[12] T. Tanaka, L. S. Mangala, P. E. Vivas-Mejia, R. Nieves-Alicea, A. P. Mann, E. Mora, H. D. Han, M. M. Shahzad, X. Liu, R. Bhavane, et-al, *Cancer Res* **2010**, *70*, 3687.
[13] E. De Rosa, C. Chiappini, D. M. Fan, X. W. Liu, M. Ferrari, E. Tasciotti, *Pharm. Res.-Dordr* **2011**, *28*, 1520.
[14] N. P. Ziats, K. M. Miller, J. M. Anderson, *Biomaterials* **1988**, *9*, 5.
[15] a) J. M. Anderson, T. L. Bonfield, N. P. Ziats, *Int. J. Artif. Organs* **1990**, *13*, 375; b) A. Rosengren, B. R. Johansson, P. Thomsen, L. E. Ericson, *Biomaterials* **1994**, *15*, 17.
[16] Y. Ku, C. P. Chung, J. H. Jang, *Biomaterials* **2005**, *26*, 5153.
[17] L. S. Chou, J. D. Firth, V. J. Uitto, D. M. Brunette, *J. Cell Sci.* **1995**, *108*, 1563.
[18] J. M. Anderson, K. M. Miller, *Biomaterials* **1984**, *5*, 5.
[19] P. Davies, R. J. Bonney, *J. Reticuloendoth. Soc.* **1979**, *26*, 37.
[20] Z. Werb, *Am. J. Anat.* **1983**, *166*, 237.
[21] a) K. M. Holgers, P. Thomsen, A. Tjellstrom, L. E. Ericson, *Biomaterials* **1995**, *16*, 83; b) C. Shannon, R. Thull, A. von Recum, *J. Biomed. Mater. Res.* **1997**, *34*, 401.
[22] K. Lehle, S. Lohn, G. Reinerth, T. Schubert, J. G. Preuner, D. E. Birnbaum, *Biomaterials* **2004**, *25*, 5457.
[23] H. Matsuno, A. Yokoyama, F. Watari, M. Uo, T. Kawasaki, *Biomaterials* **2001**, *22*, 1253.
[24] K. C. Popat, M. Eltgroth, T. J. LaTempa, C. A. Grimes, T. A. Desai, *Small* **2007**, *3*, 1878.
[25] L. T. de Jonge, S. C. Leeuwenburgh, J. G. Wolke, J. A. Jansen, *Pharm. Res.-Dordr.* **2008**, *25*, 2357.
[26] C. N. Elias, J. H. C. Lima, R. Valiev, M. A. Meyers, *JOM* **2008**, *60*, 46.
[27] a) H. Kim, S. H. Choi, J. J. Ryu, S. Y. Koh, J. H. Park, I. S. Lee, *Biomed. Mater.* **2008**, *3*; b) D. H. Li, S. J. Ferguson, T. Beutler, D. L. Cochran, C. Sittig, H. P. Hirt, D. Buser, *J. Biomed. Mater. Res.* **2002**, *60*, 325.
[28] K. de Groot, R. Geesink, C. P. Klein, P. Serekian, *J. Biomed. Mater. Res.* **1987**, *21*, 1375.
[29] H. Schliephake, D. Scharnweber, M. Dard, A. Sewing, A. Aref, S. Roessler, *J. Biomed. Mater. Res. B Appl Biomater* **2005**, *73*, 88.
[30] G. Decher, *Science* **1997**, *277*, 1232.
[31] L. T. de Jonge, S. C. G. Leeuwenburgh, J. J. J. P. van den Beucken, J. G. C. Wolke, J. A. Jansen, *Adv. Funct. Mater.* **2009**, *19*, 755.
[32] a) R. R. Ketchem, W. Hu, T. A. Cross, *Science* **1993**, *261*, 1457; b) L. Z. Song, M. R. Hobaugh, C. Shustak, S. Cheley, H. Bayley, J. E. Gouaux, *Science* **1996**, *274*, 1859.
[33] R. C. McPhedran, N. A. Nicorovici, D. R. McKenzie, G. W. Rouse, L. C. Botten, V. Welch, A. R. Parker, M. Wohlgennant, V. Vardeny, *Phys. B* **2003**, *338*, 182.
[34] a) D. Hanahan, G. Bergers, E. Bergsland, *J. Clin. Invest.* **2000**, *105*, 1045; b) R. S. Kerbel, G. Klement, K. I. Pritchard, B. Kamen, *Ann. Oncol.* **2002**, *13*, 12; c) R. S. Kerbel, B. A. Kamen, *Nat. Rev. Cancer* **2004**, *4*, 423; d) E. Pasquier, M. Kavallaris, N. Andre, *Nat. Rev. Clin. Oncol.* **2010**, *7*, 455.
[35] I. J. Fidler, L. M. Ellis, *Nat. Med.* **2000**, *6*, 500.
[36] O. G. Scharovsky, L. E. Mainetti, V. R. Rozados, *Curr. Oncol.* **2009**, *16*, 91.
[37] M. Colleoni, A. Rocca, M. T. Sandri, L. Zorzino, G. Masci, F. Nole, G. Peruzzotti, C. Robertson, L. Orlando, S. Cinieri, F. de Braud, G. Viale, A. Goldhirsch, *Annals of Oncology* **2002**, *13*, 73.
[38] W. V. Tamborlane, R. S. Sherwin, M. Genel, P. Felig, *N. Engl. J. Med.* **1979**, *300*, 573.
[39] J. L. Selam, P. Micossi, F. L. Dunn, D. M. Nathan, *Diabetes Care* **1992**, *15*, 877.
[40] S. Sharma, A. J. Nijdam, P. M. Sinha, R. J. Walczak, X. Liu, M. M. Cheng, M. Ferrari, *Expert Opin. Drug Delivery* **2006**, *3*, 379.
[41] A. Grattoni, H. F. Shen, D. Fine, A. Ziemys, J. S. Gill, L. Hudson, S. Hosali, R. Goodall, X. W. Liu, M. Ferrari, *Pharm. Res.-Dordr* **2011**, *28*, 292.
[42] R. Langer, *Science* **1990**, *249*, 1527.
[43] J. T. Santini, M. J. Cima, R. Langer, *Nature* **1999**, *397*, 335.
[44] J. H. Prescott, S. Lipka, S. Baldwin, N. F. Sheppard, J. M. Maloney, J. Coppeta, B. Yomtov, M. A. Staples, J. T. Santini, *Nat. Biotechnol.* **2006**, *24*, 437.
[45] R. Farra, N. F. Sheppard, L. McCabe, R. M. Neer, J. M. Anderson, J. T. Santini, M. J. Cima, R. Langer, *Sci. Transl. Med.* **2012**, 4.
[46] B. Gardner, A. Jamous, P. Teddy, E. Bergstrom, D. Wang, G. Ravichandran, R. Sutton, S. Urquart, *Paraplegia* **1995**, *33*, 551.
[47] B. P. C. a. A. Corporation, in *Viadur Prescribing Information* Vol. *08840302*, R.2, **2005**.
[48] S. Litster, M. E. Suss, J. G. Santiago, *Sens. Actuators A-Phys* **2010**, *163*, 311.
[49] J. G. S. Bhavaraju, A. Joshi, *Drug Delivery Technol.* **2010**, *10*, 24.
[50] a) N. Kumar, R. S. Langer, A. J. Domb, *Adv. Drug Delivery Rev.* **2002**, *54*, 889; b) J. P. Jain, S. Modi, A. J. Domb, N. Kumar, *J. Controlled Release* **2005**, *103*, 541; c) A. C. Grayson, G. Voskerician, A. Lynn, J. M. Anderson, M. J. Cima, R. Langer, *J. Biomater. Sci. Polym. Ed* **2004**, *15*, 1281.
[51] A. B. Scranton, N. A. Peppas, *Adv. Drug Delivery Rev.* **1993**, *11*, R7.
[52] L. L. Peng, A. D. Mendelsohn, T. J. LaTempa, S. Yoriya, C. A. Grimes, T. A. Desai, *Nano Lett.* **2009**, *9*, 1932.
[53] a) L. Kangasniemi, M. Koskinen, M. Jokinen, M. Toriseva, R. Ala-Aho, V. M. Kahari, H. Jalonen, S. Yla-Herttuala, H. Moilanen, U. H. Stenman, I. Diaconu, A. Kanerva, S. Pesonen, T. Hakkarainen, A. Hemminki, *Gene Ther.* **2009**, *16*, 103; b) T. Lebold, C. Jung, J. Michaelis, C. Brauchle, *Nano Lett.* **2009**, *9*, 2877.
[54] J. Hohlbein, M. Steinhart, C. Schiene-Fischer, A. Benda, M. Hof, C. G. Hubner, *Small* **2007**, *3*, 380.
[55] S. Y. Yang, J. A. Yang, E. S. Kim, G. Jeon, E. J. Oh, K. Y. Choi, S. K. Hahn, J. K. Kim, *Acs Nano* **2010**, *4*, 3817.
[56] C. J. Lo, T. Aref, A. Bezryadin, *Nanotechnology* **2006**, *17*, 3264.
[57] F. Martin, R. Walczak, A. Boiarski, M. Cohen, T. West, C. Cosentino, M. Ferrari, *J. Controlled Release* **2005**, *102*, 123.
[58] A. B. R. Walczak, M. Cohen, T. West, K. Melnik, J. Shapiro, S. Sharma, M. Ferrari, *NanoBioTechnology* **2005**, *1*, 35.
[59] N. Egberg, A. van Beek, C. Gunnervik, S. Hulkko, E. Hirvonen, U. Larsson-Cohn, H. C. Bennink, *Contraception* **1998**, *58*, 93.
[60] S. M. A. Shah, Q. D. Nguyen, H. Syyida, A. Polito, G. Hafiz, S. Tatlipinar, D. V. Do, S. Vitale, J. A. Haller, *Retina-J Ret Vit Dis* **2010**, *30*, 160.
[61] L. R. Kleinberg, J. Weingart, P. Burger, K. Carson, S. A. Grossman, K. Li, A. Olivi, M. D. Wharam, H. Brem, *Cancer Invest* **2004**, *22*, 1.
[62] M. F. D. Paolino, P. Sinha, M. Ferrari, "*Drug Delivery Systems*", Wiley & Sons, Inc., **2006**.
[63] J. H. Sakamoto, A. L. van de Ven, B. Godin, E. Blanco, R. E. Serda, A. Grattoni, A. Ziemys, A. Bouamrani, T. Hu, S. I. Ranganathan, E. De Rosa, J. O. Martinez, C. A. Smid, R. M. Buchanan, S. Y. Lee, S. Srinivasan, M. Landry, A. Meyn, E. Tasciotti, X. Liu, P. Decuzzi, M. Ferrari, *Pharmacol. Res* **2010**, *62*, 57.
[64] A. Grattoni, D. Fine, A. Ziemys, J. Gill, E. Zabre, R. Goodall, M. Ferrari, *Curr. Pharm. Biotechnol* **2010**, *11*, 343.
[65] a) W. Chu, M. Ferrari, *Proc. SPIE* **1995**, 2593; b) R. Fan, Y. Y. Wu, D. Y. Li, M. Yue, A. Majumdar, P. D. Yang, *J. Am. Chem. Soc.* **2003**, *125*, 5254; c) J. Li, D. Stein, C. McMullan, D. Branton, M. J. Aziz, J. A. Golovchenko, *Nature* **2001**, *412*, 166; d) P. Apel, *Radiat Meas* **2001**, *34*, 559; e) C. R. Song, P. S. Wang, *IEEE T Nanotechnol* **2010**, *9*, 138; f) Y. Li, Z. Y. Ling, J. C. Wang, S. S. Chen, X. Hu, X. H. He, *Chinese Sci Bull* **2008**, *53*, 1608; g) A. J. Storm, J. H. Chen, X. S. Ling, H. W. Zandbergen, C. Dekker, *Nat Mater* **2003**, *2*, 537; h) P. Mao, J. Y. Han, *Lab Chip* **2005**, *5*, 837.

© 2013 WILEY-VCH Verlag GmbH & Co. KGaA, Weinheim

[66] a) W. Chu, T. Huen, J. K. Tu, M. Ferrari, *Proc. SPIE* **1997**, 2978; b) J. K. Tu, T. Huen, R. Szema, M. Ferrari, *Prog Biom O* **1998**, *3258*, 148; c) T. A. Desai, D. J. Hansford, L. Leoni, M. Essenpreis, M. Ferrari, *Biosens. Bioelectron.* **2000**, *15*, 453; d) P. Mao, J. Han, *Lab Chip* **2009**, *9*, 586.
[67] a) T. S. Kustandi, W. W. Loh, H. Gao, H. Y. Low, *ACS Nano* **2010**, *4*, 2561; b) S. E. Jones, S. A. Ditner, C. Freeman, C. J. Whitaker, M. A. Lock, *Appl. Environ. Microb* **1989**, *55*, 529.
[68] S. A. Miller, V. Y. Young, C. R. Martin, *J. Am. Chem. Soc.* **2001**, *123*, 12335.
[69] Y. Shin, S. Lee, *Nano Lett.* **2008**, *8*, 3171.
[70] a) O. A. Saleh, L. L. Sohn, *Nano Lett.* **2003**, *3*, 37; b) S. J. Kim, J. Y. Han, *Anal. Chem.* **2008**, *80*, 3507.
[71] K. P. Nichols, J. C. T. Eijkel, H. J. G. E. Gardeniers, *Lab Chip* **2008**, *8*, 173.
[72] S. B. Lee, C. R. Martin, *Anal. Chem.* **2001**, *73*, 768.
[73] a) T. A. Desai, D. Hansford, M. Ferrari, *J. Membrane Sci.* **1999**, *159*, 221; b) L. T. Canham, C. L. Reeves, A. Loni, M. R. Houlton, J. P. Newey, A. J. Simons, T. I. Cox, *Thin Solid Films* **1997**, *297*, 304.
[74] C. H. Duan, A. Majumdar, *Nat. Nanotechnol.* **2010**, *5*, 848.
[75] D. Fine, A. Grattoni, S. Hosali, A. Ziemys, E. De Rosa, J. Gill, R. Medema, L. Hudson, M. Kojic, M. Milosevic, L. Brousseau Iii, R. Goodall, M. Ferrari, X. Liu, *Lab Chip* **2010**, *10*, 3074.
[76] G. Kittilsland, G. Stemme, B. Norden, *Sens. Actuators A - Phys.* **1990**, *23*, 904.
[77] B. Nilsson, K. N. Ekdahl, T. E. Mollnes, J. D. Lambris, *Mol. Immunol.* **2007**, *44*, 82.
[78] M. Goto, J. Tjernberg, D. Dufrane, G. Elgue, D. Brandhorst, K. N. Ekdahl, H. Brandhorst, L. Wennberg, Y. Kurokawa, S. Satomi, J. D. Lambris, P. Gianello, O. Korsgren, B. Nilsson, *Xenotransplantation* **2008**, *15*, 225.
[79] M. Brissova, A. C. Powers, *Diabetes* **2008**, *57*, 2269.
[80] I. Capila, R. J. Linhardt, *Angew. Chem. Int. Ed.* **2002**, *41*, 391.
[81] L. Ozmen, K. N. Ekdahl, G. Elgue, R. Larsson, O. Korsgren, B. Nilsson, *Diabetes* **2002**, *51*, 1779.
[82] a) L. Moberg, H. Johansson, A. Lukinius, C. Berne, A. Foss, R. Kallen, O. Ostraat, K. Salmela, A. Tibell, G. Tufveson, G. Elgue, K. Nilsson Ekdahl, O. Korsgren, B. Nilsson, *Lancet* **2002**, *360*, 2039; b) L. Inverardi, C. Ricordi, *Transplantation* **2006**, *82*, 312.
[83] a) D. Xie, C. A. Smyth, C. Eckstein, G. Bilbao, J. Mays, D. E. Eckhoff, J. L. Contreras, *Biomaterials* **2005**, *26*, 403; b) J. Y. Jang, D. Y. Lee, S. J. Park, Y. Byun, *Biomaterials* **2004**, *25*, 3663.
[84] a) P. de Vos, P. Marchetti, *Trends Mol. Med.* **2002**, *8*, 363; b) E. S. O'Sullivan, A. Vegas, D. G. Anderson, G. C. Weir, *Endocr. Re.v* **2011**, *32*, 827.
[85] P. de Vos, A. F. Hamel, K. Tatarkiewicz, *Diabetologia* **2002**, *45*, 159.
[86] T. Maki, J. P. Lodge, M. Carretta, H. Ohzato, K. M. Borland, S. J. Sullivan, J. Staruk, T. E. Muller, B. A. Solomon, W. L. Chick, *Transplantation* **1993**, *55*, 713.
[87] M. B. Gorbet, M. V. Sefton, *Biomaterials* **2004**, *25*, 5681.
[88] J. T. Wilson, W. Cui, E. L. Chaikof, *Nano Lett.* **2008**, *8*, 1940.
[89] H. Iwata, K. Kobayashi, T. Takagi, T. Oka, H. Yang, H. Amemiya, T. Tsuji, F. Ito, *J. Biomed. Mater. Res.* **1994**, *28*, 1003.
[90] K. C. Yang, Z. Qi, C. C. Wu, Y. Shirouza, F. H. Lin, G. Yanai, S. Sumi, *Biochem. Biophys. Res. Commun.* **2010**, *393*, 818.
[91] T. A. Desai, T. West, M. Cohen, T. Boiarski, A. Rampersaud, *Adv. Drug Deliv. Rev.* **2004**, *56*, 1661.
[92] T. A. Desai, W. H. Chu, J. K. Tu, G. M. Beattie, A. Hayek, M. Ferrari, *Biotechnol. Bioeng.* **1998**, *57*, 118.
[93] T. Desai, W. Chu, J. Tu, P. Shrewsbury, M. Ferrari, *Proc. SPIE* **1997**, 2978.
[94] T. A. Desai, D. J. Hansford, W. H. Chu, T. Huen, M. Ferrari, *Mater. Res. Soc. Symp. P* **1998**, *530*, 7.
[95] T. Desai, W. Chu, M. Ferrari, G. Rasi, P. Sinibaldi-Vallebona, P. Borboni, G. Beattie, A. Hayek, *Proc. SPIE* **1998**, 3258.
[96] C. Smith, R. Kirk, T. West, M. Bratzel, M. Cohen, F. Martin, A. Boiarski, A. A. Rampersaud, *Diabetes Technol. Ther.* **2005**, *7*, 151.
[97] K. E. La Flamme, G. Mor, D. Gong, T. La Tempa, V. A. Fusaro, C. A. Grimes, T. A. Desai, *Diabetes Technol. Ther.* **2005**, *7*, 684.
[98] S. Lee, M. Park, H. S. Park, Y. Kim, S. Cho, J. H. Cho, J. Park, W. Hwang, *Lab Chip* **2011**, *11*, 1049.
[99] Z. Minjing, L. Gang, W. Qiang, C. Hualei, L. Ling, *Appl. Surf. Sci.* **2008**, *255*, 2256.
[100] G. Karsenty, M. Ferron, *Nature* **2012**, *481*, 314.
[101] D. Q. Tang, L. Z. Cao, B. R. Burkhardt, C. Q. Xia, S. A. Litherland, M. A. Atkinson, L. J. Yang, *Diabetes* **2004**, *53*, 1721.
[102] a) P. M. Sinha, G. Valco, S. Sharma, X. W. Liu, M. Ferrari, *Nanotechnology* **2004**, *15*, S585; b) G. B. Lesinski, S. Sharma, K. A. Varker, P. Sinha, M. Ferrari, W. E. Carson, *Biomed. Microdevices* **2005**, *7*, 71.
[103] A. Grattoni, G. Canavese, F. M. Montevecchi, M. Ferrari, *Anal. Chem.* **2008**, *80*, 2617.
[104] C. Cosentino, F. Amato, R. Walczak, A. Boiarski, M. Ferrari, *J. Phys. Chem. B* **2005**, *109*, 7358.
[105] a) W. Sparreboom, A. van den Berg, J. C. T. Eijkel, *Nat. Nanotechnol.* **2009**, *4*, 713; b) J. C. T. Eijkel, A. van den Berg, *Chem Soc. Rev.* **2010**, *39*, 957.
[106] a) A. Ziemys, M. Kojic, M. Milosevic, N. Kojic, F. Hussain, M. Ferrari, A. Grattoni, *J. Comput. Phys.* **2011**, *230*, 5722; b) A. Ziemys, A. Grattoni, D. Fine, F. Hussain, M. Ferrari, *J. Phys. Chem.B* **2010**, *114*, 11117; c) S. Pricl, M. Ferrone, M. Fermeglia, F. Amato, C. Cosentino, M. M. C. Cheng, R. Walczak, M. Ferrari, *Biomed. Microdevices* **2006**, *8*, 277; d) F. Amato, C. Cosentino, S. Pricl, M. Ferrone, M. Fermeglia, M. M. C. Cheng, R. Walczak, M. Ferrari, *Biomed Microdevices* **2006**, *8*, 291; e) L. Bocquet, E. Charlaix, *Chem. Soc. Rev.* **2010**, *39*, 1073.
[107] D. Hanahan, R. A. Weinberg, *Cell* **2000**, *100*, 57.
[108] S. S. Bansal, M. Goel, F. Aqil, M. V. Vadhanam, R. C. Gupta, *Cancer Prev. Res.* **2011**, *4*, 1158.
[109] M. B. Sporn, *Cancer Res.* **1976**, *36*, 2699.
[110] E. Half, N. Arber, *Expert Opin. Pharmacol.* **2009**, *10*, 211.
[111] S. S. Bansal, M. V. Vadhanam, R. C. Gupta, *Pharm Res-Dordr* **2011**, *28*, 1121.
[112] S. S. Bansal, H. Kausar, M. V. Vadhanam, S. Ravoori, R. C. Gupta, *Eur J Pharm Biopharm* **2012**, *80*, 571.
[113] F. Levi, M. C. Mormont, *Cancer* **2003**, *98*, 882.
[114] S. P. A. Grattoni, F. Hussain, *Mechanical Engineering* **2011**, *133*, 22.
[115] a) P. A. v. Guggenberg, *Electrical Insulation and Dielectric Phenomena:* **1993** Annual Report 1993, 122; b) C. R. Martin, M. Nishizawa, K. Jirage, M. S. Kang, S. B. Lee, *Adv. Mater.* **2001**, *13*, 1351; c) S. Pennathur, J. G. Santiago, *Anal. Chem.* **2005**, *77*, 6772; d) S. Pennathur, J. G. Santiago, *Anal. Chem.* **2005**, *77*, 6782; e) R. Karnik, R. Fan, M. Yue, D. Y. Li, P. D. Yang, A. Majumdar, *Nano Lett.* **2005**, *5*, 943; f) R. Karnik, K. Castelino, A. Majumdar, *Appl Phys Lett* **2006**, *88*; g) R. B. M. Schasfoort, S. Schlautmann, L. Hendrikse, A. van den Berg, *Science* **1999**, *286*, 942; h) A. Plecis, R. B. Schoch, P. Renaud, *Nano Lett* **2005**, *5*, 1147; i) T. C. Kuo, L. A. Sloan, J. V. Sweedler, P. W. Bohn, *Langmuir* **2001**, *17*, 6298; j) L. Sun, R. M. Crooks, *J. Am. Chem. Soc.* **2000**, *122*, 12340; k) L. X. Chen, J. Choot, B. Yan, *Expert Opin. Drug Delivery* **2007**, *4*, 119; l) S. Scheindlin, *Mol. Interv.* **2004**, *4*, 308.
[116] M. J. Gordon, X. H. Huang, S. L. Pentoney, R. N. Zare, *Science* **1988**, *242*, 224.
[117] D. Fine, A. Grattoni, E. Zabre, F. Hussein, M. Ferrari, X. W. Liu, *Lab Chip* **2011**, *11*, 2526.
[118] P. Schulz, T. Steimer, *Cns Drugs* **2009**, *23*, 3.
[119] A. C. Liu, W. G. Lewis, S. A. Kay, *Nat. Chem. Biol.* **2007**, *3*, 630.
[120] I. C. Kowanko, M. S. Knapp, R. Pownall, A. J. Swannell, *Ann. Rheum. Dis.* **1982**, *41*, 453.
[121]F. Portaluppi, R. Manfredini, C. Fersini, *Chronobiol. Int.* **1999**, *16*, 33.

 © 2013 WILEY-VCH Verlag GmbH & Co. KGaA, Weinheim

[122] M. Gallerani, R. Manfredini, L. Ricci, E. Grandi, R. Cappato, G. Calo, P. L. Pareschi, C. Fersini, *Eur. Heart J.* **1992**, *13*, 661.
[123] T. Saitoh, Y. Watanabe, Y. Kubo, M. Shinagawa, K. Otsuka, S. Ohkawa, T. Watanabe, *Biomed. Pharmacother.* **2001**, *55*, 138s.
[124] F. Winau, O. Westphal, R. Winau, *Microbes Infect.* **2004**, *6*, 786.
[125] M. V. Blagosklonny, *Cell Cycle* **2004**, *3*, 1035.
[126] A. Hatefi, B. Amsden, *Pharm. Res.* **2002**, *19*, 1389.
[127] M. Ferrari, *Nat. Rev. Clin. Oncol.* **2010**, *7*, 485.
[128] a) M. Ferrari, *Trends Biotechnol.* **2010**, *28*, 181; b) R. K. Jain, *Cancer Res.* **1990**, *50*, 814s; c) R. K. Jain, *J. Controlled Release* **2001**, *74*, 7.
[129] a) B. Godin, W. H. Driessen, B. Proneth, S. Y. Lee, S. Srinivasan, R. Rumbaut, W. Arap, R. Pasqualini, M. Ferrari, P. Decuzzi, *Adv. Genet.* **2010**, *69*, 31; b) B. Godin, R. E. Serda, J. Sakamoto, P. Decuzzi, M. Ferrari, *Nanoparticles for Cancer Detection and Therapy*, Wiley-VCH Verlag GmbH & Co. KGaA, **2010**.
[130] a) J. R. Heath, M. E. Davis, *Annu. Rev. Med.* **2008**, *59*, 251; b) M. D. Wang, D. M. Shin, J. W. Simons, S. Nie, *Expert Rev. Anticancer Ther.* **2007**, *7*, 833; c) K. Riehemann, S. W. Schneider, T. A. Luger, B. Godin, M. Ferrari, H. Fuchs, *Angew. Chem. Int. Ed. Engl.* **2009**, *48*, 872.
[131] a) V. Wagner, A. Dullaart, A. K. Bock, A. Zweck, *Nat. Biotechnol.* **2006**, *24*, 1211; b) M. Ferrari, *Nat. Rev. Cancer* **2005**, *5*, 161; c) O. C. Farokhzad, R. Langer, *Acs Nano* **2009**, *3*, 16; d) S. Dixit, M. Hingorani, S. Achawal, I. Scott, *Brit. J. Neurosurg.* **2011**, *25*, 459.
[132] a) W. R. Sanhai, J. H. Sakamoto, R. Canady, M. Ferrari, *Nat. Nanotechnol.* **2008**, *3*, 242; b) B. Godin, J. H. Sakamoto, R. E. Serda, A. Grattoni, A. Bouamrani, M. Ferrari, *Trends Pharmacol Sci* **2010**, *31*, 199.
[133] a) H. Hashizume, P. Baluk, S. Morikawa, J. W. McLean, G. Thurston, S. Roberge, R. K. Jain, D. M. McDonald, *Am. J. Pathol.* **2000**, *156*, 1363; b) H. Maeda, *Adv. Enzyme Regul.* **2001**, *41*, 189.
[134] a) V. P. Torchilin, *Nat. Rev. Drug Discovery* **2005**, *4*, 145; b) A. A. Gabizon, H. Shmeeda, S. Zalipsky, *J. Liposome Res.* **2006**, *16*, 175.
[135] S. Kommareddy, S. B. Tiwari, M. M. Amiji, *Technol. Cancer Res. Treat* **2005**, *4*, 615.
[136] R. Duncan, *Nat. Rev. Drug Discovery* **2003**, *2*, 347.
[137] D. Sutton, N. Nasongkla, E. Blanco, J. Gao, *Pharm. Res.* **2007**, *24*, 1029.
[138] C. C. Lee, J. A. MacKay, J. M. Frechet, F. C. Szoka, *Nat. Biotechnol.* **2005**, *23*, 1517.
[139] a) J. M. Harris, R. B. Chess, *Nat. Rev. Drug Discovery* **2003**, *2*, 214; b) H. Maeda, G. Y. Bharate, J. Daruwalla, *Eur. J. Pharm. Biopharm.* **2009**, *71*, 409; c) R. Duncan, *Nat Rev Cancer* **2006**, *6*, 688.
[140] a) L. Brannon-Peppas, J. O. Blanchette, *Adv. Drug Delivery Rev.* **2004**, *56*, 1649; b) A. A. Kale, V. P. Torchilin, *J. Liposome Res.* **2007**, *17*, 197; c) G. R. Souza, F. I. Staquicini, D. R. Christianson, M. G. Ozawa, J. H. Miller, R. Pasqualini, W. Arap, *Biomed. Microdevices* **2009**; d) M. Juweid, R. Neumann, C. Paik, M. J. Perez-Bacete, J. Sato, W. van Osdol, J. N. Weinstein, *Cancer Res* **1992**, *52*, 5144; e) T. Nakanishi, S. Fukushima, K. Okamoto, M. Suzuki, Y. Matsumura, M. Yokoyama, T. Okano, Y. Sakurai, K. Kataoka, *J. Controlled Release* **2001**, *74*, 295; f) J. F. Kukowska-Latallo, K. A. Candido, Z. Cao, S. S. Nigavekar, I. J. Majoros, T. P. Thomas, L. P. Balogh, M. K. Khan, J. R. Baker Jr., *Cancer Res* **2005**, *65*, 5317.
[141] a) A. Hajitou, R. Pasqualini, W. Arap, *Trends Cardiovasc Med* **2006**, *16*, 80; b) S. Srinivasan, W. H. Driessen, B. Proneth, J. F. Alexander, W. Arap, R. Pasqualini, B. Godin, in *Mass transport of nanocarriers.*, (Ed: R. E. Serda), Pan Stanford Publishing Pte. Ltd., **2012**.
[142] E. Tasciotti, X. Liu, R. Bhavane, K. Plant, A. D. Leonard, B. K. Price, M. M. Cheng, P. Decuzzi, J. M. Tour, F. Robertson, M. Ferrari, *Nat. Nanotechnol.* **2008**, *3*, 151.
[143] B. Godin, E. Tasciotti, X. Liu, R. E. Serda, M. Ferrari, *Acc. Chem. Res.* **2011**, *44*, 979.
[144] a) P. Decuzzi, M. Ferrari, *Biomaterials* **2008**, *29*, 377; b) P. Decuzzi, R. Pasqualini, W. Arap, M. Ferrari, *Pharm. Res.* **2009**, *26*, 235.
[145] a) R. E. Serda, J. Gu, R. C. Bhavane, X. Liu, C. Chiappini, P. Decuzzi, M. Ferrari, *Biomaterials* **2009**, *30*, 2440; b) R. E. Serda, A. Mack, M. Pulikkathara, A. M. Zaske, C. Chiappini, J. Fakhoury, D. Webb, B. Godin, J. L. Conyers, X. W. Liu, J. A. Bankson, M. Ferrari, *Small* **2010**, *6*, 1329.
[146] a) P. Decuzzi, S. Lee, M. Decuzzi, M. Ferrari, *Ann. Biomed. Eng.* **2004**, *32*, 793; b) J. A. Champion, S. Mitragotri, *Proc. Natl. Acad. Sci. USA* **2006**, *103*, 4930; c) P. Decuzzi, M. Ferrari, *Biomaterials* **2007**, *28*, 2915; d) M. Ferrari, *Nat Nanotechnol* **2008**, *3*, 131; e) P. Decuzzi, M. Ferrari, *Biophys. J.* **2008**, *94*, 3790; f) S. Y. Lee, M. Ferrari, P. Decuzzi, *J Biomech* **2009**, *42*, 1885; g) S. Mitragotri, *Pharm Res* **2009**, *26*, 232.
[147] a) M. Koval, K. Preiter, C. Adles, P. D. Stahl, T. H. Steinberg, *Experimental Cell Research* **1998**, *242*, 265; b) J. Rejman, V. Oberle, I. S. Zuhorn, D. Hoekstra, *Biochem. J.* **2004**, *377*, 159; c) S. Muro, C. Garnacho, J. A. Champion, J. Leferovich, C. Gajewski, E. H. Schuchman, S. Mitragotri, V. R. Muzykantov, *Mol. Ther.* **2008**, *16*, 1450; d) N. Doshi, S. Mitragotri, *J R Soc Interface* **2010**, *7* Suppl 4, S403.
[148] H. Jin, D. A. Heller, R. Sharma, M. S. Strano, *Acs Nano* **2009**, *3*, 149.
[149] R. E. Serda, J. Gu, J. K. Burks, K. Ferrari, C. Ferrari, M. Ferrari, *Cytometry A* **2009**, *75*, 752.
[150] a) P. Decuzzi, B. Godin, T. Tanaka, S. Y. Lee, C. Chiappini, X. Liu, M. Ferrari, *J Control Release* **2010**, *141*, 320; b) A. van de Ven, P. Kim, O. Haley, J. Fakhoury, G. Adriani, J. Schmulen, P. Moloney, F. Hussain, M. Ferrari, X. Liu, S. Yun, P. Decuzzi, *JCR* **2012**, *158*, 148.
[151] A. van de Ven, M. Wu, M. A. Chaplain, S. R. McDougall, V. Cristini, J. Lowengrub, M. Ferrari, H. B. Frieboes, *AIP Advances* **2012**, *2*, 011208.
[152] a) M. H. Cohen, K. Melnik, A. A. Boiarski, M. Ferrari, F. J. Martin, *Biomed Microdevices* **2003**, *5*, 253; b) A. H. Nashat, M. Moronne, M. Ferrari, *Biotechnol. Bioeng.* **1998**, *60*, 137; c) J. Salonen, A. M. Kaukonen, J. Hirvonen, V. P. Lehto, *J Pharm Sci* **2008**, *97*, 632; d) J. Salonen, L. Laitinen, A. M. Kaukonen, J. Tuura, M. Bjorkqvist, T. Heikkila, K. Vaha-Heikkila, J. Hirvonen, V. P. Lehto, *J. Controlled Release* **2005**, *108*, 362.
[153] a) C. Chiappini, X. Liu, J. R. Fakhoury, M. Ferrari, *Adv. Funct. Mater.* **2010**, *20*, 2231; b) C. Chiappini, E. Tasciotti, J. R. Fakhoury, D. Fine, L. Pullan, Y. C. Wang, L. Fu, X. Liu, M. Ferrari, *Chemphyschem* **2010**, *11*, 1029; c) F. Gentile, C. Chiappini, D. Fine, R. C. Bhavane, M. S. Peluccio, M. M. Cheng, X. Liu, M. Ferrari, P. Decuzzi, *J Biomech* **2008**, *41*, 2312.
[154] B. Godin, C. Chiappini, S. Srinivasan, J. F. Alexander, K. Yokoi, M. Ferrari, P. Decuzzi, X. Liu, *Adv. Funct. Mater.* **2012**, *22*, 4186.
[155] R. E. Serda, B. Godin, E. Blanco, C. Chiappini, M. Ferrari, *Biochim Biophys Acta* **2010**.
[156] M. Colleoni, G. Curigliano, I. Minchella, G. Peruzzotti, F. Nole, G. Mazzarol, G. Renne, L. Orlando, A. Rocca, P. Veronesi, M. Intra, G. Viale, M. T. Sandri, G. Severi, A. Goldhirsch, *Ann. Oncol.* **2003**, *14*, 1477.
[157] S. Ferrati, A. Mack, C. Chiappini, X. Liu, A. J. Bean, M. Ferrari, R. E. Serda, *Nanoscale* **2010**, *2*, 1512.
[158] A. van de Ven, A. Mack, M. Ferrari, R. Serda, *Meth. Enzymol* **2012**, *508*, 1.
[159] P. S. Frenette, S. Subbarao, I. B. Mazo, U. H. von Andrian, D. D. Wagner, *Proc. Natl. Acad. Sci. USA* **1998**, *95*, 14423.
[160] A. P. Mann, T. Tanaka, A. Somasunderam, X. Liu, D. G. Gorenstein, M. Ferrari, *Adv. Mater.* **2011**, *23*, H278.
[161] J. S. Ananta, B. Godin, R. Sethi, L. Moriggi, X. Liu, R. E. Serda, R. Krishnamurthy, R. Muthupillai, R. D. Bolskar, L. Helm, *Nat. Nanotechnol.* **2010**, *5*, 815.

© 2013 WILEY-VCH Verlag GmbH & Co. KGaA, Weinheim

[162] J. Y. Haifa Shen, G. Zhang, A. Ziemys, Q. Li, L. Bai, X. Deng, D. R. Erm, X. Liu, C. Li, M. Ferrari, *Adv. Healthcare Mater.* **2012**, *1*, 6.
[163] K. E. Byun, K. Heo, S. Shim, H. J. Choi, S. Hong, *Small* **2009**, *5*, 2659.
[164] S. J. Qi, C. Q. Yi, S. L. Ji, C. C. Fong, M. S. Yang, *ACS Appl. Mater. Int.* **2009**, *1*, 30.
[165] a) A. K. Shalek, J. T. Robinson, E. S. Karp, J. S. Lee, D. R. Ahn, M. H. Yoon, A. Sutton, M. Jorgolli, R. S. Gertner, T. S. Gujral, G. MacBeath, E. G. Yang, H. Park, *Proc. Natl. Acad. Sci. USA* **2010**, *107*, 1870; b) B. D. Almquist, N. A. Melosh, *Proc. Natl. Acad. Sci. USA* **2010**, *107*, 5815; c) I. Obataya, C. Nakamura, S. Han, N. Nakamura, J. Miyake, *Nano Lettt.* **2005**, *5*, 27.
[166] a) Y. Geng, P. Dalhaimer, S. S. Cai, R. Tsai, M. Tewari, T. Minko, D. E. Discher, *Nat. Nanotechnol.* **2007**, *2*, 249; b) S. E. A. Gratton, P. A. Ropp, P. D. Pohlhaus, J. C. Luft, V. J. Madden, M. E. Napier, J. M. DeSimone, *Proc. Natl. Acad. Sci. USA* **2008**, *105*, 11613.
[167] D. Cai, J. M. Mataraza, Z. H. Qin, Z. P. Huang, J. Y. Huang, T. C. Chiles, D. Carnahan, K. Kempa, Z. F. Ren, *Nat. Meth.* **2005**, *2*, 449.
[168] S. W. Han, C. Nakamura, N. Kotobuki, I. Obataya, H. Ohgushi, T. Nagamune, J. Miyake, *Nanomed. Nanotechnol.* **2008**, *4*, 215.
[169] a) J. T. Robinson, M. Jorgolli, A. K. Shalek, M. H. Yoon, R. S. Gertner, H. Park, *Nat. Nanotechnol.* **2012**, *7*, 180; b) C. Xie, Z. L. Lin, L. Hanson, Y. Cui, B. X. Cui, *Nat. Nanotechnol.* **2012**, *7*, 185.
[170] K. J. Morton, G. Nieberg, S. F. Bai, S. Y. Chou, *Nanotechnology* **2008**, *19*.
[171] J. T. Hu, T. W. Odom, C. M. Lieber, *Acc. Chem. Res.* **1999**, *32*, 435.
[172] C. Yang, Z. H. Zhong, C. M. Lieber, *Science* **2005**, *310*, 1304.
[173] A. M. Morales, C. M. Lieber, *Science* **1998**, *279*, 208.
[174] S. Hofmann, C. Ducati, R. J. Neill, S. Piscanec, A. C. Ferrari, J. Geng, R. E. Dunin-Borkowski, J. Robertson, *J. Appl. Phys.* **2003**, *94*, 6005.
[175] J. D. Holmes, K. P. Johnston, R. C. Doty, B. A. Korgel, *Science* **2000**, *287*, 1471.
[176] J. L. Liu, S. J. Cai, G. L. Jin, S. G. Thomas, K. L. Wang, *J. Cryst. Growth* **1999**, *200*, 106.
[177] H. J. Fan, P. Werner, M. Zacharias, *Small* **2006**, *2*, 700.
[178] F. Cunin, T. A. Schmedake, J. R. Link, Y. Y. Li, J. Koh, S. N. Bhatia, M. J. Sailor, *Nat. Mater.* **2002**, *1*, 39.
[179] M. Xue, X. Zhong, Z. Shaposhnik, Y. Q. Qu, F. Tamanoi, X. F. Duan, J. I. Zink, *J. Am. Chem. Soc.* **2011**, *133*, 8798.
[180] L. Canham, *Properties of Porous Silicon*, Institute of Engineering and Technology, **1997**.
[181] A. I. Hochbaum, D. Gargas, Y. J. Hwang, P. D. Yang, *Nano Lett.* **2009**, *9*, 3550.
[182] Y. Q. Qu, L. Liao, Y. J. Li, H. Zhang, Y. Huang, X. F. Duan, *Nano Lett.* **2009**, *9*, 4539.
[183] Z. P. Huang, N. Geyer, P. Werner, J. de Boor, U. Gosele, *Adv. Mater.* **2011**, *23*, 285.
[184] a) K. W. K. a. J. W. Gogola, in *218th ECS Meeting*, Vol. *33* (Ed: R. B. D. Lockwood, Y. Ogata, P. Schmuki), The Electrochemical Society, Las Vegas, NV **2012**, *23*; b) K. W. Kolasinski, J. Yadlovskiy, *Phys. Status Solidi C* **2011**, 8.
[185] a) R. Langer, J. P. Vacanti, *Science* **1993**, *260*, 920; b) J. P. Vacanti, R. Langer, *Lancet* **1999**, *354*, Si32; c) R. L. Robert Lanza, J. Vacanti, *Principles of Tissue Engineering, 3rd Edition*, Academic Press, **2007**.
[186] Y. Tabata, *Drug Discovery Today* **2001**, *6*, 483.
[187] K. J. L. Burg, S. Porter, J. F. Kellam, *Biomaterials* **2000**, *21*, 2347.
[188] P. Bianco, P. G. Robey, *Nature* **2001**, *414*, 118.
[189] a) S. Yang, K. F. Leong, Z. Du, C. K. Chua, *Tissue Eng.* **2001**, *7*, 679; b) J. A. Hubbell, *Bio-Technology* **1995**, *13*, 565; c) M. N. Rahaman, D. E. Day, B. S. Bal, Q. Fu, S. B. Jung, L. F. Bonewald, A. P. Tomsia, *Acta Biomater.* **2011**, *7*, 2355.
[190] D. M. Fan, E. De Rosa, M. B. Murphy, Y. Peng, C. A. Smid, C. Chiappini, X. W. Liu, P. Simmons, B. K. Weiner, M. Ferrari, E. Tasciotti, *Adv. Funct. Mater.* **2012**, *22*, 282.
[191] a) R. F. B. Mohamed N. Rahaman, B. Sonny Bal, D. E. Day, *Sem. Arthroplasty* **2006**, *17*, 102; b) W. H. Huang, M. N. Rahaman, D. E. Day, Y. D. Li, *Phys. Chem. Glasses-B* **2006**, *47*, 647; c) M. V. H. I. D. Xynos, J. J. Batten, L. D. Buttery, L. L. Hench, J. M. Polak, *Calcified Tissue Intl.* **2000**, *67*, 321; d) I. D. Xynos, A. J. Edgar, L. D. Buttery, L. L. Hench, J. M. Polak, *Biochem Biophys Res Commun* **2000**, *276*, 461.
[192] a) I. D. Xynos, A. J. Edgar, L. D. Buttery, L. L. Hench, J. M. Polak, *J. Biomed. Mater. Res.* **2001**, *55*, 151; b) T. Kokubo, H. Takadama, *Biomaterials* **2006**, *27*, 2907; c) T. Kokubo, H. Kushitani, S. Sakka, T. Kitsugi, T. Yamamuro, *J. Biomed. Mater. Res.* **1990**, *24*, 721.
[193] a) M. Vallet-Regi, A. Ramila, S. Padilla, B. Munoz, *J. Biomed. Mater. Res. A* **2003**, *66*, 580; b) L. L. Hench, *J. Biomed. Mater. Res.* **1998**, *41*, 511; c) M. M. Pereira, A. E. Clark, L. L. Hench, *J. Biomed. Mater. Res.* **1994**, *28*, 693.
[194] a) R. Gupta, A. Kumar, *Biomed Mater* **2008**, *3*, 034005; b) J. T. Heikkila, A. J. Aho, A. Yli-Urpo, O. H. Andersson, H. J. Aho, R. P. Happonen, *Acta Orthop. Scand.* **1993**, *64*, 678.
[195] a) A. Y. Au, R. Y. Au, J. L. Demko, R. M. McLaughlin, B. E. Eves, C. G. Frondoza, *J. Biomed. Mater. Res. A* **2010**, *94*, 380; b) C. Knabe, M. Stiller, G. Berger, D. Reif, R. Gildenhaar, C. R. Howlett, H. Zreiqat, *Clin. Oral Implants Res.* **2005**, *16*, 119.
[196] a) D. L. Wheeler, K. E. Stokes, H. M. Park, J. O. Hollinger, *J. Biomed. Mater. Res.* **1997**, *35*, 249; b) D. L. Wheeler, K. E. Stokes, R. G. Hoellrich, D. L. Chamberland, S. W. McLoughlin, *J. Biomed. Mater. Res.* **1998**, *41*, 527.
[197] H. Oonishi, L. L. Hench, J. Wilson, F. Sugihara, E. Tsuji, S. Kushitani, H. Iwaki, *J. Biomed. Mater. Res.* **1999**, *44*, 31.
[198] a) A. J. Salgado, O. P. Coutinho, R. L. Reis, *Macromol. Biosci.* **2004**, *4*, 743; b) T. W. Bauer, G. F. Muschler, *Clin. Orthop. Relat. R.* **2000**, *10*.
[199] W. L. Shen, X. A. Chen, J. L. Chen, Z. Yin, B. C. Heng, W. S. Chen, H. W. Ouyang, *Biomaterials* **2010**, *31*, 7239.
[200] S. I. Ranganathan, D. M. Yoon, A. M. Henslee, M. B. Nair, C. Smid, F. K. Kasper, E. Tasciotti, A. G. Mikos, P. Decuzzi, M. Ferrari, *Acta Biomater.* **2010**, *6*, 3448.
[201] a) M. A. Whitehead, D. Fan, G. R. Akkaraju, L. T. Canha, M. J. L. Coffer, *J. Biomed. Mater. Res. A* **2007**, *83A*, 225; b) X. Li, J. L. Coffer, Y. D. Chen, R. F. Pinizzotto, J. Newey, L. T. Canham, *J. Am. Chem. Soc.* **1998**, *120*, 11706; c) J. M. Chan, L. F. Zhang, K. P. Yuet, G. Liao, J. W. Rhee, R. Langer, O. C. Farokhzad, *Biomaterials* **2009**, *30*, 1627; d) C. A. Prestidge, T. J. Barnes, C. H. Lau, C. Barnett, A. Loni, L. Canham, *Expert Opin Drug Delivery* **2007**, *4*, 101.
[202] R. A. Jain, *Biomaterials* **2000**, *21*, 2475.
[203] a) J. Heller, *Critical Reviews in Therapeutic Drug Carrier Systems* **1984**, *1*, 39; b) R. Jalil, J. R. Nixon, *J. Microencapsul.* **1990**, *7*, 297; c) C. Shih, N. Waldron, G. M. Zentner, *J. Controlled Release* **1996**, *38*, 69.
[204] a) W. J. E. M. Habraken, O. C. Boerman, J. G. C. Wolke, A. G. Mikos, J. A. Jansen, *J. Biomed. Mater. Res. A* **2009**, *91A*, 614; b) W. Linhart, F. Peters, W. Lehmann, K. Schwarz, A. F. Schilling, M. Amling, J. M. Rueger, M. Epple, *J. Biomed. Mater. Res.* **2001**, *54*, 162.
[205] S. H. Lim, H. Q. Mao, *Adv. Drug Deliver Rev.* **2009**, *61*, 1084.
[206] a) R. S. Tuan, G. Boland, R. Tuli, *Arthritis Res. Ther.* **2003**, *5*, 32; b) D. W. Hutmacher, *Biomaterials* **2000**, *21*, 2529.
[207] a) M. Manzano, D. Lozano, D. Arcos, S. Portal-Nunez, C. L. la Orden, P. Esbrit, M. Vallet-Regi, *Acta Biomater.*. **2011**, *7*, 3555; b) D. M. Fan, G. R. Akkaraju, E. F. Couch, L. T. Canham, J. L. Coffer, *Nanoscale* **2011**, *3*, 354.

 © 2013 WILEY-VCH Verlag GmbH & Co. KGaA, Weinheim

[208] a) V. Lundin, A. Herland, M. Berggren, E. W. H. Jager, A. I. Teixeira, *PLoS One* **2011**, *6*; b) Y. Cho, R. Y. Shi, A. Ivanisevic, R. Ben Borgens, *Nanotechnology* **2009**, *20*.
[209] S. H. Oh, T. H. Kim, J. H. Lee, *Biomaterials* **2011**, *32*, 8254.
[210] a) L. M. Wakefield, N. L. Thompson, K. C. Flanders, M. D. O'Connor-McCourt, M. B. Sporn, *Ann. NY Acad. Sci.* **1988**, *551*, 290; b) P. de Winter, P. Leoni, D. Abraham, *Growth Factors* **2008**, *26*, 80; c) D. O. Morgan, J. C. Edman, D. N. Standring, V. A. Fried, M. C. Smith, R. A. Roth, W. J. Rutter, *Nature* **1987**, *329*, 301.
[211] a) J. Atencia, G. A. Cooksey, L. E. Locascio, *Lab Chip* **2012**, *12*, 309; b) V. V. Abhyankar, M. W. Toepke, C. L. Cortesio, M. A. Lokuta, A. Huttenlocher, D. J. Beebe, *Lab Chip* **2008**, *8*, 1507.
[212] X. Lin, R. F. Bulleit, *Brain Res. Dev. Brain Res.* **1997**, *99*, 234.
[213] J. F. Rual, K. Venkatesan, T. Hao, T. Hirozane-Kishikawa, A. Dricot, N. Li, G. F. Berriz, F. D. Gibbons, M. Dreze, N. Ayivi-Guedehoussou, N. Klitgord, C. Simon, M. Boxem, S. Milstein, J. Rosenberg, D. S. Goldberg, L. V. Zhang, S. L. Wong, G. Franklin, S. M. Li, J. S. Albala, J. H. Lim, C. Fraughton, E. Llamosas, S. Cevik, C. Bex, P. Lamesch, R. S. Sikorski, J. Vandenhaute, H. Y. Zoghbi, A. Smolyar, S. Bosak, R. Sequerra, L. Doucette-Stamm, M. E. Cusick, D. E. Hill, F. P. Roth, M. Vidal, *Nature* **2005**, *437*, 1173.
[214] a) A. Gorg, W. Weiss, M. J. Dunn, *Proteomics* **2004**, *4*, 3665; b) H. B. Liu, R. G. Sadygov, J. R. Yates, *Anal. Chem.* **2004**, *76*, 4193; c) T. Rabilloud, *Proteomics* **2002**, *2*, 3.
[215] B. E. Collins, K. P. S. Dancil, G. Abbi, M. J. Sailor, *Adv. Funct. Mater.* **2002**, *12*, 187.
[216] a) H. J. Zhou, S. Y. Xu, M. L. Ye, S. Feng, C. Pan, X. G. Jiang, X. Li, G. H. Han, Y. Fu, H. Zou, *J. Proteome Res.* **2006**, *5*, 2431; b) Y. Hu, A. Bouamrani, X. W. Liu, E. Tasciotti, L. Li, M. Ferrari, *Nanotechnol. Conf. Expo* **2009**, Vol *3*, Technical Proceedings 2009, 238.
[217] a) Y. Hu, A. Bouamrani, E. Tasciotti, L. Li, X. Liu, M. Ferrari, *ACS Nano* **2010**, *4*, 439; b) Y. Hu, Y. Peng, K. Lin, H. Shen, L. C. Brousseau, J. Sakamoto, T. Sun, M. Ferrari, *Nanoscale* **2011**, *3*, 421.
[218] a) E. F. Petricoin, C. Belluco, R. P. Araujo, L. A. Liotta, *Nat. Rev. Cancer* **2006**, *6*, 961; b) L. A. Liotta, M. Ferrari, E. Petricoin, *Nature* **2003**, *425*, 905; c) S. H. Beachy, E. A. Repasky, *Cancer Immunol. Immunother.* **2008**, *57*, 759.
[219] a) J. D. Wulfkuhle, L. A. Liotta, E. F. Petricoin, *Nat. Rev. Cancer* **2003**, *3*, 267; b) S. M. Hanash, S. J. Pitteri, V. M. Faca, *Nature* **2008**, *452*, 571; c) R. Etzioni, N. Urban, S. Ramsey, M. McIntosh, S. Schwartz, B. Reid, J. Radich, G. Anderson, L. Hartwell, *Nat. Rev. Cancer* **2003**, *3*, 243.
[220] J. Fan, X. Y. Deng, J. W. Gallagher, H. Y. Huang, Y. Huang, J. G. Wen, M. Ferrari, H. F. Shen, Y. Hu, *Philos. Trans. R. Soc. A* **2012**, *370*, 2433.
[221] Amerisource-Bergen, *Amerisource-Bergen, Valley Forge, PA* **2009**.
[222] Commercial Perspective Provided by Leonardo Biosystems, Inc.

© 2013 WILEY-VCH Verlag GmbH & Co. KGaA, Weinheim